POLITECNICO
MILANO 1863

SCUOLA DI INGEGNERIA INDUSTRIALE
E DELL'INFORMAZIONE

# Preliminary sizing of an airport facility for refueling liquid hydrogen-powered aircraft

Tesi di Laurea Magistrale in
Aeronautical Engineering - Ingegneria Aeronautica

Author: **Antonio Filoni**

Student ID: 964835
Advisor: Prof. Lorenzo Trainelli
Co-advisors: Prof. Carlo E.D. Riboldi
Academic Year: 2022-23

# Abstract

The purpose of this thesis is to address the urgent need for an effective and rapid reduction of the environmental impact of the aeronautical sector. Aviation is a major contributor to greenhouse gas emissions and air pollution, and there is a pressing need to mitigate this phenomenon. The most promising solution currently is the transition to hydrogen-powered aircraft. Hydrogen has a high energy density and produces very low emissions when burned, generating only water and minimal $NO_x$. While research on the development of hydrogen-powered aircraft is well underway, a major limitation to their widespread adoption would be the lack of airport infrastructure for refueling.

To address this issue, this thesis presents a methodology for economically and performance-based preliminary sizing of a ground-based hydrogen production, storage, and distribution system for refueling aircraft with this innovative propulsion system. The methodology considers factors such as the specific airport's traffic volume, the characteristics of the aircraft operating the flights, and the technical data of the system elements. The methodology will be applied to real cases, including Athens Airport for regional transport with turboprop aircraft and Milan Malpensa and Paris Charles De Gaulle Airports for short-haul transport with turbojet aircraft.

**Keywords:** Preliminary sizing, Liquid hydrogen, Airport facility, Hydrogen propulsion, Sustainability.

# Abstract in lingua italiana

Lo studio presentato in questa tesi nasce dall'esigenza di limitare l'impatto ambientale del settore aeronautico in modo efficace e rapido. L'aviazione infatti contribuisce in modo significativo alle emissioni di gas serra e all'inquinamento atmosferico, ed è necessario ridurre l'entità di questo fenomeno. Attualmente, la soluzione più promettente sembra essere quella di adottare aerei con propulsione a idrogeno. L'idrogeno, infatti, oltre ad avere una densità energetica elevata, permette di avere una combustione a bassissime emissioni, poiché genera solo acqua e una quantità minima di $NO_x$. La ricerca sullo sviluppo di velivoli alimentati ad idrogeno è già ben avviata, tuttavia, la carenza di infrastrutture aeroportuali per il rifornimento di questi aerei rappresenterebbe un grosso limite alla loro adozione diffusa.

A tal proposito, questa tesi si pone l'obiettivo di presentare una metodologia che consente di effettuare un dimensionamento preliminare economico e prestazionale di un impianto di terra per la produzione, lo stoccaggio e la distribuzione dell'idrogeno, e per il rifornimento dei velivoli. Essa tiene conto di vari fattori, come il volume del traffico nello scalo specifico, le caratteristiche dei velivoli che operano i voli e i dati tecnici degli elementi dell'impianto. La metodologia presentata verrà poi applicata a dei casi reali, nello specifico all'aeroporto di Atene, per quanto riguarda il trasporto regionale con velivoli a turboelica, e agli aeroporti di Milano Malpensa e Parigi Charles De Gaulle, concentrandosi invece sul trasporto a breve raggio operato con velivoli turbogetto.

**Parole chiave:** Dimensionamento preliminare, Idrogeno liquido, Infrastrutture aeroportuali, Propulsione a idrogeno, Sostenibilità.

# Contents

# List of Figures

# List of Tables

# List of Symbols

| Symbol | Description | Unit |
|---|---|---|
| $C^{\mathrm{DU}}$ | Total dispensing unit procurement cost | € |
| $c^{\mathrm{DU}}$ | Procurement cost for the dispensing unit | € |
| $C^{e}$ | Electric energy cost | € |
| $C^{\mathrm{GNR}}$ | Total generator procurement cost | € |
| $c^{\mathrm{GNR}}$ | Procurement cost per unit of daily production for the generator | €/(kg d) |
| $c_{e}^{\mathrm{GNR}}$ | Energy required by the generator to produce one $kg$ of hydrogen | kWh |
| $C^{p}$ | Electric power cost | € |
| $c_{p}$ | Electric power cost per month | €/(kW month) |
| $c_{p}^{\mathrm{DU}}$ | Power absorbed by each dispensing unit | kW |
| $C^{\mathrm{PV}}$ | Daily cost of PV plant | € |
| $c^{\mathrm{PV}}$ | PV plant procurement cost | €/kW |
| $c_{\mathrm{O\&M}}^{\mathrm{PV}}$ | PV plant operational and maintenance costs | €/(kW year) |
| $C^{\mathrm{ST}}$ | Total storage tank procurement cost | € |
| $c^{\mathrm{ST}}$ | Procurement cost for the tank per $kg$ of stored hydrogen | €/kg |
| $d$ | Simulated time duration | d |
| $d^{\mathrm{DU}}$ | Expected lifespan of the dispensing unit | d |
| $d^{\mathrm{GNR}}$ | Expected lifespan of the generator | d |

| Symbol | Description | Unit |
|---|---|---|
| $d^{\mathrm{PV}}$ | Expected lifespan of the PV plant | d |
| $d^{\mathrm{ST}}$ | Expected lifespan of the tank | d |
| $E^0$ | Standard reduction potential | V |
| $E_t$ | Consumed electric energy at time $t$ | kWh |
| $E^{\mathrm{PV}}$ | Energy produced by the PV plant | kWh |
| $g$ | Gravity acceleration | $\mathrm{m/s^2}$ |
| $H$ | Pump head | m |
| $h_{sun}^{\mathrm{ATH}}$ | | |
| $I$ | Set of aircraft | - |
| $J$ | Cost function | € |
| $L$ | Simulated time duration | - |
| $l_t$ | Length of a time slot | h |
| $m_{\mathrm{BO},i}^{a}$ | Mass of hydrogen lost in the tank due to boil off | kg |
| $m_{i,t}^{a}$ | Mass of hydrogen in the $i$-th aircraft tank at time $t$ | kg |
| $m_{max,i}^{a}$ | Maximum mass of hydrogen that the tank of the $i$-th aircraft can store | kg |
| $m_{min,i}^{a}$ | Minimum mass of hydrogen that the tank of the $i$-th aircraft must always store | kg |
| $m_{req,i,t}^{a}$ | Mass of hydrogen required by the $i$-th aircraft at time $t$ | kg |
| $\dot{m}^{\mathrm{DU}}$ | Hourly hydrogen flow rate of the dispensing unit | kg/h |
| $m_{fuel,i}^{a}$ | Mass of hydrogen needed for the i-th aircraft to travel the distance of its mission | - |
| $\dot{m}_t^{\mathrm{GNR}}$ | Hourly production rate of hydrogen by the generator at time $t$ | kg/h |
| $m_{\mathrm{BO},t}^{\mathrm{ST}}$ | Mass of hydrogen lost due to boil off in the tank at time $t$ | kg |

| Symbol | Description | Unit |
|---|---|---|
| $m_{min}^{\mathrm{ST}}$ | Minimum amount of hydrogen that must be counted from the tank | kg |
| $m_t^{\mathrm{ST}}$ | Mass of hydrogen in the storage tank at time $t$ | kg |
| $N^{\mathrm{DU}}$ | Number of dispensing units | - |
| $N_{extra}^{\mathrm{DU}}$ | Number of reserve dispensing unit | - |
| $Q$ | Volumetric flow | $\mathrm{m}^3/\mathrm{s}$ |
| $T$ | Set of time slots | - |
| $t_{i,t}^{ref}$ | Refueling time required for aircraft $i$-th at time $t$ | h |
| $y_{i,t}^{coup}$ | Parameter indicating if the aircraft $i$ is coupled to a dispensing unit at time $t$ | - |
| $y_{i,t}^{leave}$ | Parameter indicating if the aircraft $i$ will leave the airport during the timestep $t$ | - |
| $y_{i,t}^{out}$ | Parameter indicating if the aircraft $i$ is on mission at time $t$ | - |
| $y_{i,t}^{ref}$ | Parameter indicating if the aircraft $i$ is being refueled at time $t$ | - |
| $v_{fin}$ | Fluid velocity in the storage tank | m/s |
| $v_{in}$ | Fluid velocity in the aircraft tank | m/s |
| $\Delta h$ | Aircraft tank height | m |
| $\Delta P$ | Pressure difference | Pa |
| $\eta$ | Pump efficiency | - |
| $\lambda_t$ | Electric energy price at time $t$ | €/kWh |
| $\rho$ | Liquid hydrogen density | $\mathrm{kg}/\mathrm{m}^3$ |

# Abbreviations and Acronyms

| | |
|---|---|
| **A/C** | Aircraft |
| **AHRES** | Airport Hydrogen Refueling Equipment Sizing |
| **API** | Application Programming Interface |
| **ARERA** | Autorità di Regolazione per Energia Reti e Ambiente |
| **ATH** | Athens International Airpot |
| **BOG** | Boil Off Gas |
| **CDG** | Paris Charles De Gaulle Airport |
| **CNG2020** | Carbon Neutral Growth |
| **CORSIA** | Carbon Offsetting and Reduction Scheme for International Aviation |
| **DC** | Direct Current |
| **DU** | Dispensing Unit |
| **EEA** | European Environment Agency |
| **FC** | Fuel Cell |
| **GHG** | GreenHouse Gases |
| **GNR** | Generator |
| **GPM** | Gallons Per Minute |
| **HRS** | Hydrogen Refueling Station |

| | |
|---|---|
| **HYPERION** | HYbrid PERformance simulatION |
| **IATA** | International Air Transport Association |
| **ICAO** | International Civil Aviation Organization |
| **IPEX** | Italian Power Exchange |
| **IRENA** | International Renewable Energy Agency |
| **LDD** | Least Demanding Day |
| **LH2** | Liquid Hydrogen |
| **LNG** | Liquiefied Natural Gas |
| **MDD** | Most Demanding Day |
| **MPH** | Miles Per Hour |
| **MXP** | Milan Malpensa Airport |
| **OECD** | Organisation of Economic Co-operation and Development |
| **OEW** | Operating Empty Weight |
| **PAX** | Passenger |
| **PEM** | Proton Exchange Membrane |
| **PV** | Photovoltaic |
| **PUN** | Prezzo Unico Nazionale (national single price) |
| **ST** | Storage Tank |
| **ZBO** | Zero Boil Off methods |

# Introduction

## Motivation

In 2019, the global aviation industry (including commercial, private, and military flights) emitted around 920 million metric tons of carbon dioxide ($CO_2$), which accounted for roughly 2.5% of all human-induced $CO_2$ emissions and approximately 12% of all transport-related emissions [1]. Moreover, the sector is experiencing a constant growth rate of 4.5-4.8% per year, with no signs of slowing down [2]. Apart from $CO_2$, which makes up approximately 70% of exhaust emissions, the combustion of conventional fuels also generates $NO_x$ emissions, harmful nitrogen-oxygen compounds that deplete the ozone layer and cause respiratory issues in humans, along with particulate matter [3]. The aviation industry acknowledges the imperative need for sustainable alternatives to fossil fuels. In particular, in aircraft, $CO_2$ should be reduced by 75% and $NO_x$ by 90% by 2050 compared to 2000 according to the Flightpath 2050 commitment [4]. One notable effort in this direction is the Carbon Offsetting and Reduction Scheme for International Aviation (CORSIA) initiative, launched by the International Civil Aviation Organization (ICAO) in 2016. The primary objective of CORSIA is to achieve carbon-neutral growth starting from 2020 levels (CNG2020). Considerations of fuel availability and environmental concerns place hydrogen in an excellent position to replace jet fuel when compared with other candidates [5]. Hydrogen combustion generates water as exhaust, thus eliminating $CO_2$ emissions and substantially mitigating the $NO_x$ and particulate emissions. As a result, it is regarded as the most promising option for achieving significant reductions in greenhouse gases (GHG) emissions.

Currently, hydrogen aircraft technology is advancing rapidly, e.g. Airbus plans to launch the first commercial hydrogen-powered aircraft by 2035 [6]. However, the success and deployment of hydrogen-powered aircraft are dependent on the development of ground infrastructure needed to support their operation.

The aim of this thesis is to analyze the technical and economic feasibility of a facility for the refueling of hydrogen-powered aircraft. Various technical and technological solutions will be considered, regarding hydrogen production from renewable sources, storage, and

distribution to refueling stations at airports selected for testing. Concrete and plausible results will be provided on the initial investment required by the airport and the ongoing costs of using such a facility, along with potential solutions to make this investment more sustainable.

## Mission

In the "Hydrogen-powered aviation" report by Clean Sky 2 [7], a detailed cost analysis of the main aviation sectors was conducted in order to determine which sectors would benefit the most from switching to hydrogen in a short time.

The report concluded that hydrogen propulsion is most suitable for commuter, regional, short range, and medium range aircraft. For commuter and regional aircraft, fuel cell propulsion powered by hydrogen is the most energy-efficient, climate-friendly, and economical option, with operating costs increasing by only $5 to $10 per PAX (passenger) (around 10%) compared to conventional aircraft. Entry into service is expected to occur within the next 10 to 15 years. For short-range aircraft, a hybrid propulsion approach utilizing both hydrogen combustion and fuel cells might be the most suitable option, but would result in a cost increase per PAX of 20-30%. In the medium-range aircraft segment, significantly longer fuselages for hydrogen storage would be required, resulting in a 25% increase in energy consumption compared to conventional aircraft, leading to a 30-40% cost increase per PAX. While hydrogen is technically feasible for long-range aircraft, it is less economically viable due to the increase in airframe length and energy requirements associated with hydrogen tanks, resulting in a cost increase per PAX of 40-50%.

If hydrogen-fueled aircraft are deployed in segments where they are the most cost-effective means of decarbonization, they could account for 40% of all aircraft by 2050, with the share increasing further after 2050. In this scenario, global aviation demand for hydrogen would amount to 10 million tons per year by 2040 and grow to 40 million tons per year by 2050, necessitating a significant increase in the hydrogen supply chain and airport refueling infrastructure.

Therefore, one of the main challenges lies in producing a quantity of hydrogen of this magnitude. Indeed, to ensure effective decarbonization of the sector, the entire hydrogen supply chain must be environmentally friendly, beginning with its generation. Different colors of hydrogen are identified based on the method of production and resulting emissions:

- Grey hydrogen is generated from fossil fuels, typically using the steam methane reforming (SMR) method. This method produces $CO_2$, which is eventually released into the atmosphere.

- Blue hydrogen is also derived from fossil fuels, but with the capture and storage of $CO_2$ underground through carbon sequestration, the production process is considered carbon neutral.
- Green hydrogen is produced through the electrolysis of water using renewable electricity. It is referred to as green because there are no $CO_2$ emissions during the production process. Water electrolysis involves using electricity to decompose water into hydrogen gas and oxygen.

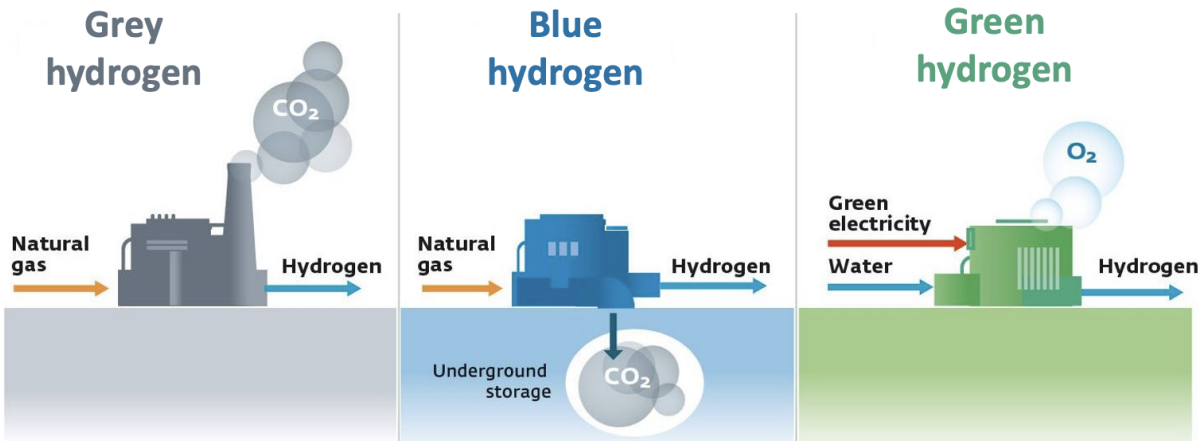


Figure 1: Depiction of grey, blue, and green hydrogen production

Although the electrolysis of water is an environmentally friendly method of hydrogen production, it is also highly energy-intensive, resulting in a significant increase in production costs. As a result, this poses a significant limitation to the widespread adoption of hydrogen as an innovative fuel. To tackle this issue, the U.S. Department of Energy has proposed its first energy EarthShot in 2021, aiming to reduce the cost of producing clean hydrogen. The primary objective is to achieve an 80% cost reduction, bringing down the cost to "$1 per 1 kilogram of hydrogen produced in 1 decade", with an intermediate target of $2/kg $H_2$ by 2025 [8]. Currently, projections estimate a higher cost of approximately $3-3.5/kg by 2040, making the production of hydrogen more costly than kerosene, which would cost $1.90 per kilogram of hydrogen in energy-equivalent cost. Nevertheless, in its International Energy Outlook 2019 [9], the U.S. Energy Information Administration predicts a potential increase in kerosene prices during the same period, making hydrogen an increasingly cost-effective option.

## State of the art

In recent years, research on hydrogen-powered aircraft has made significant progress, but the study of the necessary ground infrastructure to support flights using this innovative propulsion system still lags behind. Particularly, the refueling system, which serves as a bridge between the production process and the aircraft, is an aspect that is usually neglected [10]. However, ongoing projects are focused on exploring this crucial aspect for the widespread adoption of hydrogen aviation. Airbus, for example, is currently working on the development of a zero-emission aircraft, the Zero-E, which will be powered by hydrogen fuel cells. The company is also developing in parallel a hydrogen supply chain and infrastructure to support the operation of the Zero-E [11]. Recently, Airbus has revealed a preliminary concept of a hydrogen refueling station.

Smaller companies are also actively involved in research on hydrogen refueling systems. For instance, H2FLY, a German company that specializes in developing hydrogen fuel cell systems for aircraft, has announced the construction of a facility called the Center of Excellence for Hydrogen in Aviation at Stuttgart Airport. The facility, which is set to open in late 2024, will focus on the development and testing of hydrogen-electric propulsion systems for passenger planes. The testing stations will allow for the testing of systems up to 1 MW before the installation on an aircraft, as well as the evaluation of storage and refueling systems, and is expected to become the headquarters for companies and scientific institutes in this field [12, 13].

A noteworthy proposal comes from Universal Hydrogen, a company focused on decarbonizing air travel by offering comprehensive hydrogen transportation. One of their proposed solutions is the implementation of modular capsules for hydrogen transport and refueling. The concept is to use standardized containers that can be transported via trucks, trains, or ships to convey hydrogen from production facilities to refueling stations. These capsules would be designed to fit conventional cargo containers, enabling easy transportation using existing logistics infrastructure. At the refueling station, the modular capsules would be unloaded and connected to a dispensing system that transfers the hydrogen into the aircraft's tanks. However, it is important to note that this idea is currently only suitable for regional flights operated by small aircraft [14].

In other industries outside of aviation, hydrogen infrastructure has advanced significantly. Certainly, the most advanced infrastructures are those related to the automotive sector. Indeed, several hydrogen refueling stations are already operational worldwide, mainly located in California, Japan and Germany, needed to refuel the first fuel cell electric vehicles marketed by companies such as Toyota, Hyundai and Honda [15–17]. Rail transportation

is also seeing ambitious hydrogen-based projects, like the "H2iseO Hydrogen Valley" in Iseo, Lombardy, which aims to decarbonize public transportation services and promote a sustainable transportation system. The project includes constructing a blue hydrogen production plant at the Iseo station in the coming years to power a fleet of hydrogen trains serving the Val Camonica region. It is planned to increase production stations along the railway line, moving to fully green hydrogen production in the second phase of the project [18]. In the maritime transport sector, the Port of Valencia will be the first European port to use hydrogen in its operations under the European "H2Ports" project. The project involves the installation of a mobile hydrogen station to support the decarbonization of the port's supply chain [19]. In addition to transportation, hydrogen will be used in other sectors such as the steel industry, as demonstrated by the experimental green hydrogen production project at the Dalmine plant in Italy, which involves the use of a 20 MW electrolyzer to generate hydrogen for use in the steelmaking process instead of natural gas [20].

## Framework assumptions

Due to the complexity of hydrogen facilities and the various proposed solutions for implementing hydrogen on a large scale in aviation, it was necessary to narrow down the study to specific cases of particular interest. One of the key assumptions concerns the storage methodology used for the hydrogen, which can be stored in two ways: as pressurized gas or in liquid form. While storage in gaseous form may be suitable for shorter flights and is commercially available, this study focuses on liquid hydrogen (LH2) tanks because they require about half the volume and, as a result, are significantly lighter than hydrogen gas tanks. This is particularly crucial for short- and medium-haul flights, where several tons of hydrogen per flight need to be carried. However, it is worth noting that compared to kerosene, LH2 tanks are roughly four times larger so, to effectively integrate the tanks into the aircraft's fuselage, the airframe must be stretched, which will increase the aircraft's operating empty weight (OEW) [21].

Another important assumption, on the other hand, concerns the type of fueling station considered. There exists a variety of hydrogen production plants, but they can generally be classified into two main categories: those that provide hydrogen through steam-reforming methane, and those that produce hydrogen on-site through water electrolysis. Currently, the majority of operating stations utilize the former method. However, under the assumption of a transition toward more environmentally sustainable hydrogen production in the near future, this thesis will exclusively focus on the latter category of stations that produce hydrogen on-site through water electrolysis [22].

## Research framework: SIENA Project

The work expounded in this thesis is affiliated with the investigations conducted within the framework of the European project SIENA. SIENA (i.e. Scalability Investigation of hybrid-Electric concepts for Next generation Aircraft) is a EU funded project, coordinated by Collins aerospace, with the participation of Politecnico di Milano and is founded by the European Union as part of the Clean Sky 2 program [23].

The SIENA project aims to expedite the advancement of hybrid electric aircraft (A/C) technology for larger vehicles by identifying scalable technologies that can be utilized across various vehicle classes. Its primary goal is to conduct an in-depth investigation into different technology options within novel A/C architectures, considering their performance, operational efficiency, and economic impact, while also assessing their potential for scaling up across different categories. In this context, the methodology presented below would allow defining the impact of potential technologies on airport infrastructure and the complementary requirements during operation, which is a crucial step in determining the scalability of a technology.

## Structure of the work

This thesis work is divided in three main chapters, plus the introduction and conclusion. Each chapter covers as follows:

- **Chapter 1: AHRES methodology** – This chapter will provide a comprehensive overview of the developed methodology. Initially, it will introduce the plant under consideration and provide a detailed description of its components. Subsequently, it will outline the optimization problem and its mathematical formulation, with a thorough examination of each constraint. Finally, to ensure the efficacy of the methodology, the sanity of the code will be assessed by analyzing the outcomes of several test simulations.
- **Chapter 2: Application scenarios** – This chapter introduces the various scenarios of application of the ARES Methodology. This focuses on the aircraft models and reference airports included in the simulations, with an explanation of the selection of the specific days under investigation and the characteristics of the airports.
- **Chapter 3: Results** – Lastly, in this chapter, the outcomes of the executed simulations will be presented and evaluated critically. In order to determine the parameters that have the most significant impact on the final solution and their magnitude, off-design and sensitivity analyses will be conducted. Additionally, the hypothesis of on-site energy production will be assessed to reduce the magnitude of energy costs by decreasing the amount of energy purchased from the national power grid.

# 1 | AHRES methodology

In this chapter, the AHRES (Airport Hydrogen Refueling Equipment Sizing) methodology is presented in detail. This represents the approach used in this study that allows, by means of an optimization code, to determine the solution that requires the lowest plant cost, while still guaranteeing the performance given as input.

## 1.1. The airport facility

Before describing the methodology, it is necessary to go into a more detailed definition of the system considered throughout the study, focusing on the individual elements that compose it.

In order to achieve meaningful results with the current hardware and data at this stage of the study, it was essential to establish a simplified model of the system. Although this model may not be an exact representation of the actual system in the future, the advantage of the software design tool developed is its high level of flexibility. In fact, all parameters can be easily modulated, allowing for easy correction of results in case of updated estimates.

The considered airport facility consists of three main components. Firstly, the generator (GNR), comprising an electrolyzer, buffer tank, and liquefied, produces hydrogen by electrolyzing water using a significant amount of energy. The hydrogen gas is then cooled to cryogenic temperatures, turning it into a liquid form. Secondly, the storage tank (ST) stores the hydrogen produced in advance, e.g., during a time slot when the cost of energy is lower. Lastly, the dispensing units (DU) are responsible for transferring fuel from the ground tank to the aircraft tanks.

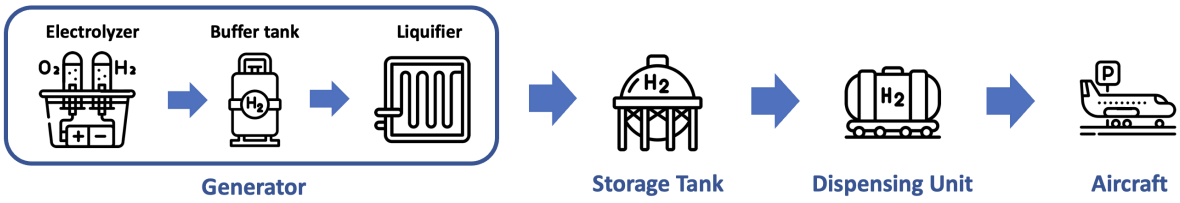


Figure 1.1: Airport facility model considered

### 1.1.1. Generator

Among the many methods of hydrogen production, the most environmentally friendly one that yields highly pure hydrogen is the electrolysis of water [24]. Water electrolysis is the process whereby water is split into hydrogen and oxygen through the application of electrical energy, as in Equation (1.6).

Typically, a water electrolysis unit consists of an anode and a cathode separated by an electrolyte, and a power supply. The electrolyte can be made of an aqueous solution containing ions, a proton exchange membrane (PEM), or an oxygen ion exchange ceramic membrane. A direct current (DC) is applied from the negative terminal of the DC source to the cathode (seat of the reduction reaction), where the hydrogen is produced. At the anode, the electrons produced by the electrochemical reaction return to the positive terminal of the DC source.

For the case of water electrolysis in an aqueous acid electrolyte, the processes that occur at the anode and the cathode are described, respectively, by Equations (1.1) and (1.2):

$$\mathrm{H_2O} \rightarrow \frac{1}{2}\mathrm{O_2} + 2\mathrm{H^+} + 2e^- \qquad \mathrm{E^0_{H_2O/O_2}} = 1.23\ \mathrm{V} \tag{1.1}$$

$$2\mathrm{H^+} + 2e^- \rightarrow \mathrm{H_2} \qquad \mathrm{E^0_{H^+/H_2}} = 0.00\ \mathrm{V} \tag{1.2}$$

The half-reactions occurring on the cathode and anode respectively can be written as:

$$2\mathrm{H_2O} + 2e^- \rightarrow \mathrm{H_2} + 2\mathrm{OH^-} \qquad \mathrm{E^0_{H_2O/H_2}} = -0.83\ \mathrm{V/ENH} \tag{1.3}$$

$$2\mathrm{OH^-} \rightarrow \frac{1}{2}\mathrm{O_2} + \mathrm{H_2O} + 2e^- \qquad \mathrm{E^0_{OH^-/O_2}} = 0.4\ \mathrm{V} \tag{1.4}$$

The global reaction is:

$$\mathrm{H_2O} \rightarrow 2\mathrm{H_2} + \frac{1}{2}\mathrm{O_2} \qquad \Delta\mathrm{E^0} = \mathrm{E^0_{H_2O/H_2}} - \mathrm{E^0_{OH^-/O_2}} = -1.23\ \mathrm{V} \tag{1.5}$$

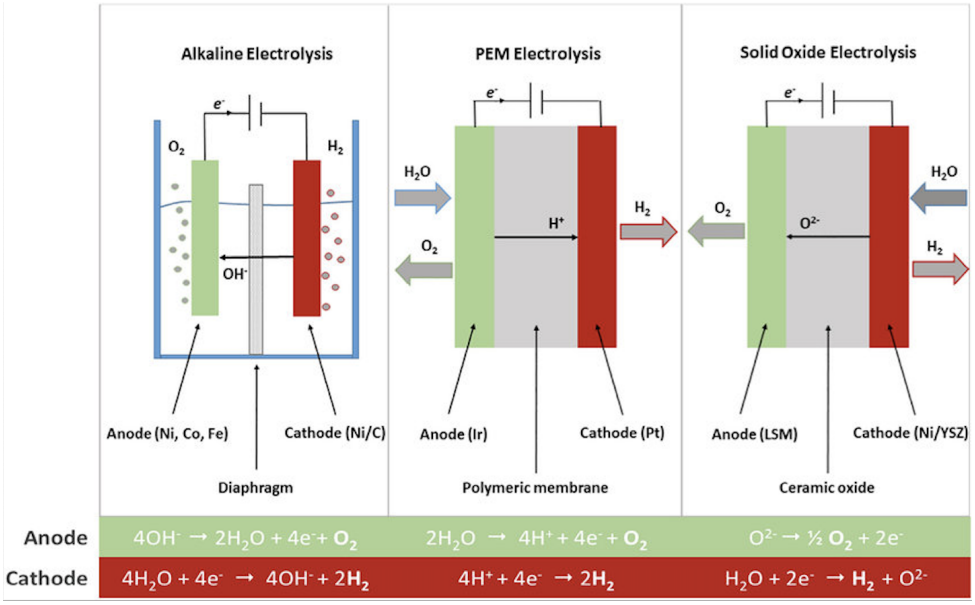


Figure 1.2: Operation principles of alkaline, PEM and solid oxide water electrolysis

Electrolysis of water is not a spontaneous phenomenon because the standard global reaction potential is negative [25]. Therefore, it needs an external intervention (power source) and the global reaction can be written as:

$$\mathrm{H_2O} + \mathit{electricity} \rightarrow \mathrm{H_2} + \frac{1}{2}\mathrm{O_2} \tag{1.6}$$

Once gaseous hydrogen is produced by this method, it requires liquefaction so as to greatly increase its density and thus store and transport it more easily [26], to do this it is necessary to cool the gas at a temperature below -253°C, and keep it below this limit to prevent it from re-evaporating. A buffer tank is located between the electrolyzer and the compressor, in order to regulate the hydrogen flow between the two elements, since in most cases the electrolyzer is going to have a different flow rate than the compressor [27].

Both production and liquefaction processes require considerable consumption of energy, in fact, currently, the production of one kilogram of hydrogen requires about 50 kWh [28], and its liquefaction between 10-12 kWh [29], and this represents one of the main limitations for the production and therefore the use of hydrogen on a large scale [30].

Typically, a plant like this does not require continuous operation. Nonetheless, it may be advantageous not to shut down the generator entirely during periods when hydrogen production is unnecessary. This is because frequent restarts can hasten the plant's

deterioration, and long restart times can limit the flexibility to adjust to changes in hydrogen demand. Hence, maintaining a constant minimum production level that keeps the plant operational at all times would be more advantageous.

Since the developed code bases the optimization on the cost of the system, for the solution it is necessary to estimate the cost of supplying the generator, this value is not certain since to date there is no electrolyzer of this size, but the cost was estimated as a function of the needed daily production. In [30], the cost of the generator per kilogram of hydrogen produced daily is 1 250 €/(kg/d). To this the operating and maintenance costs must be added, estimated at 10% of the capital cost per year, over the first ten years of the system.

### 1.1.2. Storage Tank

To ensure a reliable hydrogen supply and meet variations in hydrogen demand, a storage system is required between the central production plant and refueling stations. Cryogenic tanks are probably the plant elements with the highest level of technological readiness, with several suppliers offering solutions for different volumes. The spacecraft industry boasts the largest existing cryogenic tanks in the world, including NASA's 3 800 $m^3$ tank in Florida, USA, which can store 270 tons of liquid hydrogen [31], and JAXA's 540 $m^3$ tank in Japan, with a capacity of 38 tons [32]. In the future, liquid hydrogen storage tanks could be up to 13 times larger than the NASA tank, with a maximum capacity of 3 500 tons of hydrogen, according to a report by CleanTech [33].

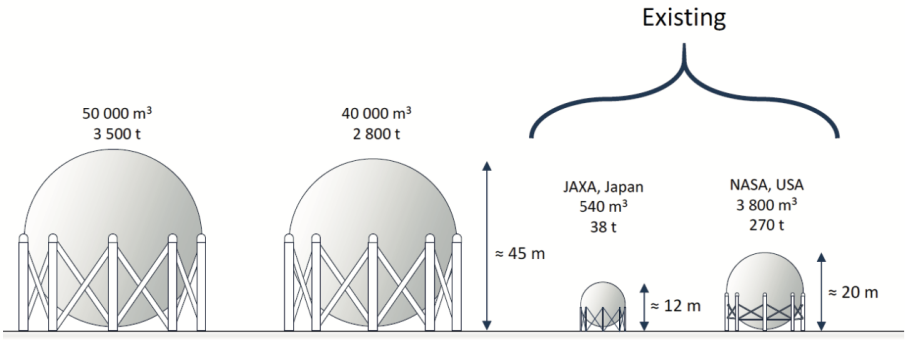


Figure 1.3: Current Liquid Hydrogen Storage

As mentioned in the previous section, it is necessary to keep the liquid hydrogen at a temperature of -253°C to prevent it from evaporating, so it is mandatory for the ground tank to provide very effective insulation from the external environment. The three main possibilities to achieve the required level of insulation are presented here [34]:

- Vacuum-insulated, double-wall tanks with perlite in the annulus. This tank con-

figuration consists of a cold inner liquid container, typically in austenitic stainless steel, because of its resistance to hydrogen embrittlement as well as its weldability and formability, a warm outer vessel, that can be in ordinary carbon steel, and an evacuated annulus which is filled with a powder insulation, typically perlite;

- Vacuum-insulated, double-wall tanks with multilayer insulation. This configuration is the same as for the powder insulation except that the powder is replaced by alternate layers of low emissivity metal foil (usually aluminum) and a thin, low conductance spacer (usually glass fiber paper);
- Single-wall, external foam insulation. This configuration has the advantage, by eliminating the outer casing, of reducing complexity and cost of the structure. This simplification, however, makes it more difficult to achieve a high level of thermal performance. One method of achieving good insulation, as used for the storage of liquified natural gas (LNG), is to bury the tank in the ground and take advantage of the insulating effect of the frozen soil surrounding the tank. However, this solution would be impractical in most cases and inefficient for liquid hydrogen due to the extremely low storage temperature.

In any case, it is preferable to use a spherical shape for cryogenic tanks, because this allows for the same tank volume, the smallest surface area through which heat exchange with the outside occurs.

The substantial temperature gradient between the liquid hydrogen stored in a tank and its surroundings inevitably results in a heat flux into the tank, that causes the liquid hydrogen to evaporate. The evaporated hydrogen is termed boil-off gas (BOG) [35] and its generation leads to a rise in pressure in the storage tank. In order to avoid structural failure due to excessive pressure, a vent must be installed in the tank to release the pressure, which unfortunately results in the loss of a fraction of hydrogen [36]. The entity of the BOG generation depends on various factors, such as the insulation quality and the tank's surface-to-volume ratio. In this study, it is approximated on the order of 1% of the maximum mass stored per day [34, 36, 37]. This value would be somewhat overestimated considering only the tank, but the boil-off phenomenon, and consequently the associated hydrogen loss, occurs along the entire hydrogen pathway [38], particularly during refueling [39], so using this estimate, all losses are concentrated in one element of the system, in order to have a leaner model. Since boil-off would represent the most significant form of hydrogen loss, especially for future large-scale storage and transport applications [38], many numerical models have been developed [40]. This development has led, among other things, to the so-called zero-boil-off methods (ZBO), in which hydrogen gas is re-liquefied,

thus completely preventing boil-off [41]. However, in this thesis, the phenomenon will not be explored further.

New insulation technologies are currently being investigated, for example, the NASA Cryogenics Test Laboratory at Kennedy Space Center has developed a new material, K1 glass bubbles, that would guarantee a significant reduction in boil-off in future cryogenic vessels [42], however, more traditional insulation with perlite will be considered from now on.

The storage of cryogenic fluids entails a crucial factor related to the reservoir's filling level. It is necessary to ensure that the tank does not exceed 80% of its capacity, since gas expansion may cause an excessive pressure buildup [43]. Moreover, to maintain temperature stability in the tank, it is essential to have a minimum quantity of fluid in storage [44], which is set at 5% of the maximum storable mass.

The cost of storage is still unclear. In fact, consulting several sources, the cost estimate is extremely variable, even depending on the technology used for the tank, and in general, the cost of storing one kilogram of hydrogen decreases significantly as the size of the tank increases, as can be seen in the Table 1.1 obtained from [37].

Table 1.1: Liquid Hydrogen Tanks Costs

| **Size [kg]** | **Cost [€]** | **Cost/kg [€/kg]** |
|---|---|---|
| 0.089 – 8.9 | n/a | €455 – €645 |
| 8.9 – 890 | n/a | €20 – €34 |
| 270 | €110 000 | €415 |
| 300 000 | €5 000 000 | €17 |

An average storage value of 200 €/kg was chosen to be used, however, this value will decrease significantly in the near future [33]. Again, operation and maintenance costs, estimated at 10% of the capital cost per year, were added for the first ten years of the system's life.

### 1.1.3. Dispensing Unit

At this point, it is necessary to assume in the considered airport the presence of a hydrogen distribution system that connects the storage tank to the various refueling stations and

allows all necessary refueling when needed. In particular, there are two types of systems, not unlike those used in current airports for kerosene distribution:

- distribution by pipeline;
- distribution by tanker trucks.

The cost of supplying the two systems varies considerably, mainly because the pipeline would require specialized pipes that could provide adequate cryogenic insulation [45]. Alternatively, a distribution system using cryogenic trucks, although requiring a significant initial investment by the airport, presents a more adaptable approach that uses more established and consequently less expensive technologies, leading to greater efficiency, especially in the short term, as in the scenario being analyzed [46]. Consequently, the latter distribution method is the chosen option.

Each liquid hydrogen truck consists of a truck cab and a large single liquid hydrogen tank mounted on a trailer (see Figure 1.4). The capital cost of the individual truck is about €800 000 [47].


Figure 1.4: PRAXAIR liquid hydrogen truck

However, the cost of the truck is only one cost item of the entire refueling station, which will be much more complex and expensive. In fact, there is also a necessity for ground static hydrogen storage, a system to aspirate the boil-off gas that is generated during refueling, ground equipment and utility fluids needed for refueling operations, and infrastructure to ensure safety. In late 2022 Airbus and ArianeGroup, a joint venture equally owned by Airbus and Safran, and a world leader in space propulsion technologies, announced that they will work together to build the first liquid hydrogen refueling facility for ZEROe aircraft (a zero emission concept aircraft from Airbus) at Toulouse-Blagnac airport [48].

The station will be operational in 2025. At the announcement, the first rendering of the station was also released in which all the elements mentioned above are visible (Figure 1.5). In [30] the total cost for the entire refueling station is estimated at about €3 200 000. For each dispensing unit, operation and maintenance costs were considered, estimated at 10% of capital cost per year for the first ten years of the system's life.

Figure 1.5: Liquid hydrogen refueling station for ZEROe aircraft

Following the arrival of the hydrogen tanker truck at the refueling station, a sufficiently powerful pump is required for refueling the aircraft. For the transfer of cryogenic liquids with high flow rates, centrifugal turbopumps turn out to be the ideal pumps. In order to estimate the flow rate required by the hydrogen dispensing units, the mass flow rate was assumed to be the same as that of pumps used today to refuel conventional kerosene aircraft. Currently, pumps of 300 GPM (Gallons Per Minute) are used to refuel most civilian aircraft [49], especially for the short- and medium-haul flights that will be considered later, which in the case of kerosene results in about 830 kg/min. This same value will also be assumed for liquid hydrogen refueling, which means about 11 667 L/min. When analyzing bigger aircraft or longer flights, it may be necessary to consider pumps with higher flow rates or to refuel a single aircraft with two dispensing units, to avoid having excessively long refueling times. However, in the cases that will be analyzed below, a 300 GPM pump always guarantees acceptable refueling times.

It is possible to estimate the power absorbed by the dispensing unit during refueling. Considering a centrifugal cryogenic pump, the absorbed power (P) can be calculated with the Formula (1.7):

$$\mathrm{P} = \frac{\mathrm{Q}\,\rho\,g\,\mathrm{H}}{\eta} \tag{1.7}$$

where:

- Q is the volumetric flow of fluid through the pump which in this case is equal to 0.21 $m^3$/s;
- $\rho$ is the density of the fluid being pumped, in this case, 70.99 kg/$m^3$;
- $g$ is the gravity (9.81 kg/$m^3$);
- H is the head produced by the pump, computed by the Formula (1.8):

$$\mathrm{H} = \Delta h + \frac{\Delta \mathrm{P}}{\rho\,g} + \frac{{v_{fin}}^2 - {v_{in}}^2}{2g} \tag{1.8}$$

  Here, $\Delta h$ is the height above the ground of the tank in an average aircraft, approximated to 5 m, $\Delta P$ is the pressure difference we have between the aircraft tank (125 000 Pa [50]) and the ground tank (103 400 Pa [50]), so it is equal to 21 600 Pa. Finally, the third term will be zero since the fluid is at rest in both the ground tank and the aircraft tank ($v_{in} = v_{fin} = 0$).

  So the value of H in our case will be equal to 38 m;

- $\eta$ is the pump efficiency which in the case of the centrifugal pump is around 0.75 [51].

By substituting all values in (1.7), the power consumed by the pump turns out to be about 7 500 W.

This study did not consider pump head pressure losses, which are energy losses due to frictional resistance when pumping fluid through a pipeline [52] and must be added to the pump head H calculated above [53]. This is because accurate estimation requires specific data on the pipes, which were unavailable at the time of the study (April 2023). Furthermore, in tanker truck distribution, the pipeline length is typically short, making pressure losses less significant as they increase with length. However, for a piped distribution system in the future, these losses may become more important and will require further analysis.

Moreover, the dispensing hose serves another crucial function of aspirating the boil-off gas generated in the aircraft tank, which is greater in the aircraft tank than that generated in the ground tank due to the lower insulating capacity that can be guaranteed onboard the aircraft. Therefore, once refueling is concluded, it is necessary for the hose to still remain connected to the aircraft until just before takeoff to avoid excessive pressure buildup in the tank.

## 1.2. Preliminary definition

Since the problem involves a large number of variables and parameters, it is treated as an optimization problem. An objective function, in this specific case, the daily cost of the system, is defined and the aim is to determine the solution that will minimize this function while satisfying all relevant constraints presented in Section 1.5. This is applied to a given time frame for which a detailed flight schedule is known. The solution is provided as optimal values of the hydrogen generator production capacity, the size of the ground storage tank, the number of necessary dispensing units, the maximum power absorbed by the system, and the detailed time scheduling of the refueling process.

In seeking the minimum of the cost function $J$ as a function of an array of optimization variables $\mathbf{x}$, the dynamics of the refueling operations are integrated over a time duration $L$, subdivided into a number of slots of length $l_t$, providing a discrete time grid for the problem. The set of all time slots is denoted by $T$ and each time slot is identified by the index $t \in T$. Therefore, $L = \Sigma_{t \in T} l_t$. The set of all aircraft is denoted by $I$ and each aircraft is identified by the index $i \in I$.

The hydrogen demand over time is defined by the flight scheduling at the considered airport. The amount of fuel required by the aircraft depends on its model and thus on the specific fuel consumption but more importantly, on the distance of the flight the aircraft has to travel. Furthermore, it is conservatively assumed that the state of filling of aircraft tanks before each flight is equal to the minimum allowable value.

The cost function and constraint equations will be described in detail in the following.

## 1.3. Cost function

From the standpoint of an airport operator, the goal is to grant an assigned operational capability, to satisfy a given flight schedule, while minimizing procurement and operational costs. Therefore, the cost function $J$ is defined as the sum of all involved costs over the

time duration $L$ as

$$J = C^e + C^p + C^{\mathrm{GNR}} + C^{\mathrm{ST}} + C^{\mathrm{DU}}; \tag{1.9}$$

where $C^e$ represents the cost of the electric energy purchased from the grid, $C^p$ the cost of the corresponding peak power, and $C^{\mathrm{GNR}}$, $C^{\mathrm{ST}}$ and $C^{\mathrm{DU}}$ are the depreciation cost of the generator, storage tank, and dispensing units, respectively. Each cost component in Equation (1.9) is discussed below.

The cost of the energy supply $C^e$ is bound to the energy amount $E_t$ purchased from the grid in the time slot $t$ and to the corresponding monetary value per energy unit $\lambda_t$. In particular, the latter parameter is highly variable depending on the historical time in which the analysis is carried out and the national energy market of the airport considered, so this topic will be discussed in more detail in Section 1.4.

Due to the very low frequencies in the evolution of both quantities as functions of time (compared to a daytime scale), providing definitions in discrete time is more typical to this type of problem [54]. Therefore, it is possible to write

$$C^e = \sum_{t \in T} \lambda_t E_t; \tag{1.10}$$

where the value of $E_t$ represents the energy acquired in the current time slot $t$, this can be estimated by the following formula [54]:

$$E_t = \dot{m}_t^{\mathrm{GNR}} c_e^{\mathrm{GNR}} l_t + c_p^{\mathrm{DU}} \left( \sum_{i \in I} t_{i,t}^{ref} \right); \tag{1.11}$$

where $\dot{m}_t^{\mathrm{GNR}}$ is the hourly hydrogen production in the time slot $t$, $c_e^{\mathrm{GNR}}$ is the energy required by the generator to produce one $kg$ of hydrogen, $c_p^{\mathrm{DU}}$ is the power absorbed by each dispensing unit and $t_{i,t}^{ref}$ is the refueling time required for the $i$-th aircraft in timestep $t$ for which the dispensing unit is then in operation.

The cost of peak power can be expressed as

$$C^p = \max_{t \in T} \left( \frac{E_t}{l_t} \right) c_p \frac{d}{30}; \tag{1.12}$$

where the ratio $E_t/l_t$ represents required power in the time slot $t$, while $c_p$ represents the cost per unit peak-power per month, and $d$ the number of days in the considered analysis. This is simply the time duration expressed in days, so that $d = L/1440$, when $L$ is given in minutes.

The procurement cost of the generator can be written as

$$C^{\mathrm{GNR}} = \dot{m}^{\mathrm{GNR}}_{daily} c^{\mathrm{GNR}} \left( \frac{d}{d^{\mathrm{GNR}}} \right); \tag{1.13}$$

where $\dot{m}^{\mathrm{GNR}}_{daily}$ is the daily hydrogen production of the generator, $c^{\mathrm{GNR}}$ is the procurement cost per unit of daily production for the generator and $d^{\mathrm{GNR}}$ is the expected lifespan of the device measured in days.

The procurement cost of the storage tank can be written as

$$C^{\mathrm{ST}} = m^{\mathrm{ST}}_{max} c^{\mathrm{ST}} \left( \frac{d}{d^{\mathrm{ST}}} \right); \tag{1.14}$$

where $m^{\mathrm{ST}}_{max}$ is the maximum mass of hydrogen stored in the tank throughout the day, $c^{\mathrm{ST}}$ is the cost of the tank per kilogram of stored hydrogen, and $d^{\mathrm{ST}}$ is the expected lifespan of the device, measured in days.

Whereas, the procurement cost of the dispensing unit can be written as

$$C^{\mathrm{DU}} = \left( N^{\mathrm{DU}} + N^{\mathrm{DU}}_{extra} \right) c^{\mathrm{DU}} \left( \frac{d}{d^{\mathrm{DU}}} \right); \tag{1.15}$$

The number of dispensing units required for the system is denoted by $N^{\mathrm{DU}}$. Additionally, $N^{\mathrm{DU}}_{extra}$ reserve dispensing units are added to this number, with one extra unit for every five units needed. These reserves are used in case of malfunction or maintenance of one of the dispensing units. The parameters $c^{\mathrm{DU}}$ and $d^{\mathrm{DU}}$ represent the procurement cost and expected lifespan in days of each dispensing unit, respectively.

## 1.4. Electricity pricing

The energy cost certainly represents the dominant cost of the whole system, so the results that will be obtained will be particularly sensitive to variations in the parameter $\lambda_t$. However, the energy market is extremely variable even in the short term, and it is impossible to define an unambiguous value for this parameter that can be valid all the time. It is necessary to define an average value by analyzing energy price trends. Specifically in this thesis, reference will be made to the Italian energy market.

The most important parameter to be analyzed for energy cost estimation is the PUN (Italian acronym for Prezzo Unico Nazionale, "National Single Price"), which is the wholesale reference price of electricity purchased on the "Borsa Elettrica Italiana" market

(IPEX - Italian Power Exchange). At the Italian Power Exchange, the transactions between producers and suppliers of electricity are regulated. The PUN, therefore, represents the national weighted average of the zonal sales prices of electricity for each hour and for each day [55].

The Figure 1.6 shows the average Italian PUN values from 2017 to the end of 2022 obtained from [56]. Excluding the last year, it can be seen that the value is around 60 €/MWh. For greater generality of the results that will be obtained from the simulations, the energy cost data that will be used later will refer to the period prior to 2022, also in consideration that the forecasts for the next few years are optimistic and see a decline in the energy price by 2025, with the PUN settling back to values close to those that were in place before the energy crisis of recent months [57].

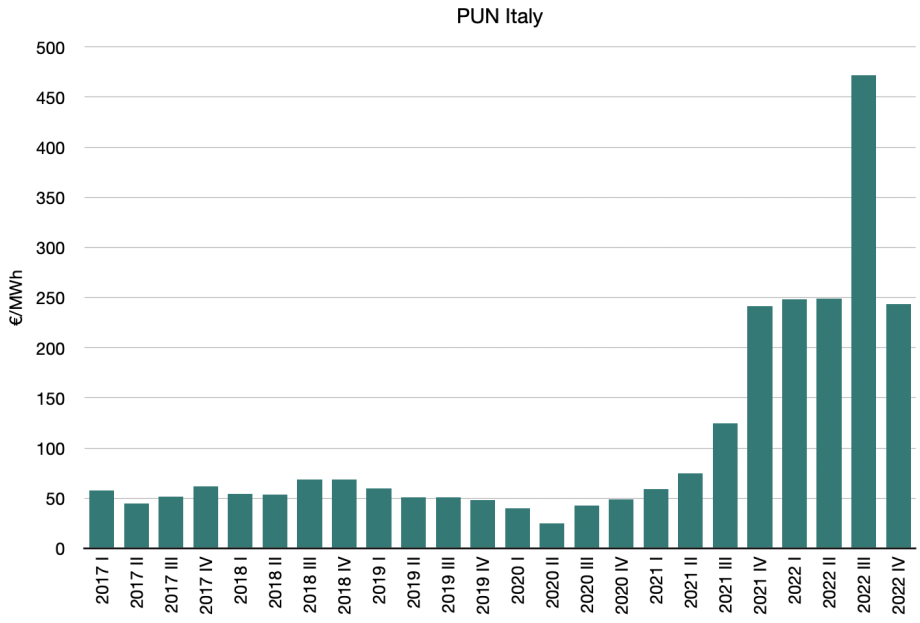


Figure 1.6: Italian PUN trend over the last 6 years

It is possible to have two types of energy pricing:

- In the simple tariff, the consumer pays electricity at the same price for all hours of the day.
- In the bi-hourly tariff, the consumer pays electricity at two different prices for two corresponding hourly consumption periods. Considering a midweek day, the two cost bands are:
  - F1: 8 am to 7 pm, higher cost interval;

– F23: 7 pm to 8 am, lower cost interval.

The final cost of selling energy in the various tariffs is in direct relation to the value of the PUN, which is increased with the addition of some fees. The price that will be used in the study (in Table 1.2), refers to the first quarter of 2021. The data were obtained from the official website of ARERA (Autorità di Regolazione per Energia Reti e Ambiente), the Italian regulator of electricity, gas and water markets.

Table 1.2: Electricity price

| Simple tariff [€/kWh] | Bi-hourly [€/kWh] | |
|---|---|---|
| | F1 | F23 |
| 0.05657 | 0.06662 | 0.05336 |

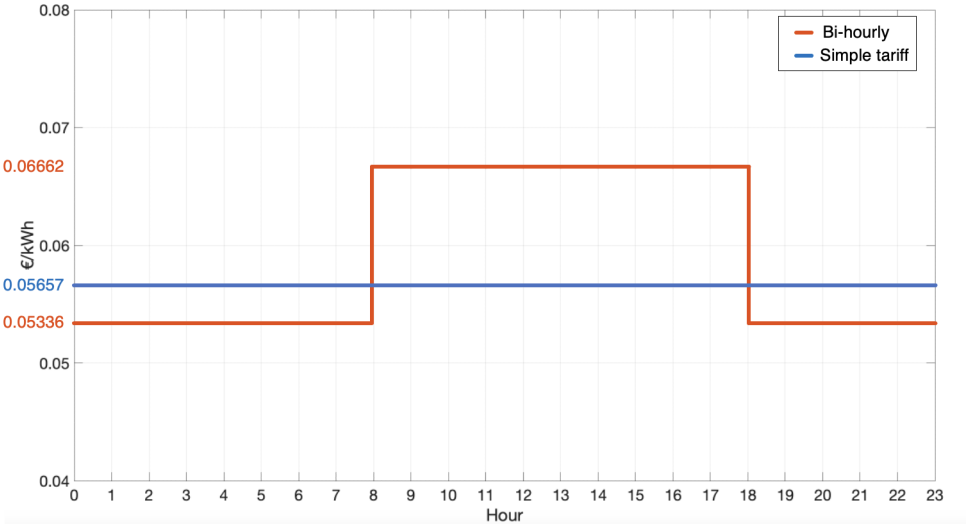


Figure 1.7: Electricity price during the day

Another cost related to the price of energy that will be significant in the case of the system considered, is the amount to be paid in proportion to the committed power, even in the absence of energy consumption. This parameter, denoted in this thesis by $c_p$, assumes a value of approximately 30 €/(kW·year) in the case of non-household users [58].

In this study, reference will also be made to non-Italian airports, particularly Athens International Airport and Paris Charles de Gaulle Airport. By analyzing the trend of energy purchase prices in France and Greece, it is observed that these are very similar to

the Italian ones (as shown in Figure 1.8). Therefore, the same energy prices will be kept for all cases analyzed.

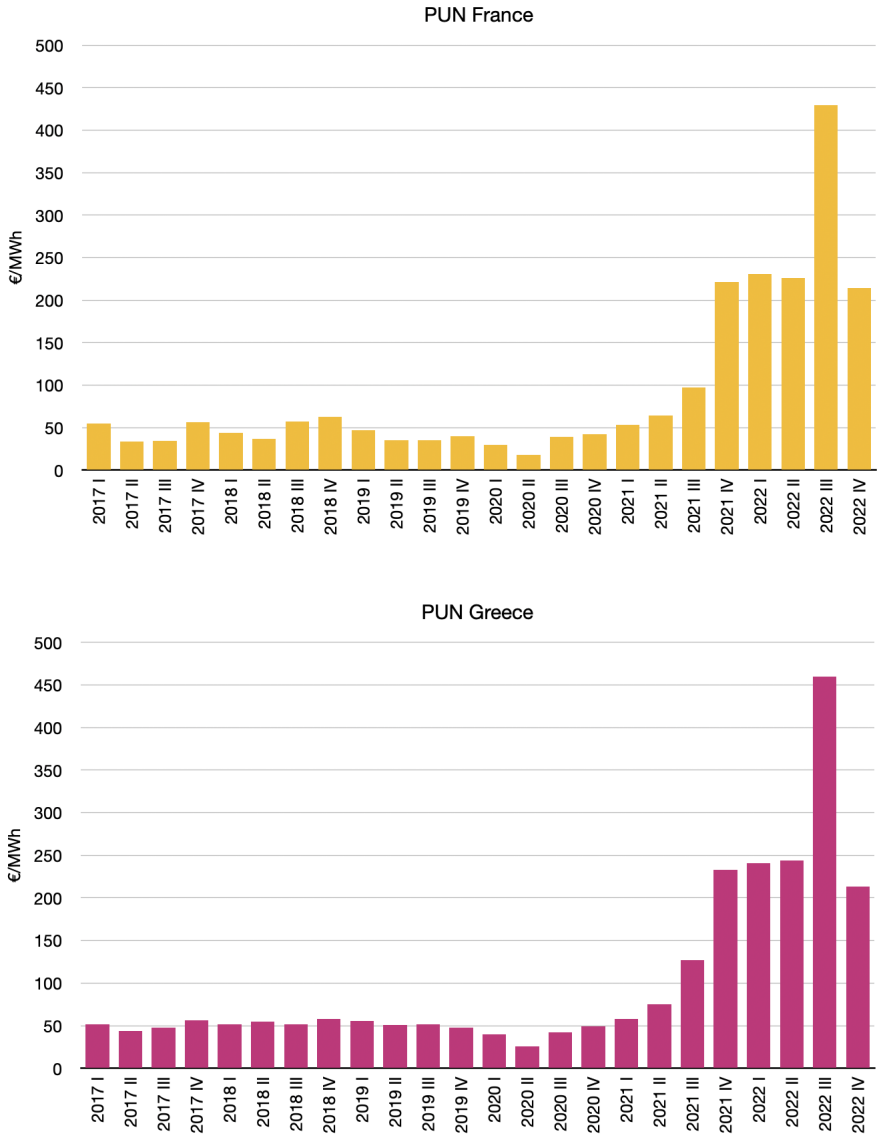


Figure 1.8: French and Greek PUN trend over the last 6 years

## 1.5. Constraints

The parameters influencing the components of the cost function need to satisfy an array of constraints, which reflect both technological limits and models of the refueling processes. As seen in the following, these constraints can be formalized mathematically as a set of 14 relations: 4 equations and 10 inequalities.

### 1.5.1. Filling of aircraft tanks

The mass of hydrogen stored in the tank of the $i$-th aircraft at time index $t$ should always range between a maximum $m^a_{max,i}$, calculated as the amount of fuel required for the specific aircraft model to travel its maximum range plus a 10% safety reserve, and a minimum $m^a_{min,i}$ equal to the 10% safety reserve mentioned before.

This is expressed by:

$$m^a_{min,i} \leq m^a_{end,i,t} \leq m^a_{max,i}. \tag{1.16}$$

### 1.5.2. Filling of the storage tank

At any given time $t$, the hydrogen mass stored in the ground storage tank should always be maintained within the limits of a minimum mass $m^{\text{ST}}_{min}$ and a maximum mass $m^{\text{ST}}_{max}$. The minimum mass, which is set at 5% of the maximum amount of hydrogen stored, ensures that the tank never becomes completely empty and temperature stability is maintained. The maximum mass, on the other hand, is equal to the maximum amount of hydrogen that the tank should be able to store.

This is expressed by:

$$m^{\text{ST}}_{min} \leq m^{\text{ST}}_{end,t} \leq m^{\text{ST}}_{max}. \tag{1.17}$$

### 1.5.3. Requested fuel

The fuel required by the $i$-th aircraft at time $t$ can be computed by the following formula:

$$m^a_{req,i,t} = y^{leave}_{i,t} m^a_{fuel,i}; \tag{1.18}$$

where the variables $y^{leave}_{i,t}$ can assume only 2 values:

$$y^{leave}_{i,t} = \begin{cases} 1, & \text{if aircraft } i \text{ leaves the airport at time } t, \\ 0, & \text{otherwise;} \end{cases} \tag{1.19}$$

while $m^a_{fuel,i}$ is the amount of hydrogen required by the $i$-th aircraft to travel the distance of its mission. This value is computed based on consumption estimates, which will be detailed for each aircraft model in Section 2.1, and evaluated for the mission's length using a second-degree interpolation.

### 1.5.4. Full tanks before take off

Obviously, each aircraft must have the required amount of fuel ($m^a_{req,i,t}$) before take off. Hence, the following equation is needed:

$$m^a_{start,i,t} \geq m^a_{req,i,t}. \tag{1.20}$$

### 1.5.5. Aircraft availability for refueling

Since the aircraft cannot be refueled during the mission, it is necessary to introduce two variables, $y^{ref}_{i,t}$ and $y^{out}_{i,t}$:

$$y^{ref}_{i,t} = \begin{cases} 1, & \text{if aircraft } i \text{ is being refueled at time } t, \\ 0, & \text{otherwise;} \end{cases} \tag{1.21}$$

$$y^{out}_{i,t} = \begin{cases} 1, & \text{if aircraft } i \text{ is out of the airport at time } t, \\ 0, & \text{otherwise;} \end{cases}. \tag{1.22}$$

The constraint is satisfied if the following condition is valid:

$$y^{ref}_{i,t} \leq 1 - y^{out}_{i,t}. \tag{1.23}$$

The simulations below assumed that all aircraft were available for refueling only 30 minutes before takeoff, in order to simulate the actual operation of a civil airport that also accommodates low-cost airlines with very dense flight schedules and minimal turnaround times.

### 1.5.6. Coupling of aircraft to dispensing unit

After the aircraft tank is refueled, it is crucial for the dispensing unit to remain connected to it, as its primary function is to aspirate the boil-off gas and maintain the pressure within the tank below the limit. Consequently, a new variable is introduced:

$$y^{coup}_{i,t} = \begin{cases} 1, & \text{if aircraft } i \text{ is coupled to a dispensing unit at time } t, \\ 0, & \text{otherwise.} \end{cases} \tag{1.24}$$

It must satisfy the following equation:

$$y_{i,t}^{coup} = \min\left(1, \left(m_{start,i,t}^{a} - m_{min,i}^{a}\right)\right) - y_{i,t}^{leave}. \tag{1.25}$$

Thus, coupling occurs if the tank is full ($m_{start,i,t}^{a}$-$m_{min,i}^{a} > 1$) and the aircraft will not leave the airport in the timestep $t$ ($y_{i,t}^{leave} = 0$)

### 1.5.7. Update of aircraft tank mass

In each time step, we need to update the mass stored in the tank of the $i$-th aircraft, which at the end of the time step $t$ will be:

$$m_{end,i,t}^{a} = m_{start,i,t}^{a} + t_{i,t}^{ref}\dot{m}^{\mathrm{DU}} - \left(y_{i,t}^{coup} m_{\mathrm{BO},i}^{a}\right) - y_{i,t}^{leave}\left(m_{start,i,t}^{a} - m_{min,i}^{a}\right). \tag{1.26}$$

Hence, to the initial mass we add the mass coming in from the dispensing units (if the aircraft is being refueled, and thus $t_{i,t}^{ref} \neq 0$) and subtract the mass lost due to boil-off, which occurs only when the aircraft is connected to the dispensing units ($y_{i,t}^{coup}$=1) and, in case the aircraft takes off, we assume that the tank empties instantaneously returning to the minimum value since what happens in flight is not influential for the purpose of this study.

As stated earlier, the estimated amount of boil-off in the aircraft tank is greater compared to that of the ground tank. This is mainly due to the assumption that the aircraft tank has less efficient insulation, which results in higher heat entering the tank. This is necessary to avoid excessive weight. Therefore, a boil-off value per hour of 3% of the maximum storable mass was considered for each aircraft model.

### 1.5.8. Refueling continuity

It is necessary for refueling to continue until the mass in the tank is sufficient. This condition can be expressed by the following inequation:

$$y_{i,t}^{ref} \geq y_{i,t-1}^{ref} - floor\left(\frac{m_{start,i,t}^{a}}{m_{next,i,t}^{a}}\right). \tag{1.27}$$

Then the second term of the right-hand side will be null until the mass in the tank has reached the amount of hydrogen required in the following take-off ($m_{next,i,t}^{a}$), at which point it will take on a value of 1 so the refueling can be terminated.

### 1.5.9. Minimum generator flow

The generator probably does not have to operate continuously during the day, especially when considering bi-hourly electricity pricing. In fact, in this case, to reduce energy costs, the plant will produce most of the hydrogen needed during off-rate hours. However, it is not recommended to shut down the plant completely when production is not needed, both because this would damage the plant in the long run and because restarting would incur higher costs than maintaining a constant minimum production, so a minimum production flow ($\dot{m}_{min}^{\mathrm{GNR}}$) of 2.5% of maximum hourly production is imposed.

$$\dot{m}_t^{\mathrm{GNR}} \geq \dot{m}_{min}^{\mathrm{GNR}}. \tag{1.28}$$

### 1.5.10. Update of storage tank mass

In each time step, we need to update the mass stored in the storage tank, which at the end of the time step $t$ will be:

$$m_{end,t}^{\mathrm{ST}} = m_{start,t}^{\mathrm{ST}} + \dot{m}_t^{\mathrm{GNR}} l_t - \left( \sum_{i \in I} t_{i,t}^{ref} \right) \dot{m}^{\mathrm{DU}} - m_{\mathrm{BO},t}^{\mathrm{ST}}. \tag{1.29}$$

Therefore, mass entering from the generator is added to the initial mass, while mass lost due to boil-off and mass delivered to aircraft by the active dispensing units in timestep $t$ is subtracted.

### 1.5.11. Maximum requested power

The maximum available power must also meet the system's demand at all times, even when this is the maximum.

$$P_{max} \geq \max \left( \dot{m}_t^{\mathrm{GNR}} c_e^{\mathrm{GNR}} + c_p^{\mathrm{DU}} \left( \sum_{i \in I} y_{i,t}^{ref} \right) \right). \tag{1.30}$$

On the right-hand side, the first term represents the power absorbed by the generator, the second term represents the power absorbed by the dispensing units working in the time interval $t$.

### 1.5.12. Necessary dispensing units

The number of dispensing units must meet the plant's demand at all times, even at the timestep of maximum use. Considering the two purposes of the dispensing unit, i.e., refueling the aircraft and venting the gas produced due to boil-off, the number of dispensing units needed by the plant must be at least equal to the maximum number used at the same time.

$$N^{\mathrm{DU}} \geq \max\left(\sum_{i\in I}\left(y_{i,t}^{ref} + y_{i,t}^{coup}\right)\right). \tag{1.31}$$

## 1.6. Problem statement

In order to apply the methodology on a large scale, a mathematical formalization of the problem described above is required. The optimization variables are represented by 7 arrays grouped in the global array $\mathbf{x}$ defined as

$$\mathbf{x} = \left(\{E_t\}, \{\dot{m}_t^{\mathrm{GNR}}\}, \{m_t^{\mathrm{ST}}\}, \{N^{\mathrm{DU}}\}, \{m_{i,t}^{a}\}, \{y_{i,t}^{ref}\}, \{y_{i,t}^{coup}\}\right), \tag{1.32}$$

and are detailed in Table 1.3. Through the derivations detailed in Section 1.3, it is seen that the cost function $J$ depends on $\mathbf{x}$. The problem statement is then

$$\begin{aligned} &\underset{\mathbf{x}}{\text{minimize}} \quad J(\mathbf{x}) \\ &\text{subject to} \quad \text{Equations (1.16–1.18, 1.20, 1.28, 1.23–1.31)} \end{aligned} \tag{1.33}$$

with the constraints holding $\forall t \in T$ and $\forall i \in I$. To facilitate the comprehension of the meaning of the variables involved in AHRES, the inputs to the problem are listed in Table 1.4, while the outputs are shown in Table 1.5. At the end of the optimization, the final values of the optimization variables are also provided as outputs. The general concept of the optimization tool is sketched in Figure 1.9

The problem was implemented in MATLAB®(MATLAB R2021b, 9.7, MathWorks, Natick, MA, USA) and solved using the GUROBI solver (Gurobi Optimizer, 9.1, Gurobi Optimization LLC, Beaverton, OR, USA).

Table 1.3: AHRES optimization variables

| Variable | Type | Description |
|---|---|---|
| $E_t$ | real | Consumed electric energy at time $t$ |
| $\dot{m}_t^{\mathrm{GNR}}$ | real | Hourly production rate of hydrogen by the generator at time $t$ |
| $m_t^{\mathrm{ST}}$ | real | Mass of hydrogen in the storage tank at time $t$ |
| $m_{i,t}^a$ | real | Mass of hydrogen in the $i$-th aircraft tank at time $t$ |
| $t_{i,t}^{ref}$ | real | Refueling time required for aircraft $i$-th at time $t$ |
| $N^{\mathrm{DU}}$ | integer | Number of dispensing units |
| $y_{i,t}^{ref}$ | binary | Parameter indicating if the aircraft $i$ is being refueled at time $t$ |
| $y_{i,t}^{coup}$ | binary | Parameter indicating if the aircraft $i$ is coupled to a dispensing unit at time $t$ |

Table 1.4: AHRES input parameters

| **Aircraft-related** | |
|---|---|
| $I$ | Set of aircraft |
| $m_{max,i}^a$ | Maximum mass of hydrogen that the tank of the $i$-th aircraft can store |
| $m_{min,i}^a$ | Minimum mass of hydrogen that the tank of the $i$-th aircraft must always store |
| $m_{req,i,t}^a$ | Mass of hydrogen required by the $i$-th aircraft at time $t$ |
| $m_{\mathrm{BO},i}^a$ | Mass of hydrogen lost in the tank due to boil off |
| $y_{i,t}^{out}$ | Parameter indicating if the aircraft $i$ is on mission at time $t$ |
| $y_{i,t}^{leave}$ | Parameter indicating if the aircraft $i$ will leave the airport during the timestep $t$ |
| $m_{fuel,i}^a$ | Mass of hydrogen needed for the i-th aircraft to travel the distance of its mission |

Table 1.4: *Cont.*

| | |
|---|---|
| **Generator-related** | |
| $c_e^{\mathrm{GNR}}$ | Energy required by the generator to produce one $kg$ of hydrogen |
| $c^{\mathrm{GNR}}$ | Procurement cost per unit of daily production for the generator |
| $d^{\mathrm{GNR}}$ | Expected lifespan of the generator measured in days |
| **Storage tank-related** | |
| $m_{min}^{\mathrm{ST}}$ | Minimum amount of hydrogen that must be counted from the tank |
| $m_{\mathrm{BO},t}^{\mathrm{ST}}$ | Mass of hydrogen lost due to boil off in the tank at time $t$ |
| $c^{\mathrm{ST}}$ | Procurement cost for the tank per $kg$ of stored hydrogen |
| $d^{\mathrm{ST}}$ | Expected lifespan of the tank measured in days |
| **Dispensing unit-related** | |
| $\dot{m}^{\mathrm{DU}}$ | Hourly hydrogen flow rate of the dispensing unit |
| $c_p^{\mathrm{DU}}$ | Power absorbed by each dispensing unit |
| $c^{\mathrm{DU}}$ | Procurement cost for the dispensing unit |
| $d^{\mathrm{DU}}$ | Expected lifespan of the dispensing unit measured in days |
| **Energy supply-related** | |
| $\lambda_t$ | Electric energy price at time $t$ |
| $c_p$ | Electric power cost per month |
| **Simulation-related** | |
| $T$ | Set of time slots |
| $L$, $d$ | Simulated time duration |
| $l_t$ | Length of a time slot |

Table 1.5: AHRES output parameters

| | |
|---|---|
| $C^{\mathrm{GNR}}$ | Total generator procurement cost |
| $C^{\mathrm{DU}}$ | Total dispensing unit procurement cost |
| $C^{\mathrm{ST}}$ | Total storage tank procurement cost |
| $C^{e}$ | Electric energy cost |
| $C^{p}$ | Electric power cost |
| $J$ | Cost function |

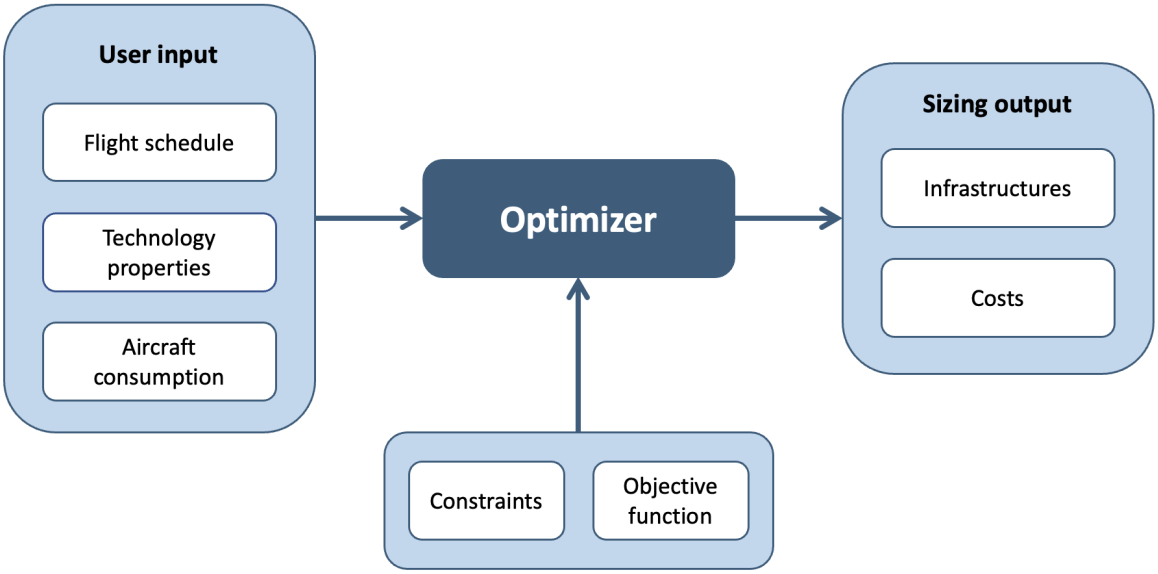


Figure 1.9: Scheme of the optimization process

## 1.7. Sanity check

The validation of the developed code is difficult to perform due to the lack of reliable public data concerning a plant of this type. However, quality control of the implemented algorithm can be performed by testing it with instances of increasing complexity. The testing began with smaller problems that can be solved manually to verify that the output generated by the solver matches the expected result.

The simplest case that will be analyzed first consists of a single flight, operated with an Airbus A320, with a length of 1 000 km that takes off at 1 pm. For a flight of this length, an Airbus A320 would consume an amount of liquid hydrogen equal to 1 442.3 kg; the details of the consumption calculation for different aircraft models will be discussed in more detail in Section 2.1.

The output provides four graphs, representing the activities of the main system elements on the operating day under consideration. In the first graph, the amount of hydrogen produced by the generator is displayed. Each blue bar represents the production every 10 minutes, while the red line represents the energy pricing during the day. The second graph displays the mass stored in the ground tank, where each blue bar represents the amount of hydrogen in the tank in each timestep. The third graph shows the flow rate of hydrogen passing through the dispensing units, with each bar representing the cumulative flow of all active dispensing units in the relevant timestep. Lastly, the last graph displays the distribution of takeoffs over the day.

As shown in Figure 1.10, the solver correctly distributes the production over the 24-hour period in order to minimize the energy peak, since in the case of monorail pricing there is no penalty for consuming energy even during daylight hours. Hence the ground tank fills up during the day and then refuels the aircraft just before takeoff in order to minimize the mass of hydrogen lost to boil off since this phenomenon is greater in the aircraft tank than in the ground tank. The total liquid hydrogen produced results to be 1 503.5 kg. It is necessary to specify that a periodicity constraint is set in the code, so the schedule considered in the simulation repeats every day. Therefore, after the aircraft has taken off, the plant starts producing hydrogen again to supply to the aircraft that will take off the next day.

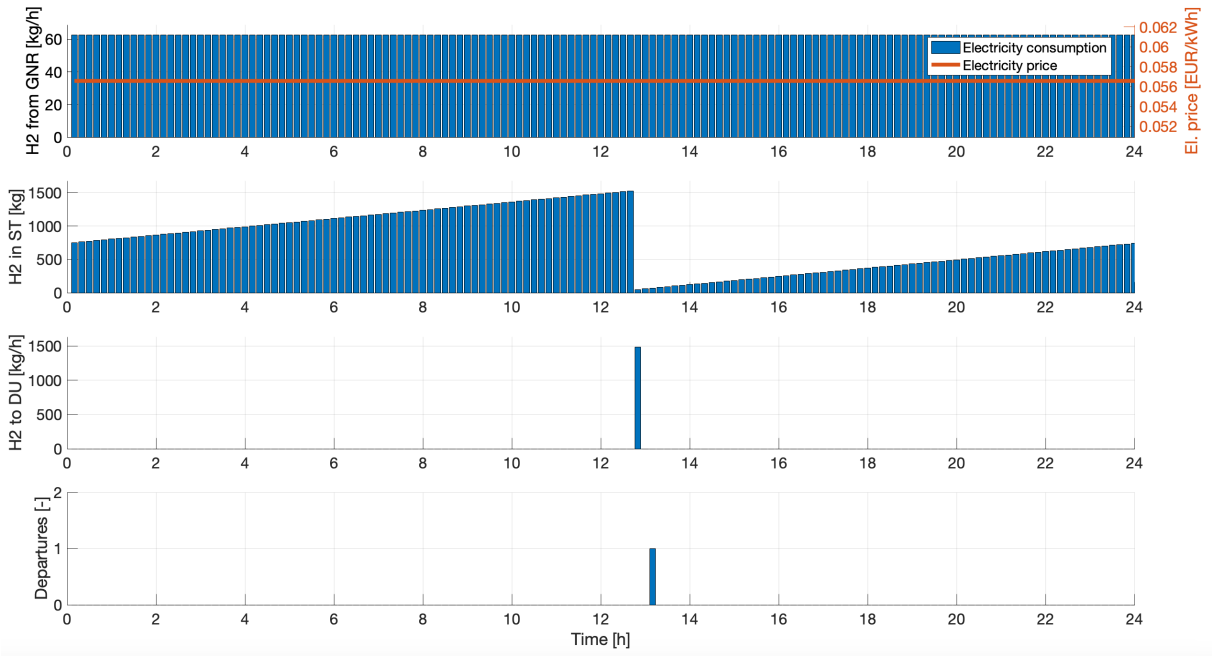


Figure 1.10: Single flight test

To increase the scale of the study, the test is performed with a more dense flight schedule, assuming one flight per hour from 8 a.m. to 6 p.m., except at 1 p.m. when there are two flights departing at the same time, in order to test the code even in the case of simultaneous takeoffs.

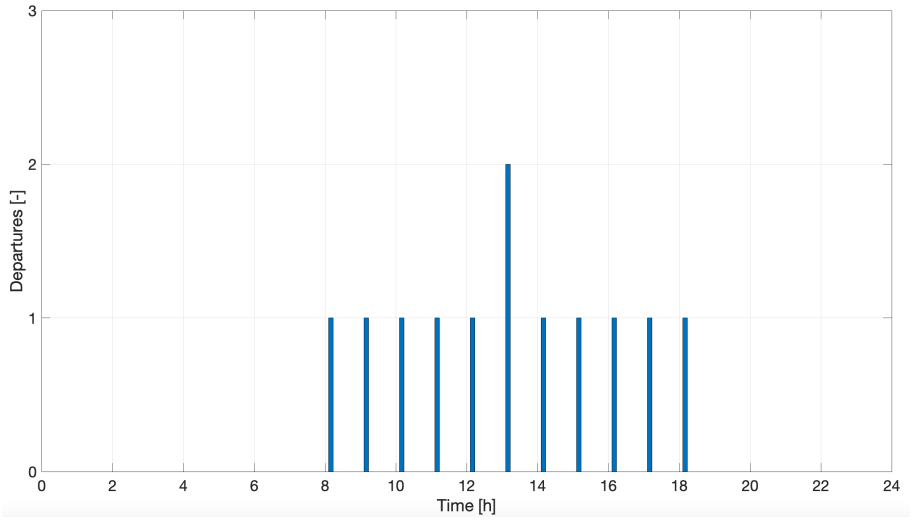


Figure 1.11: Aircraft departures in the test simulation

Once again, the results, shown in Figure 1.12, are consistent with those expected:

- production is distributed over the 24-hour period;

- each aircraft is refueled just before takeoff when it is actually available for refueling;
- due to the two flights leaving at the same time the solver correctly adds a dispensing unit. In fact, as explained in Section 1.1.3, even if one of the aircraft were to be refueled before the other, it is necessary to maintain a connection with the dispensing unit nozzle to allow the aspiration of gas generated by the boil off and prevent excessive pressure buildup within the tank.

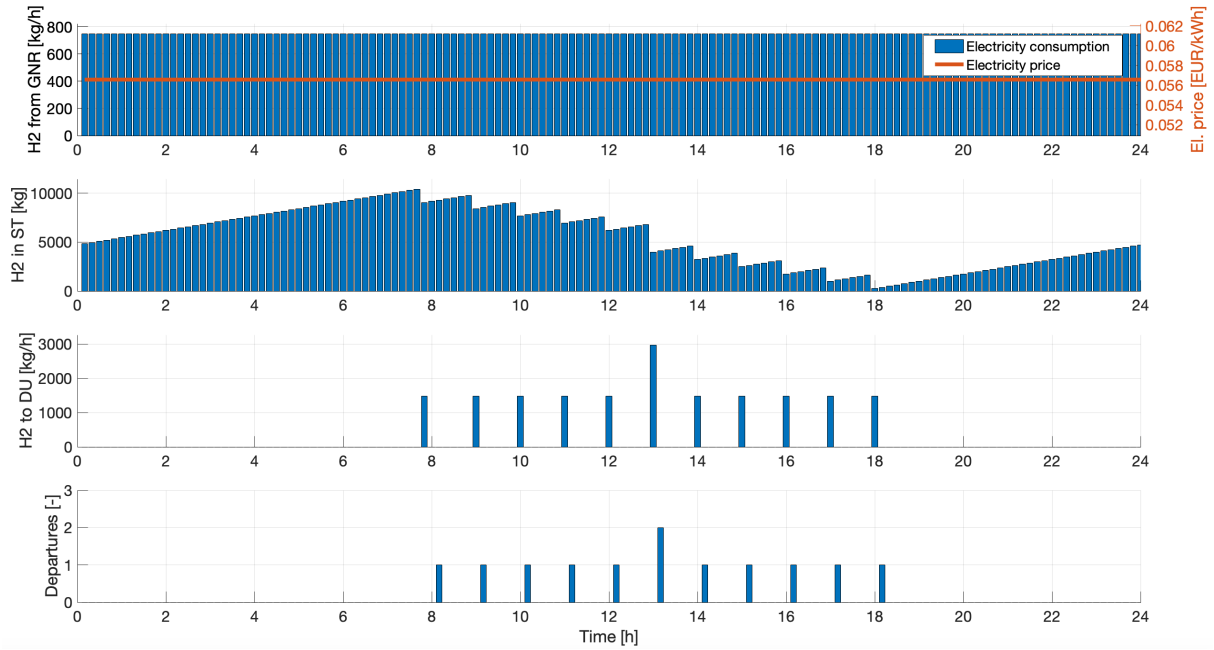


Figure 1.12: 12 flights and simple tariff test

Finally, the test was repeated by assuming bi-hourly energy pricing with the same flight schedule.

The primary difference, in this case, is that all hydrogen production is concentrated during the low-price hours, while the generator is idle during the rest of the day. Consequently, the ground tank's size increases considerably as it must have the capacity to store sufficient hydrogen to meet the demand for the next ten hours when the high-price hours commence at 8 am. Although the hydrogen production in both scenarios is roughly the same, the ground generator's size increases from 10 420 kg to 17 571 kg. However, the results are logical in this case as well.

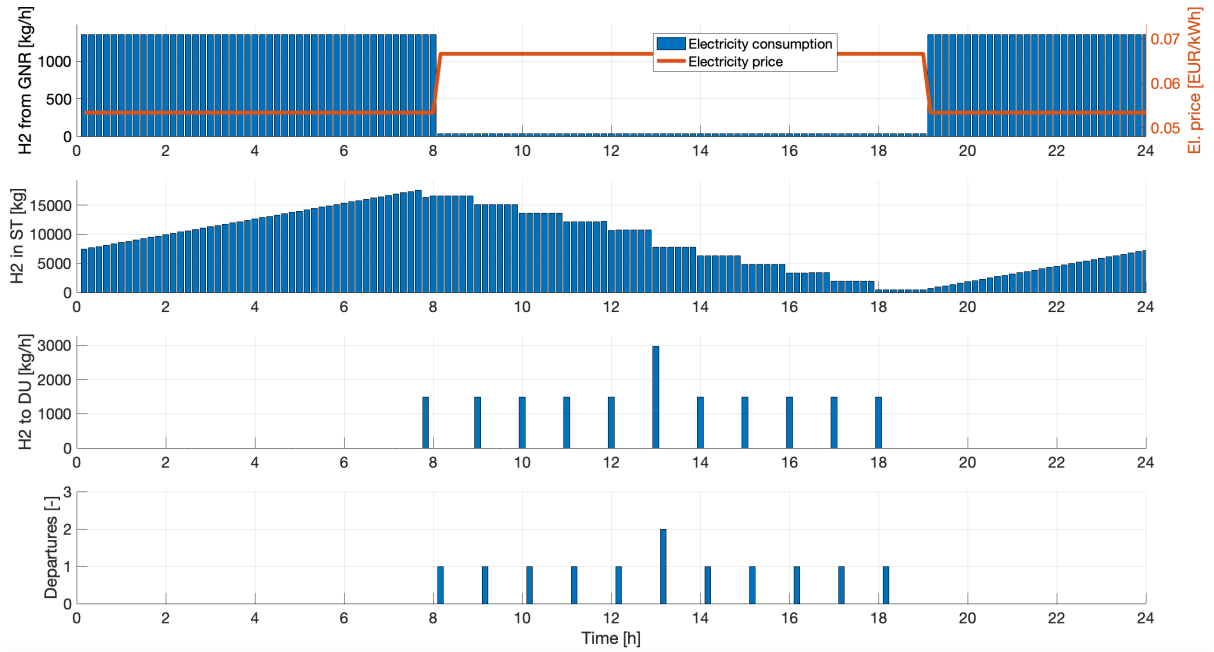


Figure 1.13: 12 flights and bi-hourly tariff test

# 2 | Application scenarios

In this chapter, the scenarios used for the study will be presented, including the airports, aircraft models, and flight schedules. These scenarios will be analyzed using the methodology described in Chapter 1. The cases are divided into two classes, with the first involving regional-type transport that typically utilizes smaller propeller-driven aircraft, while the second class considers short-range transport using jet-powered aircraft.

## 2.1. Airliners

Below are presented all the aircraft models that will be used in the simulations, divided into regional airliners (propeller-driven aircraft) and short/medium-range commercial airliners (jet-powered aircraft). Minor ariants within each aircraft class have not been divided, as they do not involve significant variation in fuel consumption.

### 2.1.1. Regional airliners

A regional airliner or feederliner is a small-sized aircraft, designed for short-haul flights that can accommodate up to 100 passengers. These types of aircraft are commonly operated by regional airlines, which may be contracted by or subsidiaries of larger airlines. Typically, regional airliners are utilized for short trips between smaller towns or from a larger city to a smaller city. As these aircraft are mainly used for serving small airports with short runways, they are often equipped with turboprop engines that use propellers instead of jet engines [59].

For aircraft of this size intended for short-distance flights, a fuel cell can be used as a power source. This method of utilizing hydrogen as fuel is considered the most eco-friendly option available [60]. A fuel cell is an electrochemical device that generates mechanical energy by converting chemical energy produced through redox reactions that take place between hydrogen (as fuel) and oxygen sourced from the surrounding ambient air. The main issues related to the use of hydrogen with a fuel cell, primarily concern the low power density which currently makes it impossible to employ this technology for larger-sized

aircraft or for longer flights [61].

Specifically, the fleet used in the simulations presented in this thesis consists of 3 propeller-driven aircraft: ATR72, ATR42, and Bombardier Dash8; presented in detail below. The crucial information regarding aircraft is the hydrogen consumption based on mission length. These were estimated using HYPERION (HYbrid PERformance simulatION), a software developed at Politecnico di Milano. Hyperion can conduct preliminary sizing of conventional, thermal hybrid-electric and hydrogen hybrid propeller aircraft and of conventional and hydrogen-burning jet aircraft, enabling the evaluation of energy consumption, performance, and innovative design capabilities. For a more detailed understanding of HYPERION and its application in calculating hydrogen consumption for propeller-driven aircraft, consult Gabriele Sirtori's Msc thesis [62].

## ATR 42

The ATR 42 is a regional turboprop aircraft manufactured by ATR, a joint venture between Airbus and Leonardo. It can carry up to 50 passengers and has a range of 842 nautical miles. The aircraft has a wingspan of 24.6 meters and a length of 22.67 meters. It is powered by two Pratt & Whitney Canada PW120 turboprop engines, which provide a maximum cruising speed of 345 mph. The ATR 42 is designed for short to medium-haul flights and is popular with regional airlines, as well as military and government operators. It has a reputation for being reliable and efficient, with low operating costs and excellent performance in hot and high conditions.

Table 2.1: ATR 42 - Specification

| **Specification** | **Value** |
|---|---|
| Length | 22.67 m |
| Wing Span | 24.57 m |
| Wing Surface | 54.50 $m^2$ |
| Design range | 1 560 km |
| No. of passengers | 42-50 |

Table 2.2: ATR 42 - LH2 consumption

| **Distance [km]** | **Consumption [kg]** |
|---|---|
| 250 | 54.5 |
| 500 | 101.7 |
| 750 | 149.9 |
| 1000 | 199.1 |


Figure 2.1: ATR 42

## ATR 72

The ATR 72 is a twin-engine turboprop aircraft that was first introduced in 1989 by ATR. The aircraft is primarily designed for regional flights and can carry up to 74 passengers. It has a range of up to 810 nautical miles and a maximum cruise speed of 317 mph. One of the main characteristics of the ATR 72 is its fuel efficiency, thanks to its turboprop engines, which consume less fuel than comparable jet engines. This makes it an ideal choice for airlines operating regional routes with smaller passenger loads.

Table 2.3: ATR 72 - Specification

| Specification | Value |
|---|---|
| Length | 24.16 m |
| Wing Span | 27.06 m |
| Wing Surface | 61.00 $m^2$ |
| Design range | 1 500 km |
| No. of passengers | 66-74 |

Table 2.4: ATR 72 - LH2 consumption

| Distance [km] | Consumption [kg] |
|---|---|
| 250 | 78.4 |
| 500 | 146.3 |
| 750 | 215.6 |
| 1000 | 286.4 |


Figure 2.2: ART 72

## De Havilland Canada Dash 8

The De Havilland Canada Dash 8, also known as the DHC-8, is a family of twin-engine turboprop aircraft designed and produced by De Havilland Canada, now part of Longview Aviation Capital. The Dash 8 is primarily used for regional flights and can accommodate up to 40 passengers. The Dash 8 has a range of up to 820 nautical miles and a maximum cruise speed of 305 mph. It is powered by two Pratt & Whitney Canada PW100 turboprop engines, which provide a high level of reliability and fuel efficiency. One of the key features of the Dash 8 is its short takeoff and landing capabilities, which allows it to operate from smaller airports and runways, making it ideal for regional airlines. It has become a popular choice for regional airlines around the world, with over 1 200 aircraft delivered to date.

Table 2.5: Dash 8 - Specification

| Specification | Value |
|---|---|
| Length | 22.95 m |
| Wing Span | 25.91 m |
| Wing Surface | 54.4 $m^2$ |
| Design range | 1 520 km |
| No. of passengers | 30-40 |

Table 2.6: Dash 8 - LH2 consumption

| Distance [km] | Consumption [kg] |
|---|---|
| 250 | 112.6 |
| 500 | 189.5 |
| 750 | 281.5 |
| 1000 | 373.9 |
| 1250 | 467.0 |


Figure 2.3: De Havilland Canada Dash 8

In order to provide an easier point of reference, Figure 2.4 shows graphs of the liquid hydrogen consumption of the aircraft analyzed above based on distance traveled.

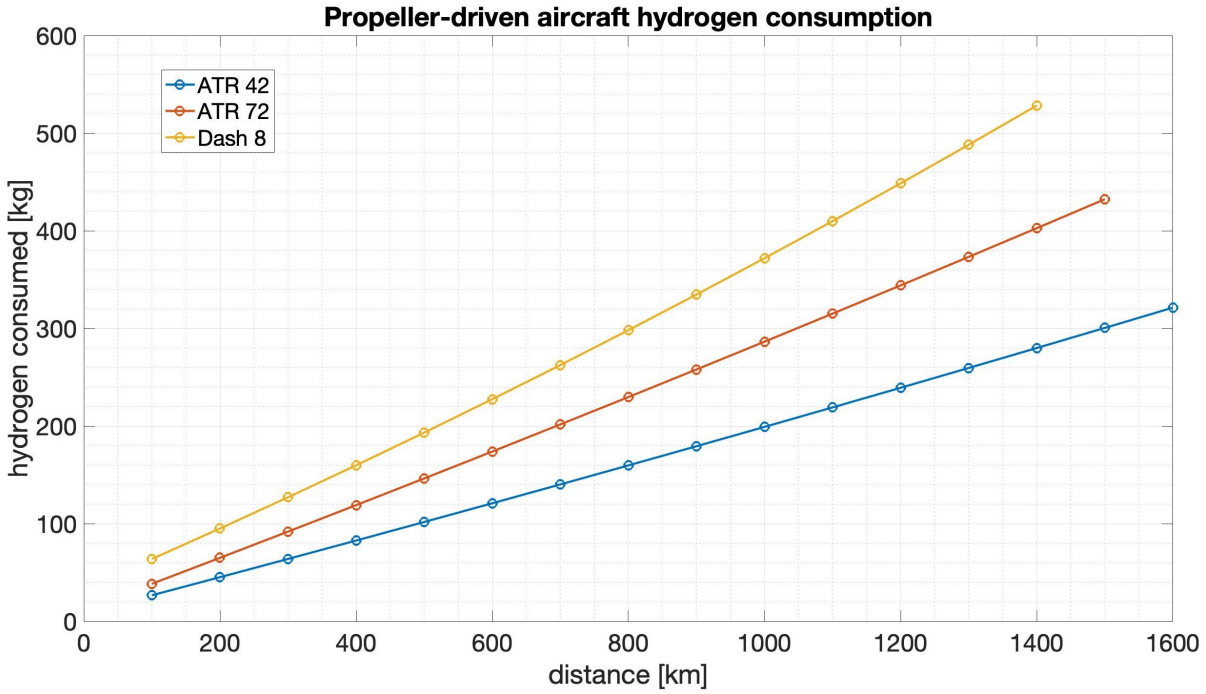


Figure 2.4: Graph of propeller-driven aircraft hydrogen consumption

### 2.1.2. Short/medium-range commercial airliners

Short/Medium-range airliners are a category of jet-powered aircraft designed to transport passengers on relatively short flights, typically with a range of 500 to 4 000 kilometers. These aircraft are typically designed to carry between 70 and 250 passengers, with a range of seating configurations to meet the needs of different airlines and their customers. Some of the most popular Short/Medium-range Airliners include the Boeing 737, the Airbus A320 family, and the Embraer E-Jet family, presented in detail below.

As previously mentioned, it is currently not possible to use fuel cells to power aircraft of this size due to the low energy density of hydrogen on a volumetric basis. The only solution in this case is to burn the hydrogen. Aircraft powered by hydrogen fuel cells have zero emissions during operation, while those using hydrogen as a fuel for an internal combustion engine are emission-free for $CO_2$, but not for nitrogen oxides. In fact, the burning of hydrogen in air leads to the production of $NO_x$, and the $H_2 + {}^1\!/_2\, O_2 \rightarrow H_2O$ reaction in a nitrogen-rich environment also causes the production of $NO_x$ [63]. However, hydrogen combustion produces up to 90% less nitrogen oxides than kerosene fuel, and it eliminates the formation of particulate matter [64].

Again, as in Section 2.1.1, the hydrogen consumption for hydrogen-burning aircraft were calculated using an extension of the HYPERION software. The procedure for the computation is presented in detail in Luca Caccetta's Msc thesis [65].

#### Airbus A320

The Airbus A320 aircraft is a narrow-body, commercial passenger jetliner produced by Airbus. It is part of the A320 family, which also includes the A319, A321, and A318 models. The A320 has a seating capacity of up to 180 passengers in a typical two-class configuration, a range of around 3 300 nautical miles and a maximum cruise speed of 540 mph. It is powered by two CFM International CFM56 or International Aero Engines V2500 turbofan engines, which provide high levels of reliability and fuel efficiency. The aircraft features advanced technology, such as fly-by-wire controls and a glass cockpit, which enhance safety and reduce pilot workload. It has been a popular choice for airlines around the world due to its versatility and efficiency. Its popularity is also due to its compatibility with the other members of the A320 family, allowing airlines to save on maintenance and training costs. The A320 is commonly used for short-to-medium haul flights.

Table 2.7: A320 - Specification

| Specification | Value |
|---|---|
| Length | 37.57 m |
| Wing Span | 35.80 m |
| Wing Surface | 124.0 $m^2$ |
| Design range | 4 000 km |
| Number of passengers | 180 |

Table 2.8: A320 - LH2 consumption

| Distance [km] | Consumption [kg] |
|---|---|
| 500 | 770.9 |
| 1000 | 1 442.3 |
| 1500 | 2 119.5 |
| 2000 | 2 806.1 |
| 2500 | 3 498.3 |
| 3000 | 4 194.7 |
| 3500 | 4 902.0 |
| 4000 | 5 614.3 |


Figure 2.5: Airbus A320

## Airbus A319

The Airbus A319 aircraft is a short-to-medium range, narrow-body, commercial passenger jetliner produced by Airbus. It is a member of the Airbus A320 family. The A319 has a seating capacity of up to 160 passengers in a typical two-class configuration, a range of around 3 750 nautical miles and a maximum cruise speed of 540 mph. It is powered by two CFM International CFM56 or International Aero Engines V2500 turbofan engines, which provide high levels of reliability and fuel efficiency. The A319 is 3.73 m shorter than the A320 and can carry fewer passengers.

Table 2.9: A319 - Specification

| Specification | Value |
|---|---|
| Length | 33.84 m |
| Wing Span | 35.80 m |
| Wing Surface | 124.0 $m^2$ |
| Design range | 4 600 km |
| No. of passengers | 160 |

Table 2.10: A319 - LH2 consumption

| Distance [km] | Consumption [kg] |
|---|---|
| 500 | 748.6 |
| 1000 | 1 416.8 |
| 1500 | 2 086.9 |
| 2000 | 2 765.6 |
| 2500 | 3 450.5 |
| 3000 | 4 141.4 |
| 3500 | 4 835.1 |
| 4000 | 5 537.9 |


Figure 2.6: Airbus A319

## Airbus A321

The Airbus A321 aircraft is a narrow-body, commercial passenger jetliner produced by Airbus. It is part of the A320 family. The A321 is the largest member of the A320 family, with a length of 44.51 meters and a seating capacity of up to 240 passengers in a typical two-class configuration. It has a range of around 3,600 nautical miles, a maximum cruise speed of 540 mph, and is powered by two CFM International CFM56 or International Aero Engines V2500 turbofan engines, which provide high levels of reliability and fuel efficiency. Its larger size and capacity make it well-suited for high-density routes, and it has proven to be a valuable asset for airlines operating in these markets.

Table 2.11: A321 - Specification

| Specification | Value |
|---|---|
| Length | 44.51 m |
| Wing Span | 35.8 m |
| Wing Surface | 128.0 $m^2$ |
| Design range | 4 100 km |
| No. of passengers | 236 |

Table 2.12: A321 - LH2 consumption

| Distance [km] | Consumption [kg] |
|---|---|
| 500 | 880.3 |
| 1000 | 1 640.4 |
| 1500 | 2 406.2 |
| 2000 | 3 175.6 |
| 2500 | 3 958.1 |
| 3000 | 4 740.9 |
| 3500 | 5 530.8 |
| 4000 | 6 335.6 |


Figure 2.7: Airbus A321

## Airbus A220-300

The Airbus A220-300 (ICAO code BCS3), formerly known as the Bombardier CSeries, is a family of narrow-body, twin-engine, medium-range jet airliners designed and produced by Airbus Canada Limited Partnership. The aircraft comes in two variants, the A220-100 and A220-300, which can seat 100-150 passengers, respectively. The A220 features advanced aerodynamics, advanced materials, and Pratt & Whitney PW1500G geared turbofan engines. The A220 has gained popularity among airlines around the world due to its fuel efficiency and versatility. As of 2021, there were over 170 A220s in service with airlines such as Delta Air Lines, Air France, and Swiss International Air Lines.

Table 2.13: A220 - Specification

| Specification | Value |
|---|---|
| Length | 38.70 m |
| Wing Span | 35.10 m |
| Wing Surface | 112.3 $m^2$ |
| Design range | 4 050 km |
| No. of passengers | 100-150 |

Table 2.14: A220-300 - LH2 consumption

| Distance [km] | Consumption [kg] |
|---|---|
| 500 | 591.6 |
| 1000 | 1 112.6 |
| 1500 | 1 639.6 |
| 2000 | 2 170.5 |
| 2500 | 2 704.9 |
| 3000 | 3 241.6 |
| 3500 | 3 783.3 |
| 4000 | 4 331.2 |


Figure 2.8: Airbus A220-300

## Boeing 737

The Boeing 737, commonly known as the B737, is a narrow-body aircraft produced by Boeing Commercial Airplanes. It is one of the best-selling jet airliners in the history of aviation and has been in production since 1967. The B737 is designed for short to medium-range flights and can accommodate up to 230 passengers, depending on the model. It has a range of up to 3,600 nautical miles, a maximum cruise speed of 838 mph and can fly at a maximum altitude of 41,000 feet. It featured CFM56 high bypass turbofan engines. There are several models of the B737, including the B737-300, B737-400, and B737-800, each with different passenger capacities and range capabilities.

Table 2.15: B737 - Specification

| Specification | Value |
|---|---|
| Length | 30.53 m |
| Wing Span | 28.8 m |
| Wing Surface | 91.04 $m^2$ |
| Design range | 4 100 km |
| No. of passengers | 230 |

Table 2.16: B737 - LH2 consumption

| Distance [km] | Consumption [kg] |
|---|---|
| 500 | 780.2 |
| 1000 | 1 423.9 |
| 1500 | 2 070.6 |
| 2000 | 2 723.6 |
| 2500 | 3 384.8 |
| 3000 | 4 049.6 |
| 3500 | 4 720.3 |
| 4000 | 5 393.9 |


Figure 2.9: Boeing 737

## Embraer 190

The Embraer 190, or E190, is a narrow-body, twin-engine commercial jet produced by Brazilian aircraft manufacturer Embraer. It entered commercial service in 2005 and is designed for short to medium-range flights. The E190 can accommodate up to 114 passengers and has a range of up to 2 800 nautical miles. It is powered by two General Electric CF34-10E engines and has a maximum cruising speed of 541 mph. Embraer has produced several models of the E190, including the E170, E175, and E195, each with different passenger capacities and range capabilities.

Table 2.17: E190 - Specification

| Specification | Value |
|---|---|
| Length | 36.25 m |
| Wing Span | 28.73 m |
| Wing Surface | 92.53 $m^2$ |
| Design range | 3 300 km |
| No. of passengers | 114 |

Table 2.18: E190 - LH2 consumption

| Distance [km] | Consumption [kg] |
|---|---|
| 500 | 523.5 |
| 1000 | 954.8 |
| 1500 | 1 389.3 |
| 2000 | 1 826.9 |
| 2500 | 2 267.7 |
| 3000 | 2 711.6 |


Figure 2.10: Embraer 190

Figure 2.11 displays graphs illustrating the liquid hydrogen consumption of the previously analyzed aircraft based on distance traveled, in order to provide a more straightforward point of reference.

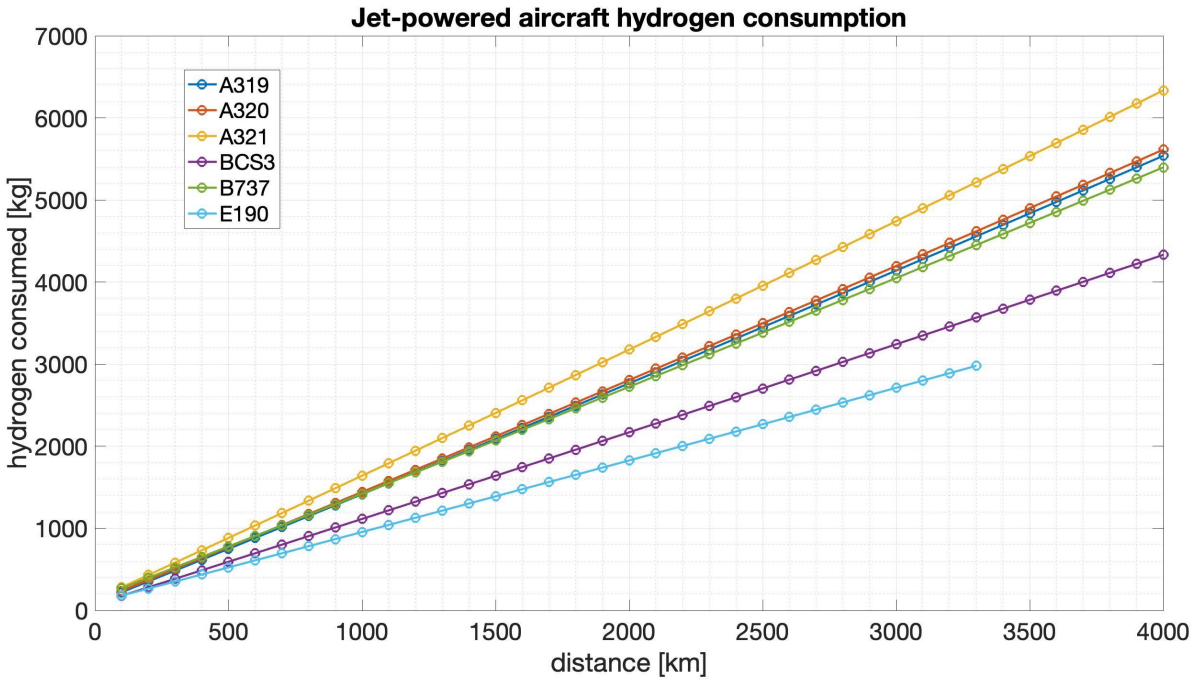


Figure 2.11: Graph of jet-powered aircraft hydrogen consumption

## 2.2. Regional operations

### 2.2.1. The airport: Athens International Airport (ATH)

Athens International Airport Eleftherios Venizelos (IATA: ATH, ICAO: LGAV), is the largest international airport in Greece, serving the city of Athens and region of Attica. In 2022 it was the 19th-busiest airport in Europe and the busiest and largest in the Balkans, with passenger traffic of 22.7 million and total aircraft movements of 213 352 [66].


Figure 2.12: Athens Airport location in Greece

This has been selected for this study since it was the European airport with the largest number of propeller-driven regional aircraft movements since 2015 [67]. Approximately 50% of the traffic is represented by domestic flights, as can be seen from the Table 2.19, which is due to the geographical characteristics of Greece and the need for frequent connections between the capital and the various Aegean islands. The analysis in this particular application will focus only on these flights in order to understand if the use of liquid hydrogen could be a viable alternative for this type of traffic characterized by short and frequent flights operated by relatively small aircraft.

Table 2.19: Total passenger percentage per country destination

| **Country destination** | **Passenger percentage** |
|---|---|
| Domestic | 47.16% |
| Germany | 10.11% |
| France | 7.38% |
| United Kingdom | 6.22% |
| Italy | 5.94% |
| Cyprus | 5.71% |

All regional flights from the airport are operated by two companies: Olympic air and Sky express, for which the Athens airport represents the main hub. The Table 2.20 show the destinations of the regional flight with their respective distances from Athens.

Table 2.20: Regional flight destinations

| Destination airport | IATA code | Distance [km] | Operated by: | |
|---|---|---|---|---|
| | | | Sky Express | Olympic Air |
| Alexandroupoli | AXD | 367 | ✓ | ✓ |
| Astypalaia | JTY | 262 | ✓ | |
| Chania | CHQ | 267 | ✓ | |
| Chios | JKH | 197 | ✓ | ✓ |
| Corfu | CFU | 396 | ✓ | |
| Heraklion | HER | 308 | ✓ | |
| Ikaria | JIK | 213 | ✓ | ✓ |
| Ioannina | IOA | 334 | | ✓ |
| Izmir | ADB | 284 | | ✓ |
| Kalymnos | JKL | 285 | ✓ | |
| Karphathos | AOK | 400 | ✓ | ✓ |
| Kavalla | KVA | 335 | | ✓ |
| Kefalonia | EFL | 303 | ✓ | ✓ |
| Kos | KGS | 445 | ✓ | ✓ |
| Kythira | KIT | 202 | ✓ | ✓ |
| Lemnos | LXS | 246 | ✓ | ✓ |
| Leros | LRS | 373 | | ✓ |
| Milos | MLO | 145 | ✓ | ✓ |
| Mykonos | JMK | 135 | ✓ | ✓ |
| Mytilene | MJT | 262 | ✓ | ✓ |
| Naxos | JNX | 248 | ✓ | ✓ |
| Paros | PAS | 146 | ✓ | ✓ |
| Rhodes | RHO | 405 | | ✓ |
| Samos | SMI | 262 | ✓ | ✓ |
| Santorini | JTR | 218 | ✓ | ✓ |
| Sitia | JSH | 358 | | ✓ |
| Skiathos | JSI | 143 | ✓ | ✓ |
| Skyros | SKU | 127 | | ✓ |
| Syros | JSY | 228 | ✓ | |
| Zakynthos | ZTH | 270 | ✓ | ✓ |

### 2.2.2. Flight schedules

The simulations were conducted using the real schedules of the airports under consideration to ensure more accurate results. The analysis specifically took place in the year 2022. From [68] the trend of total aircraft movements at the airport, i.e., the number of arrivals and departures of aircraft into and out of the airport, during the calendar year was derived. The total movement data are shown in the graph in Figure 2.13. The days with the highest and lowest number of movements were considered in particular, July 15th (842 movements) and January 25th (285 movements), respectively. For all airports considered, reference will be made to the busiest day with MDD (Most Demanding Day) and the least busy day with LDD (Least Demanding Day).

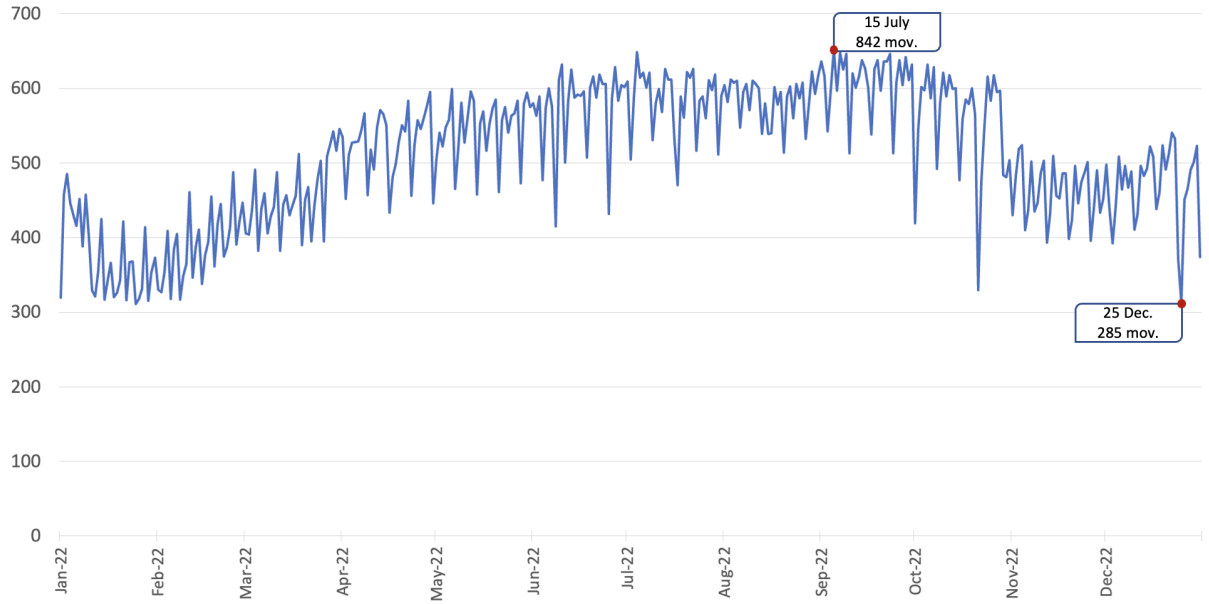


Figure 2.13: Trend in the number of aircraft movements at Athens Airport in 2022

The flight schedules used in the simulation referred to these specific days are detailed in Appendix A. It includes for each flight: the flight number, takeoff time, destination, airline, and the model of aircraft operating it. This information was obtained using the Python API furnished by Flightlabs [69]. Considering only regional flights departing from Athens, 106 flights depart in the MDD with a total of 25 625 kilometers flown, and 30 flights depart in the LDD with a total of 8 434 kilometers flown. The number of flights operated with each of the 3 aircraft models is shown in Table 2.21.

Table 2.21: Number of flights operated with each of the 3 aircraft models at ATH airport

| | MDD | LDD |
|---|---|---|
| **ATR42** | 32 | 5 |
| **ATR72** | 50 | 14 |
| **DHC8** | 24 | 11 |
| **Total flights** | 106 | 30 |

## 2.3. Short-haul operations

### 2.3.1. The airport: Milan Malpensa Airport (MXP)

Milan Malpensa Airport (IATA: MXP, ICAO: LIMC), is the largest international airport in northern Italy, serving Lombardy, Piedmont and Liguria, as well as the Swiss Canton of Ticino. In 2022, Malpensa Airport handled 21.3 million passengers and was the 23rd busiest airport in Europe in terms of passengers and 2nd busiest airport in Italy in terms of passengers after Rome Fiumicino Airport [70].


Figure 2.14: Milan Malpensa Airport location in Italy

### 2.3.2. Flight schedules

As in Section 2.2.2, the schedules to be used in the simulations are chosen from the analysis of the number of aircraft movements at the airport, shown in Figure 2.15 and obtained from [68]. Considering the year 2022, the day with the highest number of movements was September 5th when there were 653 movements, while the day with the lowest number was January 25th with 311 movements.

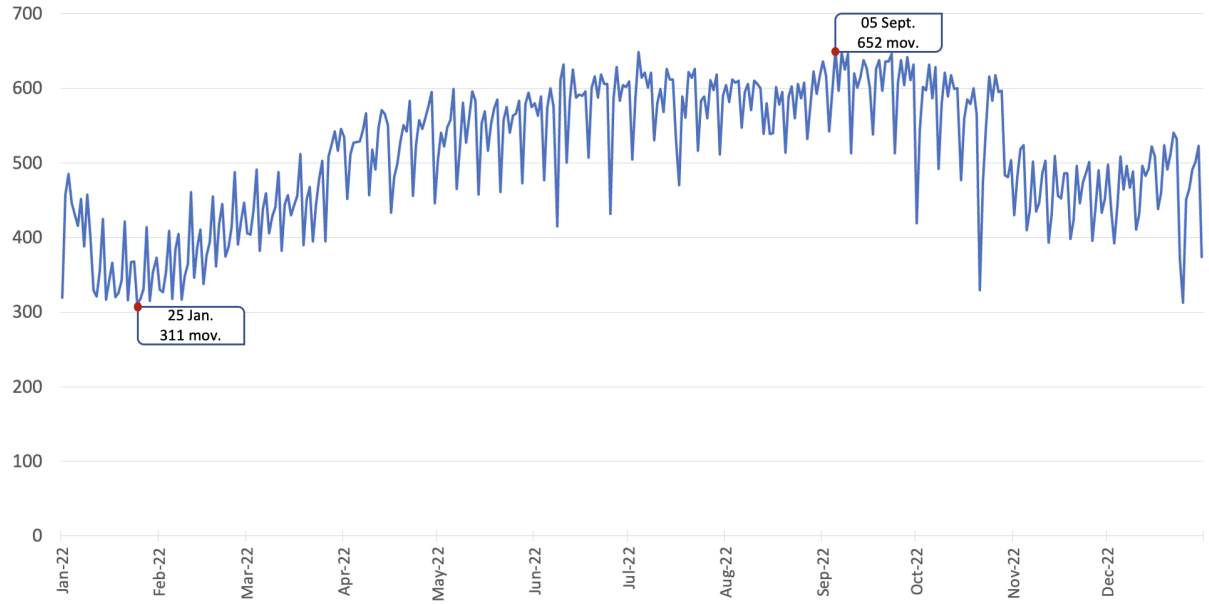


Figure 2.15: Trend in the number of aircraft movements at Milan Malpensa Airport in 2022

The flight schedules used in the simulation referred to these specific days are detailed in Appendix A. Considering only short-haul flights departing from Malpensa, 239 flights depart in the MDD with a total of 263 802 kilometers flown, and 135 flights depart in the LDD with a total of 158 963 kilometers flown. The number of flights operated with each of the 6 aircraft models is shown in Table 2.22.

Table 2.22: Number of flights operated with each of the 6 aircraft models at MXP airport

| | MDD | LDD |
|---|---|---|
| **A320** | 71 | 41 |
| **A319** | 30 | 11 |
| **A321** | 55 | 37 |
| **BCS3** | 2 | 2 |
| **B737** | 56 | 33 |
| **E190** | 25 | 11 |
| **Total flights** | 239 | 135 |

### 2.3.3. Scaling up the study: Paris Charles de Gaulle Airport (CDG)

Paris Charles de Gaulle Airport ( IATA: CDG, ICAO: LFPG), also known as Roissy Airport, is the principal airport serving the French capital, Paris (and its metropolitan area), and the largest international airport in France. In 2019, the airport handled 76 150 007 passengers and 498 175 aircraft movements, thus making it the world's ninth busiest airport and Europe's second busiest airport (after London Heathrow Airport) in terms of passenger numbers [71].


Figure 2.16: Paris Charles de Gauelle Airport location in France

Also here, the schedules are chosen from the analysis of the number of aircraft movements at the airport, shown in Figure 2.17 and obtained from [68]. In the year 2022, August 30th had the highest number of movements, with a total of 1 360, while January 22nd had the lowest number of movements, with 720.

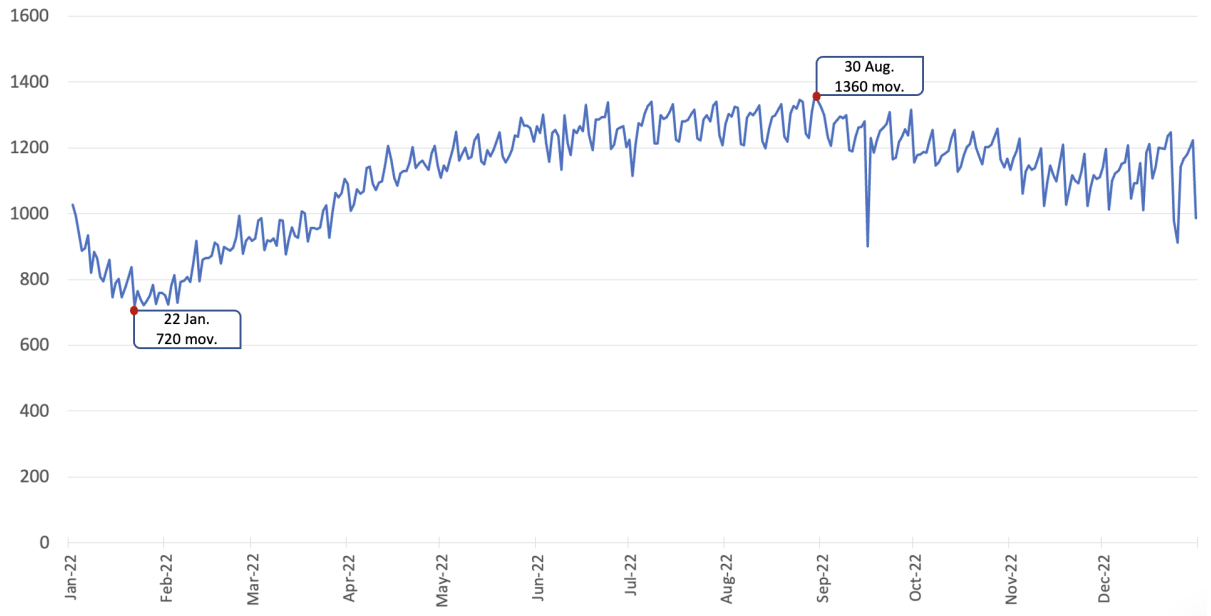


Figure 2.17: Trend in the number of aircraft movements at Paris Charles de Gaulle Airport in 2022

Considering only short-haul flights departing from Charles De Gaulle Airport, 452 flights depart in the MDD with a total of 513 344 kilometers flown, and 327 flights depart in the LDD with a total of 373 187 kilometers flown. The number of flights operated with each of the 6 aircraft models is shown in Table 2.23.

Table 2.23: Number of flights operated with each of the 6 aircraft models at CDG airport

| | MDD | LDD |
|---|---|---|
| **A320** | 84 | 67 |
| **A319** | 91 | 65 |
| **A321** | 74 | 69 |
| **BCS3** | 37 | 21 |
| **B737** | 83 | 46 |
| **E190** | 83 | 59 |
| **Total flights** | 452 | 327 |

The choice to consider these two airports, both referring to a transport operated with jet aircraft, makes it possible to have two different scales with different traffic volumes for the next simulations.

# 3 | Results

In this chapter, the results of the simulations conducted on the airports used as examples will be presented. Additionally, some analyses will be performed on specific cases to better understand some of the facility's characteristics.

## 3.1. Athens International Airport

The sizing of the Athens airport plant starts by considering the schedule of the MDD. Indeed, if the airport can fulfill the airport's requirements on this day, it will be capable of meeting the demand throughout the remainder of the year, when the number of flights operated, and thus the demand for hydrogen, will be lower.

It is important to observe that using only the actual flight schedule would eventually result in a system that would work at its maximum even under steady-state conditions, with no possibility of increasing production or storing more hydrogen if needed. To ensure that all elements of the system work with a margin of safety, an additional 5% of dummy flights were included in the schedule in all simulations conducted from here on. These flights are randomly dispersed throughout the day by the software, flown by an aircraft with average characteristics compared to others used that day, and cover a distance equal to the daily average of all flights.

Figure 3.1 represents the distribution of takeoffs in the MDD. The x-axis represents the time, and each vertical bar shows the number of takeoffs in that particular time step. The different colors on the graph represent the various aircraft models operating the flights.

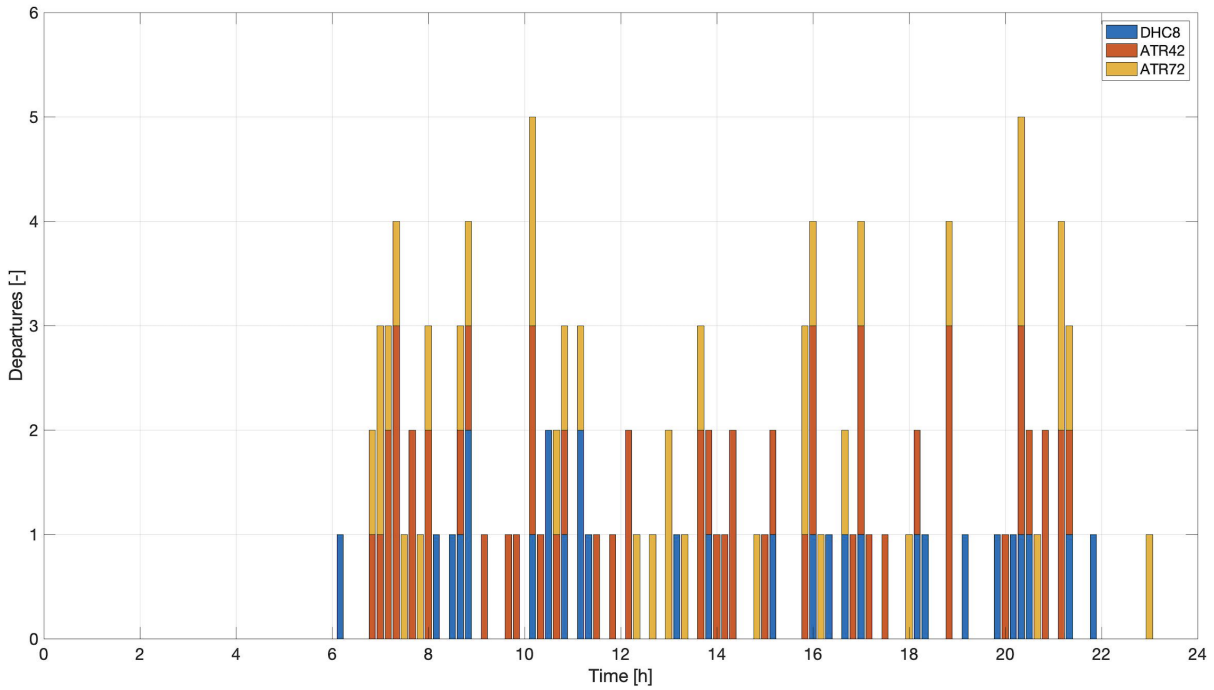


Figure 3.1: Takeoffs in Athens Airport on MDD

The optimization process is initially conducted using simple energy pricing, and the outcomes are presented in Figure 3.2. The figure includes four graphs that respectively show the hydrogen flow rate produced by the generator, the mass of hydrogen stored in the ground tank, the hydrogen flow rate through the dispensing units, and the takeoffs during the day. As previously discussed in Section 1.7, in the case of a single-rate tariff for electricity, the code distributes the hydrogen production evenly over the day.

Afterward, the simulation is repeated using a bi-hourly electricity pricing, and the outcomes are depicted in Figure 3.3. Once again, similar to the case analyzed in Section 1.7, hydrogen production is concentrated during periods of lower electricity prices. As a result, the size of the storage tank increases, the power absorbed by the plant also rises, while the overall electricity costs decrease due to the discount in the production time slots.

Table 3.1 summarizes the main results regarding the plant size and the cost of the various components in the two cases analyzed.

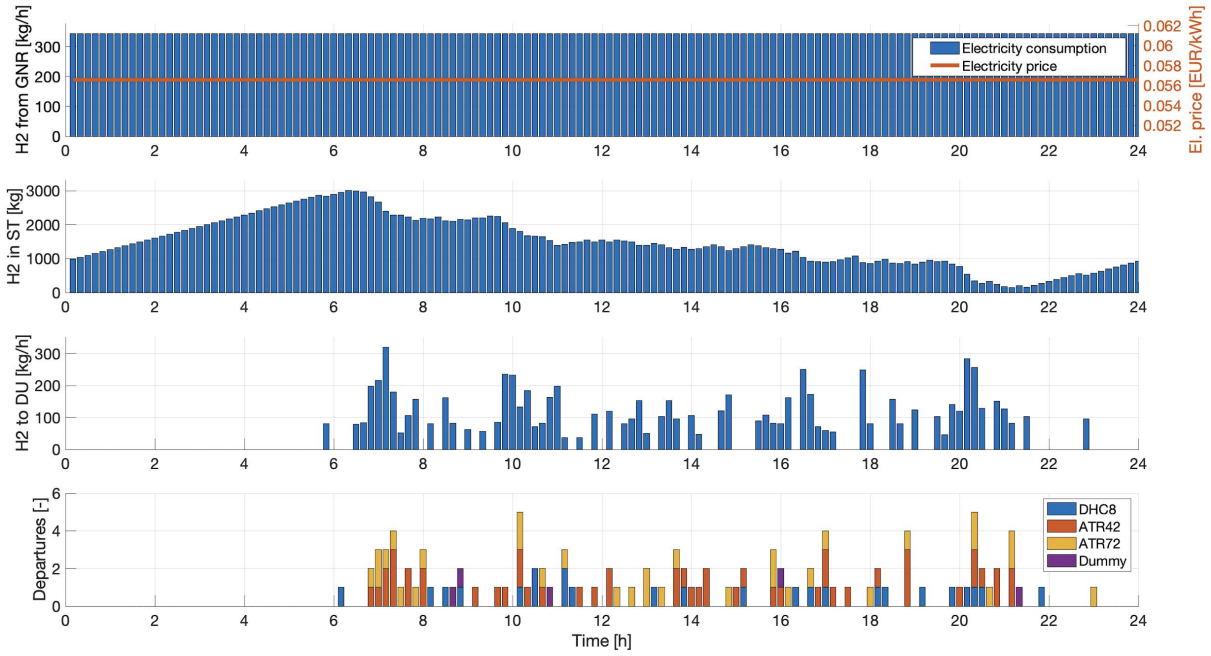


Figure 3.2: Results on MDD at ATH Airport with a simple electricity tariff

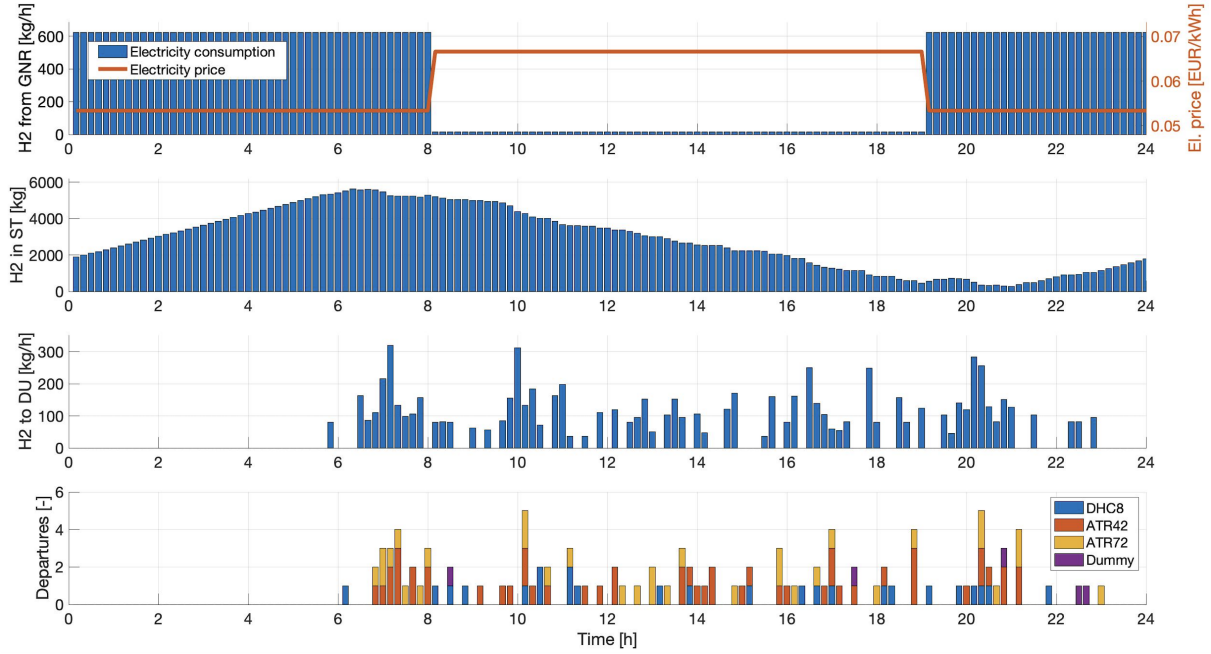


Figure 3.3: Results on MDD at ATH Airport with a bi-hourly electricity tariff

Table 3.1: Athens Airport on MDD: results

| | Simple tariff | Bi-hourly tariff | Change |
|---|---|---|---|
| Ele. consumption | 512 510 kWh | 514 140 kWh | |
| Ele. cost | €28 993 | €27 576 | -5.1% |
| Power absorbed | 21 420 kW | 38 734 kW | |
| Power cost | €1 786 | €3 238 | 44.8% |
| LH2 production | 8 266 kg/d | 8 292 kg/d | |
| GNR cost | €2 831 | €2 840 | 0.3% |
| Max mass in ST | 3 017 kg | 5 647 kg | |
| ST cost | €165 | €309 | 46.6% |
| No. of DU | 5 | 5 | |
| DU cost | €5 260 | €5 260 | 0.0% |
| Total cost | €39 035 | €39 223 | 0.5% |
| Cost per kg of LH2 | €4.72 | €4.73 | 0.2% |

Based on the results, bi-hourly pricing has the potential to lower energy costs by taking advantage of the nighttime energy discount. However, this benefit is counterbalanced by a higher power input due to the concentration of hydrogen production within a shorter time frame and the need for a larger tank. Consequently, the daily cost is roughly the same, with increased performance demands on system elements.

### 3.1.1. Off-design analysis

Under realistic conditions, it is not feasible to size a system every day based on the specific schedule. Instead, once the size of the infrastructure is determined, it must be able to adapt to different demands from the system, which inevitably leads to an increase in cost. In order to estimate this cost increase, an off-design analysis of the facility is conducted in this section, which evaluates the system under operating conditions that are different from those for which it was originally sized.

The first step in this analysis, referred to as case A, involves sizing the system based on the demands of the LDD for Athens Airport. Figure 3.4 shows the distribution of flights for that day. The optimal solution to the problem is obtained from this sizing.

Next, in Case B, the size of the facility is held constant, assuming that it was sized considering the MDD schedule, while keeping the LDD schedule. In this scenario, the daily cost will be higher in Case B than in Case A, as the depreciation costs of the system are higher in the former, where the elements are larger and more expensive. The complete results are presented in Table 3.2.

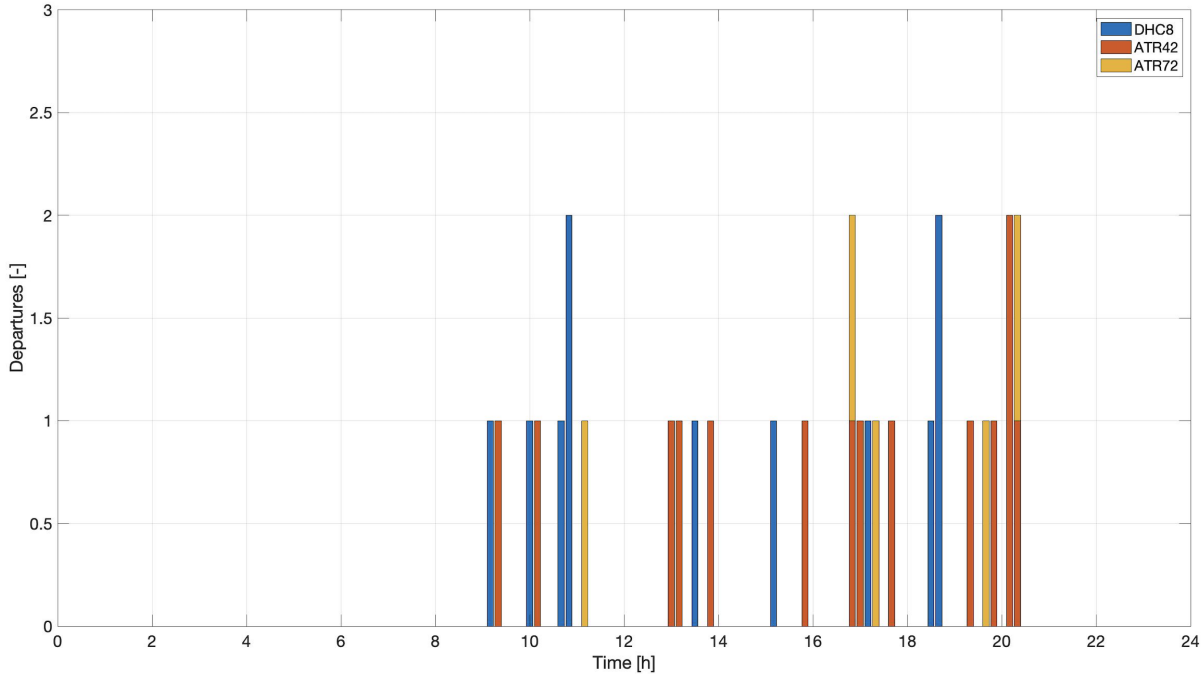


Figure 3.4: Takeoffs in Athens Airport on LDD

Table 3.2: ATH off-design analysis: results

| | Case A | Case B | Change |
|---|---|---|---|
| Ele. consumption | 176 090 kWh | 177 000 kWh | |
| Ele. cost | €9 960 | €10 010 | 0.5% |
| Power absorbed | 7 362 kW | 7 400 kW | |
| Power cost | €613 | €617 | 0.5% |
| LH2 production | 2 840 kg/d | 2 854 kg/d | |
| GNR cost | €973 | €2 831 | 65.6% |
| Max mass in ST | 1 549 kg | 1 551 kg | |
| ST cost | €85 | €165 | 48.6% |
| No. of DU | 2 | 5 | |
| DU cost | €2 104 | €5 260 | 60.0% |
| Total cost | €14 263 | €18 886 | 24.5% |
| Cost per kg of LH2 | €5.02 | €6.61 | 24.1% |

The results reveal a significant rise in the plant's cost, particularly in terms of cost per kilogram. This is due to the substantial difference in volumes between high and low seasons for regional flights at Athens Airport, as can be clearly seen in the airport movement graph (Figure 2.13). The total kilometers flown in the MDD by all the flights are 25 625, while in the LDD, it is only 8 434, indicating a decrease of 67%.

The airport could consider the following solutions:

- Use multiple storage tanks instead of a single, with one tank in use throughout the year and the other operational during peak demand periods to limit boil-off losses, which would be higher in a larger tank.
- Invest in a smaller generator that can meet demand for most days of the year, and procure hydrogen from external sources to supplement the supply during peak demand days. However, a comprehensive economic and feasibility analysis is required to evaluate the cost-effectiveness of this approach.

### 3.1.2. Sensitivity analysis

As previously mentioned, many of the parameters and assumptions in the presented work are subject to uncertainty and variability, despite extensive research. This is because cost estimates and performance properties of the plant may change significantly over time due to ongoing technological advancements and studies. Therefore, an initial sensitivity analysis is conducted here in order to identify the key parameters that significantly influence the results.

Considering the distribution of the total cost of the plant among its five main cost items (electricity, power, GNR, ST, and DU), the parameters for analysis are chosen. It is clear from Figure 3.5 that, for a simple energy pricing, the energy cost is the most significant, making it the first parameter to be analyzed.

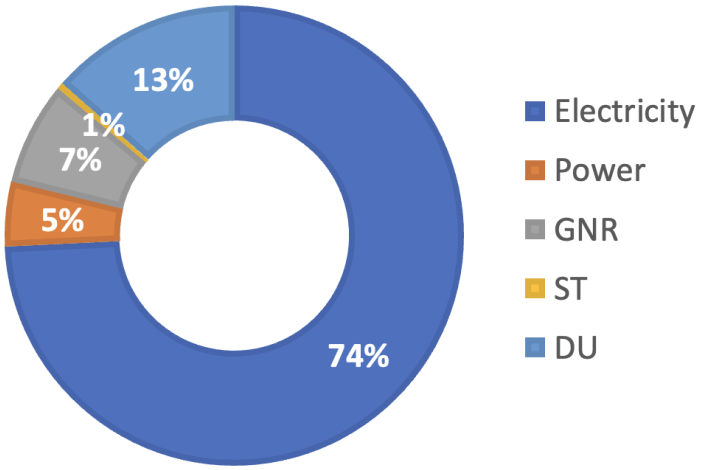


Figure 3.5: Distribution of the total cost at ATH

Although the study uses the standard energy tariff for non-domestic users, it is plausible that electricity tariffs will be negotiated directly with the supplier for energy-intensive users such as the plant under investigation, leading to considerable discounts. Hence, simulations will be performed by gradually decreasing the energy tariff from the standard tariff to a 50% discount (resulting in a cost of 28.28€/MWh) while keeping the MDD schedule constant.

Table 3.3 displays the tariffs used in each simulation, and the resulting total plant cost; while Figure 3.6 illustrates the cost percentages of the various elements as the energy tariff decreases.

Table 3.3: ATH sensitivity analysis: total cost

| Case | A | B | C | D | E | F |
|---|---|---|---|---|---|---|
| **Discount** | 0% | -10% | -20% | -30% | -40% | -50% |
| **Tariff** [€/MWh] | 56.57 | 50.91 | 45.26 | 39.60 | 33.94 | 28.28 |
| **Total cost** | € 39 035 | € 36 135 | € 33 236 | € 30 337 | € 27 436 | € 24 536 |

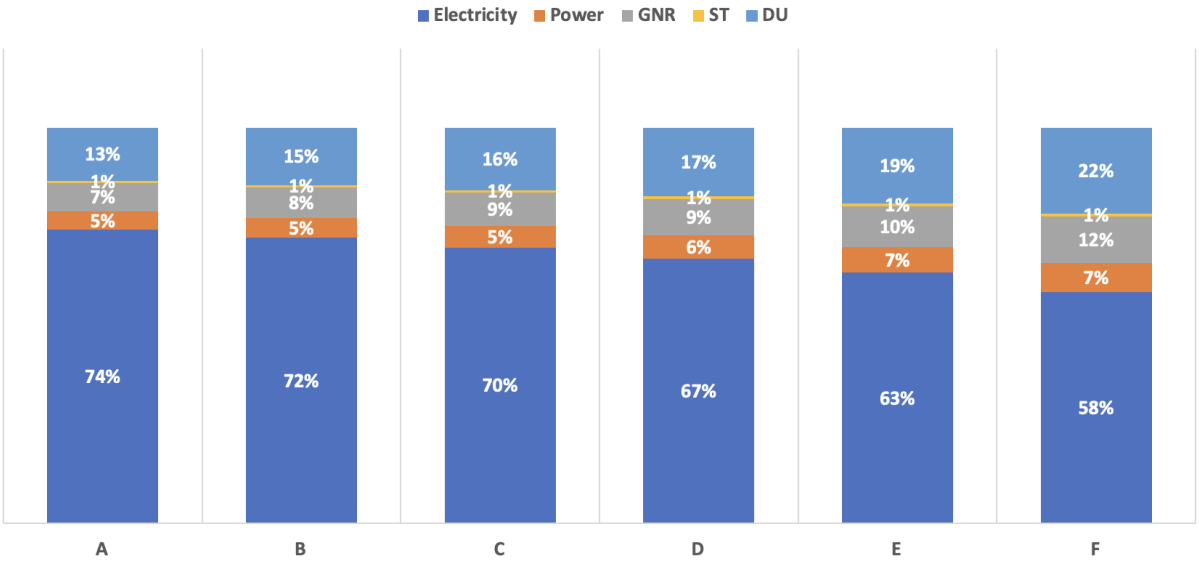


Figure 3.6: ATH sensitivity analysis: distribution of the total cost

Hence, an energy rebate can have a substantial impact on the total cost of the plant, in this case, the cost decreases from € 39 035 in the first scenario to € 24 536 euros in case F, resulting in a reduction of 37%. As a result, the cost per kilogram of hydrogen drops to € 2.97 when the energy tariff is cut in half.

Moving to a bi-hourly energy tariff, the parameter that can be varied becomes the percentage discount between the low and high-cost tariffs. In the current scenario, a 20% discount is applied during nighttime hours. This tariff has resulted in the generator prioritizing production during nighttime hours. However, even if the discount during night hours is reduced to 15% or 10%, this tendency persists (although in the second case it slightly increases production during daily hours). Finally, if the discount is reduced to less than 10%, the production is spread over the entire 24-hour period, as was the case with simple pricing. This is because the savings from nighttime production are not significant enough to offset the rising cost of a larger power consumption and a bigger ST.

Hence, it can be concluded that, for tariffs with nighttime discounts below 10%, there is no advantage to choosing a bi-hourly pricing system over a simple tariff for electricity.

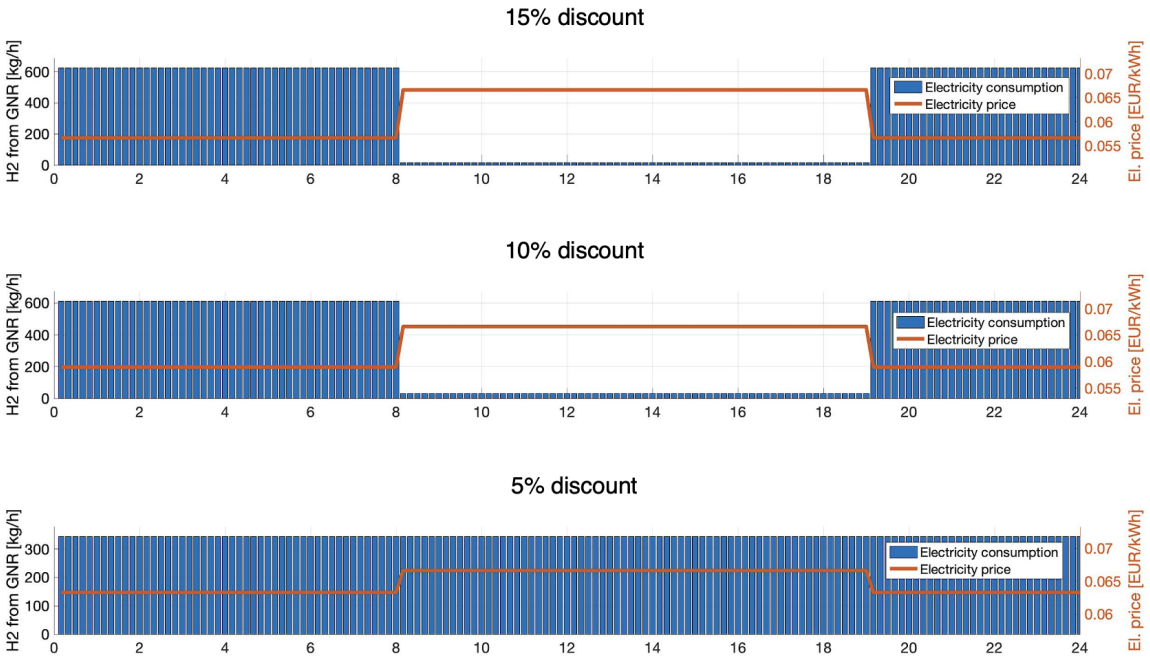


Figure 3.7: ATH sensitivity analysis: bi-hourly tariff percentage discount

According to the analysis of cost distribution, the cost of dispensing units in the Athens Airport case is another significant factor. Although the estimated cost of these units ranges from €2 400 000 to €4 000 000, simulations indicate that modifying the DU cost parameter would not have a significant impact on the final outcomes. Any changes in the overall cost would be equivalent to the changes made to the DU cost parameter, which would not significantly affect any other parameter. This also holds true, for changes in the cost of generator or storage tanks. Thus, the analysis concludes that only the energy cost parameters can significantly impact the results. As a result, the methodology employed is robust to cost estimate variations, and the results obtained are fairly reliable.

### 3.1.3. Impact of a self-generation energy plant

Among the more common and widely applicable renewable energy projects at airport sites are photovoltaic (PV) systems, which convert sunlight into electricity. PV systems are well-suited for many existing airport designs due to the vast horizontal surfaces on which they can be installed. They can be mounted on terminal buildings or placed on new or otherwise unproductive airport property. Some airports have even used the harnessed

solar energy to power ground vehicles or to deploy charging stations for electric cars in parking areas [72]. Especially in Athens, which is one of the sunniest cities in Europe [73], a PV system could be an extremely favorable option.

In this section, an initial evaluation will be performed on the size of the plant and the percentage of energy that must be self-generated to realize an economic benefit in the production cost of hydrogen, consequently decreasing dependence on the national electricity network. The source of the cost estimates used in this analysis is the "Renewable Power Generation Cost in 2020" report by IRENA [74]. The estimation begins with determining the procurement cost of the PV plant, which is dependent on the power generation capacity and is approximately $\$\,883/\text{kW}$ (equivalent to $€\,799/\text{kW}$), denoted as $c^{\text{PV}}$. To this, the operational and maintenance costs are added, which, in OECD (i.e., Organisation of Economic Co-operation and Development) member countries, of which Greece is a member, are estimated at $\$\,17.8/(\text{kW year})$, equivalent to $€\,16.1/(\text{kW year})$. This value will be denoted by $c^{\text{PV}}_{\text{O\&M}}$. The quantity of energy generated by the plant, as well as its power output, will also depend on the amount of sunshine hours available for energy conversion. In Athens, the average duration of sunshine per day ($h^{\text{ATH}}_{sun}$) is approximately 7.5 hours [75].

The daily cost of a photovoltaic system, based on the amount of energy it can produce ($E^{\text{PV}}$), is equal to:

$$C^{\text{PV}} = \frac{E^{\text{PV}}}{h^{\text{ATH}}_{sun}} \left( \frac{c^{\text{PV}}\, d}{d^{\text{PV}}} + \frac{c^{\text{PV}}_{\text{O\&M}}\, d}{365} \right). \tag{3.1}$$

where the first factor in the equation calculates the power required for the plant. The parameter $d^{\text{PV}}$, indicates the expected lifespan of the plant in days. In this case, it was set equal to 20 years.

At this point, it is assumed that a percentage of the energy required by the system will be generated by the photovoltaic system, while the remaining portion will still be purchased from the national power grid.

The cost of producing one kilogram of hydrogen is illustrated in Figure 3.8 as the proportion of energy generated by the photovoltaic system varies. It is evident from the figure that producing almost 75% of energy from renewable sources is essential to meet the 2025 target of achieving a production cost of $\$\,2/\text{kg}$ (almost $€\,1.83/\text{kg}$).

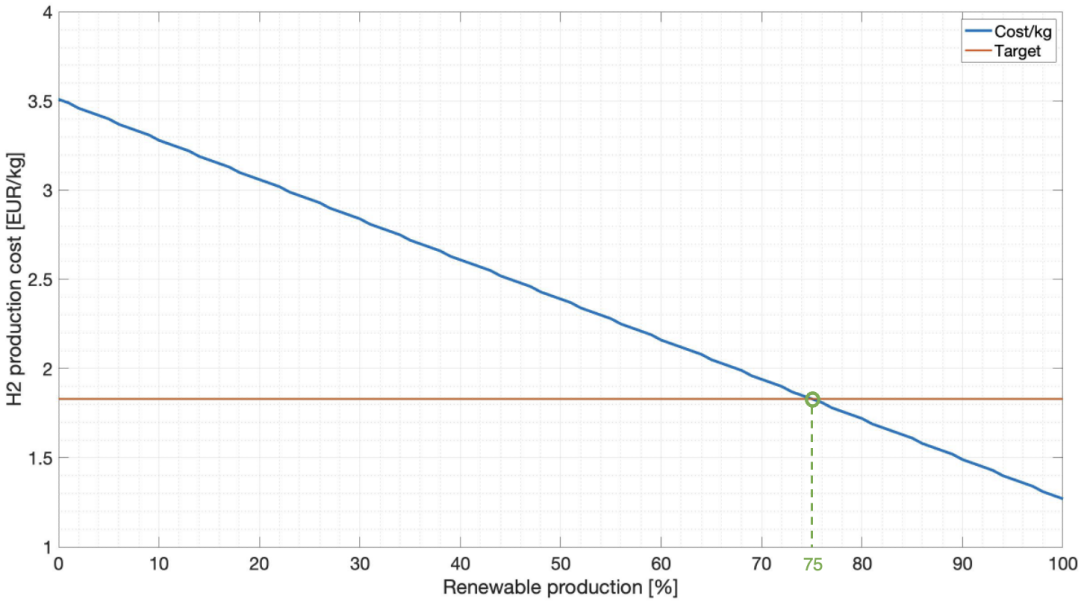


Figure 3.8: Cost of H2 production per kg changes with the rate of PV energy generation

Using the equations provided earlier, it can be deduced that the PV plant needs to have a capacity of around 51.25 MW. A photovoltaic system capable of producing 1 MW of power requires approximately 6 acres of land [76]. Therefore, a system designed for this purpose would occupy around 307 acres, which means 1.25 square kilometers. Figure 3.9 illustrates the size of this plant (represented by a yellow rectangle) in comparison to Athens Airport.

Figure 3.9: Size of the solar farm compared to the Athens Airport

## 3.2. Milan Malpensa Airport

The same analysis conducted for Athens airport in Section 3.1 will be applied here to Malpensa Airport. However, since short-haul flights will be considered at this airport, there will be a higher volume of traffic with longer flights operated by jet aircraft, which, as shown in Section 2.1, have higher fuel consumption than turboprops. The combination of these factors results in a significantly higher demand for hydrogen.

The analysis starts with considering the MDD schedule and simple energy pricing. Figure 3.10 represents the distribution of takeoffs during the day. Figure 3.11 shows the operation of the various elements of the system in this case. Then, a bi-hourly energy pricing is considered, and the simulation results are depicted in Figure 3.12. The trend observed in both simulations is similar to the one observed in the Athens Airport case. However, the facility's costs and performance requirements differ significantly between the two airports, as can be seen by comparing Table 3.4 and 3.1.

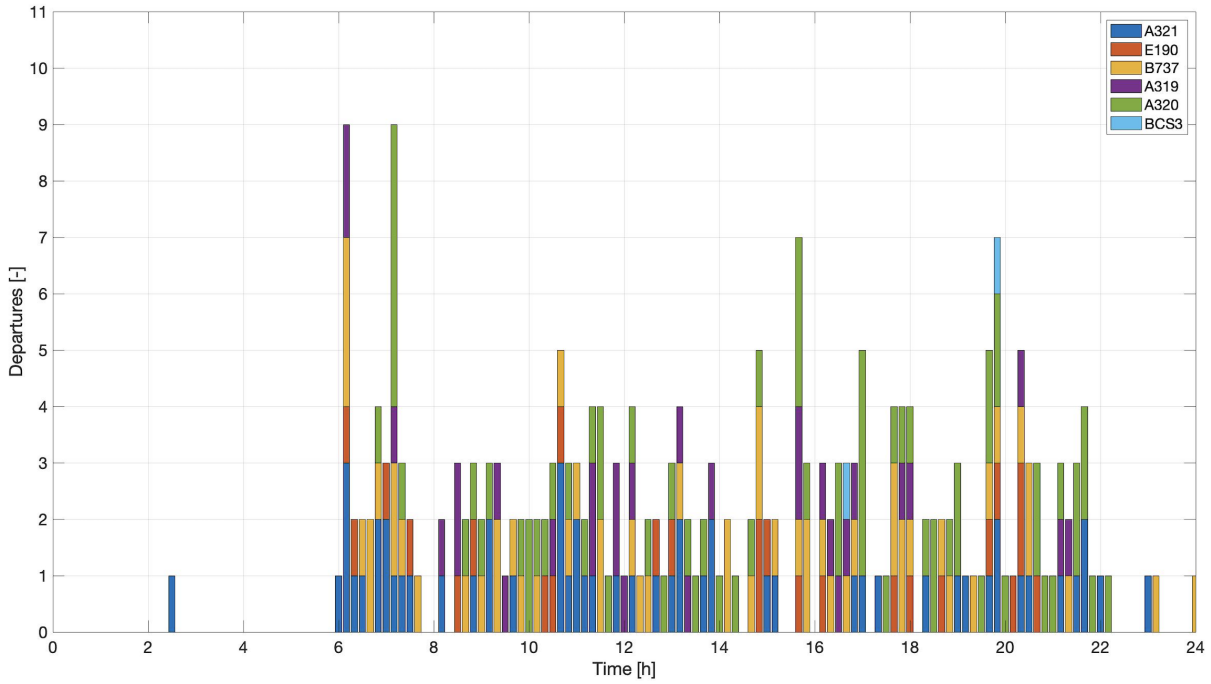


Figure 3.10: Takeoffs in Malpensa Airport on MDD

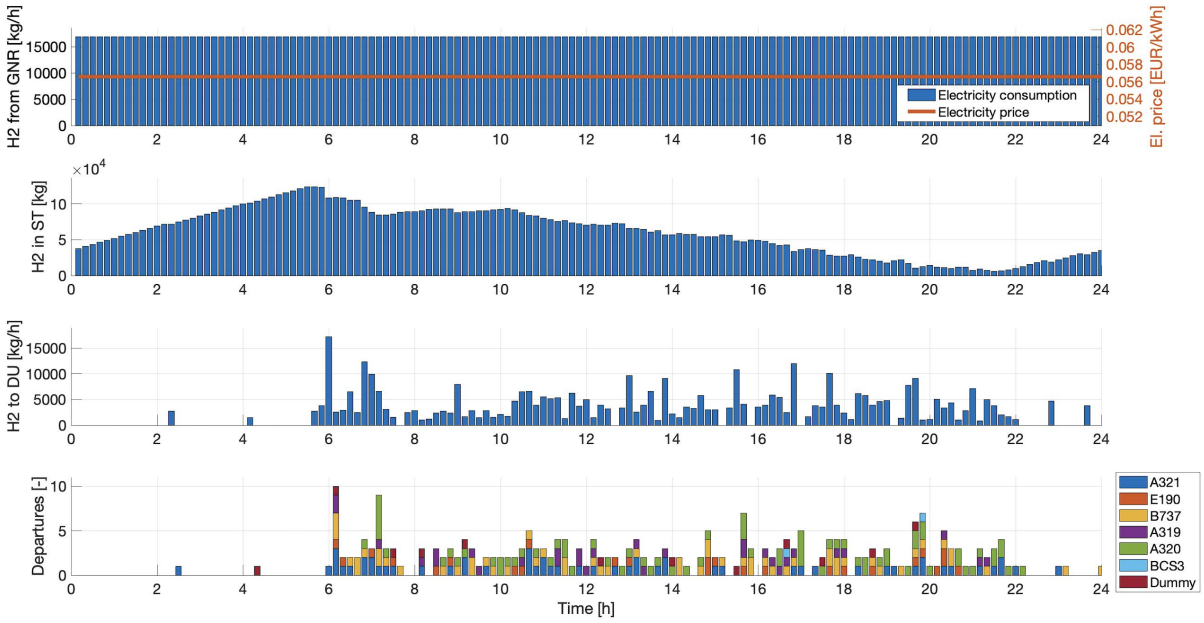


Figure 3.11: Results on MDD at MXP Airport with a simple electricity tariff

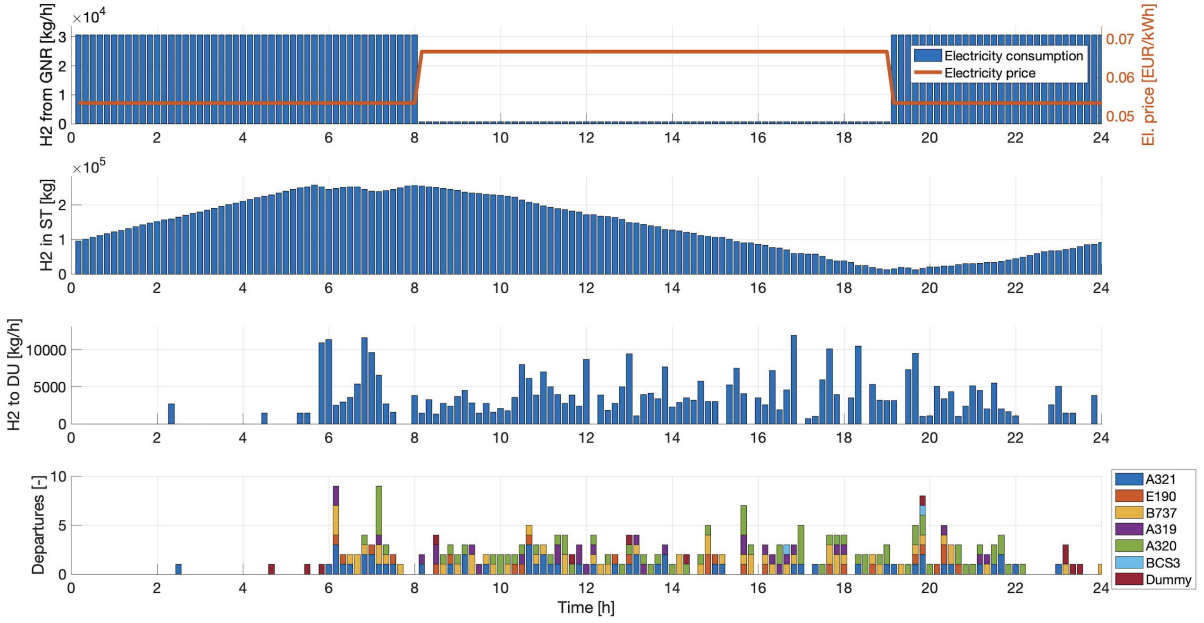


Figure 3.12: Results on MDD at MXP Airport with a bi-hourly electricity tariff

Table 3.4: Malpensa Airport on MDD: results

| | Simple tariff | Bi-hourly tariff | Change |
|---|---|---|---|
| Ele. consumption | 25 228 000 kWh | 25 311 000 kWh | 0.3% |
| Ele. cost | €1 427 200 | €1 357 600 | -5.1% |
| Power absorbed | 1 054 560kW | 1 906 700 kW | |
| Power cost | €87 880 | €159 400 | 44.9% |
| LH2 production | 406 901 kg/d | 408 250 kg/d | |
| GNR cost | €139 350 | €139 810 | 0.3% |
| Max mass in ST | 123 950 kg | 257 740 kg | |
| ST cost | €6 792 | €14 123 | 51.9% |
| No. of DU | 9 | 9 | |
| DU cost | €9 468 | €9 468 | 0.0% |
| Total cost | €1 670 648 | €1 680 500 | 0.6% |
| Cost per kg of LH2 | €4.10 | €4.12 | 0.5% |

Comparing the variances observed by switching to a bi-hourly energy pricing with those of the Athens Airport case, it was found that the savings in energy costs and the increase in power costs are approximately the same. However, the tank size increased more substantially, leading to a slightly higher cost per kilogram of hydrogen for Malpensa, at 0.5%, as opposed to 0.2% for Athens.

### 3.2.1. Off-design analysis

Off-design analysis is now performed for Malpensa Airport, which includes two scenarios. In Case A, the facility is sized based on the LDD demand (takeoff distribution throughout the day is depicted in Figure 3.13), while in Case B, a facility sized according to the MDD demand is utilized for LDD. Table 3.5 presents a comparison of the primary results for both cases.

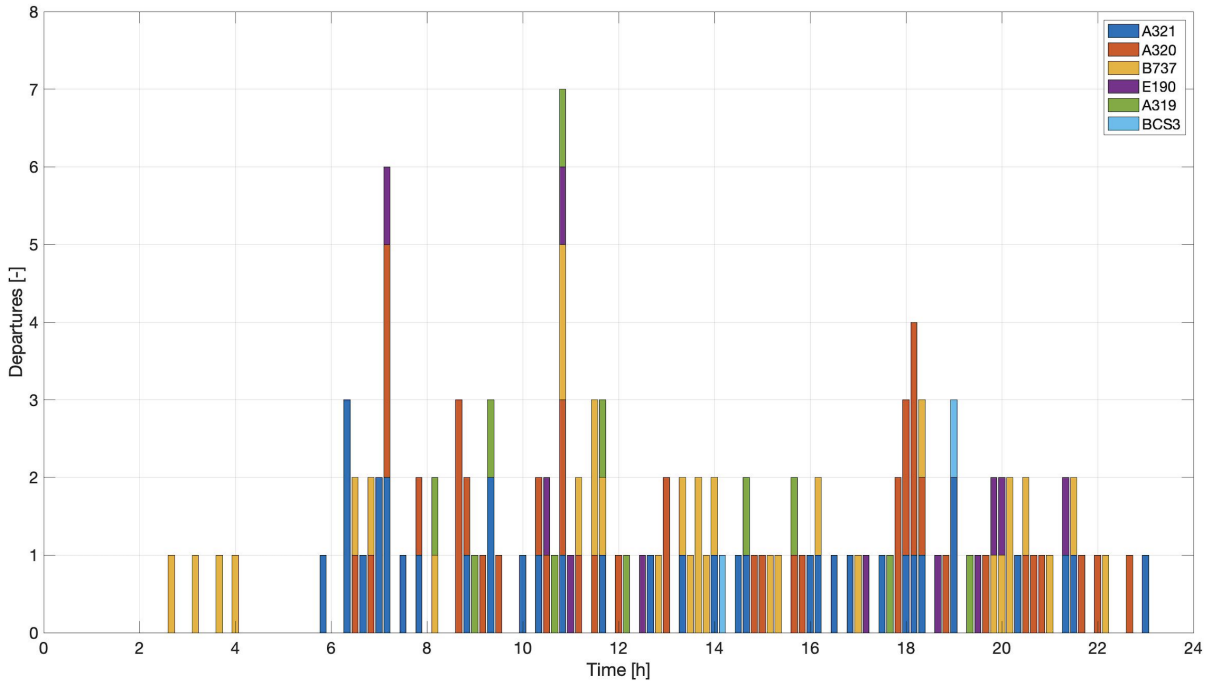


Figure 3.13: Takeoffs in Malpensa Airport on LDD

Table 3.5: MXP off-design analysis: results

| | **Case A** | **Case B** | **Change** |
|---|---|---|---|
| Ele. consumption | 15 456 000 kWh | 15 485 000 kWh | |
| Ele. cost | €874 330 | €875 980 | 0.2% |
| Power absorbed | 646 056 kW | 647 980 kW | |
| Power cost | €53 838 | €53 940 | 0.2% |
| LH2 production | 249 290 kg/d | 249 760 kg/d | |
| GNR cost | €85 372 | €139 350 | 38.7% |
| Max mass in ST | 76 958 kg | 123 950 kg | |
| ST cost | €4 217 | €6 792 | 37.9% |
| No. of DU | 7 | 10 | |
| DU cost | €7 364 | €10 521 | 30.0% |
| Total cost | €1 025 700 | €1 086 600 | 5.6% |
| Cost per kg of LH2 | €4.11 | €4.35 | 5.4% |

In contrast to the Athens Airport case, a relatively smaller difference is observed between cases A and B, particularly considering the cost per kg of hydrogen, which is the most crucial parameter in the analysis. In this case, the increase is only 5.4%, compared to the 24.1% increase seen in the Athens case. This disparity can be attributed to the fact that the Malpensa Airport experiences a much smaller variation of flights between high and low seasons. Specifically, the total number of kilometers flown at Malpensa drops from 263 802 to 158 965 (a reduction of 40%), whereas the Athens airport saw a reduction of 67%.

### 3.2.2. Sensitivity analysis

In this section, a sensitivity analysis will be conducted. Figure 3.14 depicts the distribution of the plant costs with a simple pricing tariff for electricity. Similarly to the Athens case, the energy cost represents almost all of the plant's total costs, and this is even more pronounced here. Therefore, simulations are performed by modulating the energy pricing. Table 3.6 presents the tariffs utilized in the different cases and the corresponding total cost of the resulting plant. Figure 3.15 illustrates the distribution of costs among the five items in each scenario.

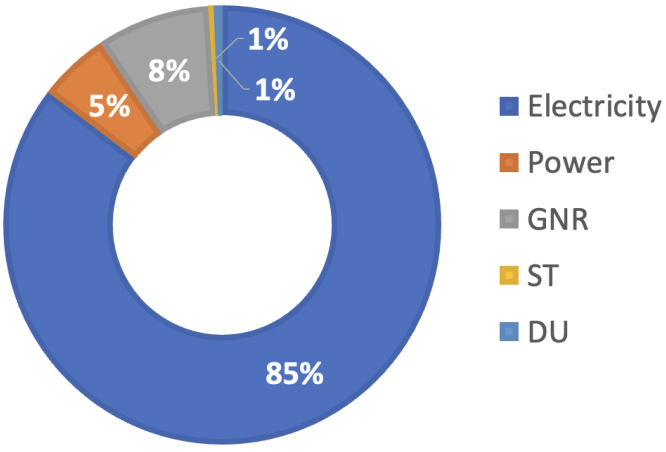


Figure 3.14: Distribution of the total cost at MXP

Table 3.6: MXP sensitivity analysis: total cost

| Case | A | B | C | D | E | F |
|---|---|---|---|---|---|---|
| **Discount** | 0% | -10% | -20% | -30% | -40% | -50% |
| **Tariff** [€/MWh] | 56.57 | 50.91 | 45.26 | 39.60 | 33.94 | 28.28 |
| **Total cost** | € 1 673 317 | € 1 530 521 | € 1 387 977 | € 1 245 182 | € 1 102 386 | € 959 464 |

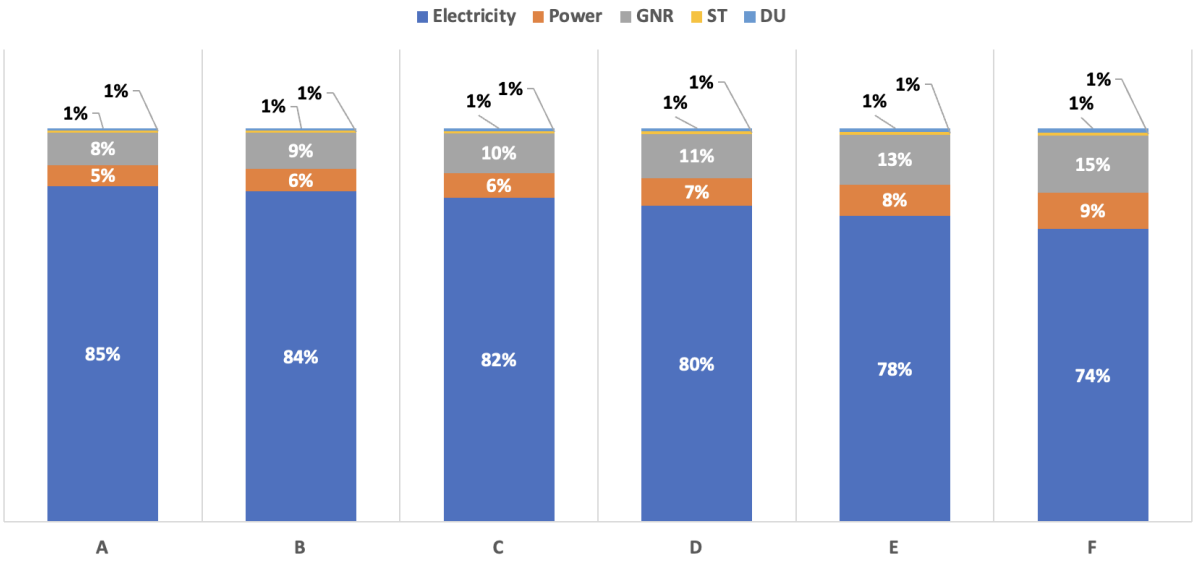


Figure 3.15: MXP sensitivity analysis: distribution of the total cost

Similarly as before, a significant reduction in plant costs can be achieved in this scenario through an energy discount. The plant cost drops from €1 673 317 in the first case to €959 464 in case F, a reduction of 43%. This cost reduction then results in a decrease in the cost per kilogram of hydrogen, which drops to €2.35 when the energy tariff is cut in half.

The analysis now shifts to the case of a bi-hourly tariff, where the percentage discount on energy that occurs at nighttime hours will be varied. Similar to the Athens case discussed in Section 3.1.2, the production is still limited to nighttime hours even when the discount is reduced from 20% to 15%. However, in the Malpensa case, reducing the rebate to 10% already results in a continuous production during the day. Therefore, it can be concluded that a bi-hourly tariff would be even less advantageous in the Malpensa case and should be avoided if the discount during night hours is less than 15%.

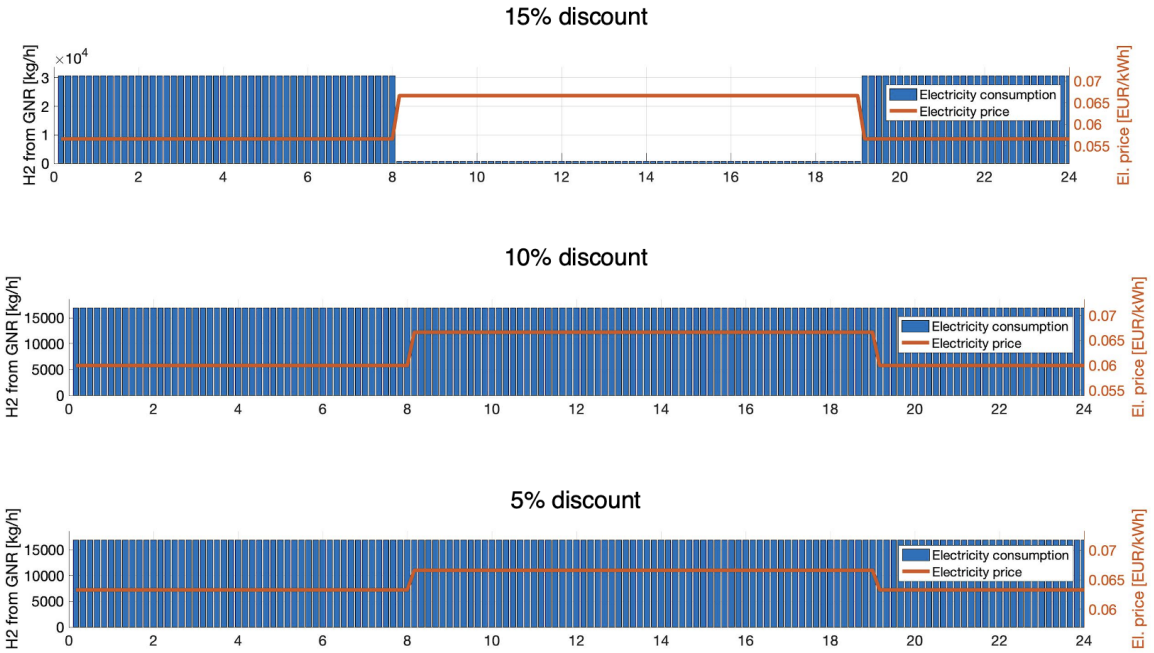


Figure 3.16: MXP sensitivity analysis: bi-hourly tariff percentage discount

## 3.3. Parigi Charles De Gaulle Airport

Concluding, the results obtained for Paris Charles De Gaulle Airport are examinated here. Although only short-haul flights operated by jet-powered aircraft are also considered here, it is worth noting that the airport has a significantly higher number of flights compared to Malpensa Airport. Figure 3.17 provides an overview of the distribution of flights in the MDD, revealing 452 flights covering a total distance of 513 344 km, representing a 94% increase compared to Malpensa.

Despite the higher traffic volume, the facility's performance is similar to what has been observed in previous cases, under both simple and biorary tariff scenarios (Figure 3.18 and 3.19, respectively). Further analysis of the results presented in Table 3.7 indicates that also the cost per kilogram of hydrogen remains almost the same as that of Malpensa.

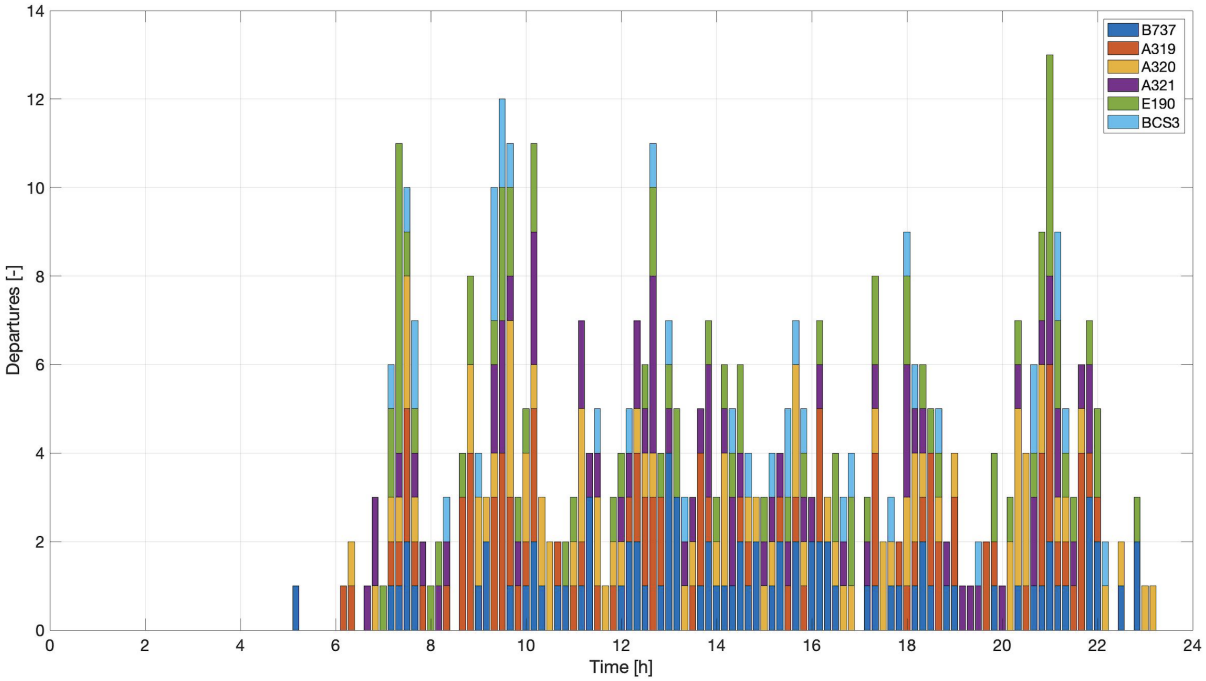


Figure 3.17: Takeoffs in Charles De Gaulle Airport on MDD

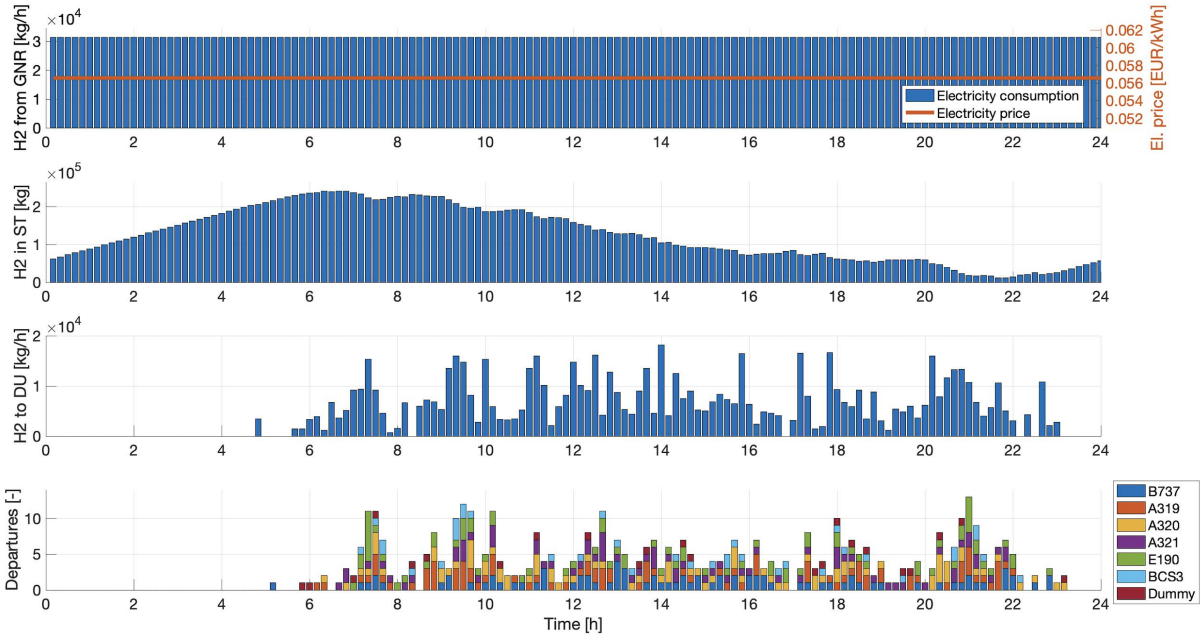


Figure 3.18: Results on MDD at CDG Airport with a simple electricity tariff

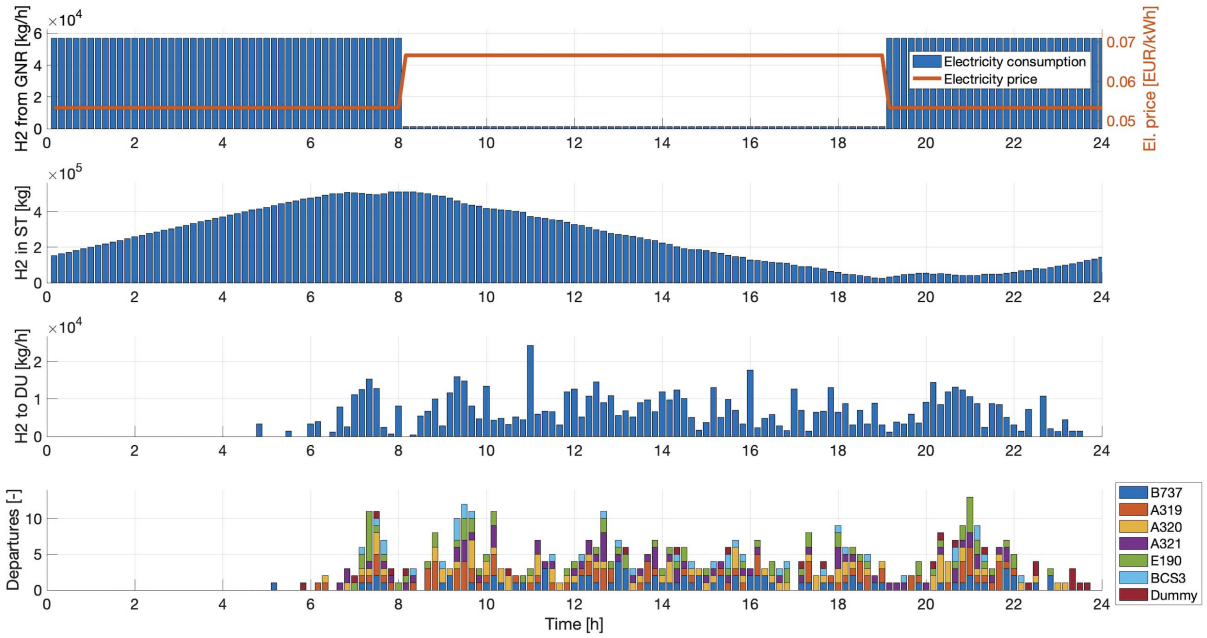


Figure 3.19: Results on MDD at CDG Airport with a bi-hourly electricity tariff

Table 3.7: Charles De Gaulle Airport on MDD: results

| | **Simple tariff** | **Bi-hourly tariff** | **Change** |
|---|---|---|---|
| Ele. consumption | 46 838 000 kWh | 47 007 000 kWh | |
| Ele. cost | €2 649 700 | €2 521 200 | -5.1% |
| Power absorbed | 1 957 920 kW | 3 541 000 kW | |
| Power cost | €163 160 | €296 030 | 44.9% |
| LH2 production | 755 460 kg/d | 758 170 kg/d | |
| GNR cost | €258 720 | €259 650 | 0.4% |
| Max mass in ST | 241 110 kg | 512 380 kg | |
| ST cost | €13 211 | €28 076 | 52.9% |
| No. of DU | 13 | 13 | |
| DU cost | €13 677 | €13 677 | 0.0% |
| Total cost | €3 098 000 | €3 119 000 | 0.7% |
| Cost per kg of LH2 | €4.10 | €4.11 | 0.2% |

### 3.3.1. Airport simulation with long-term traffic forecasts

In order to assess the cost of the facility in the future, the latest analysis will consider the forecast of the expected growth of the aviation sector. Charles De Gaulle Airport, one of the world's busiest airports, will be specifically examined in this analysis.

The analysis begins with an examination of worldwide traffic trend forecasts, particularly for France, conducted by EUROCONTROL in Aviation Outlook 2050 [77]. The report predicts a yearly increase of about 0.7% in air traffic for France, as with many central European countries, in the coming years. This would result in nearly 25% more traffic by 2050, a year that represents an important milestone in the decarbonization process of the aviation sector. The assumption is made that CDG will experience the same growth as France.

Using the AHRES methodology, the daily cost of the hydrogen plant is then estimated for future scenarios concurrent with the predicted growth. Figure 3.20 shows that the daily cost growth increases almost linearly with traffic growth. All the same, the slope of the straight line would appear to decrease for increasing numbers of flights. However, the resulting cost per kilogram of hydrogen is, except for slight fluctuations, stable at the value of €4.1/kg in all cases considered.

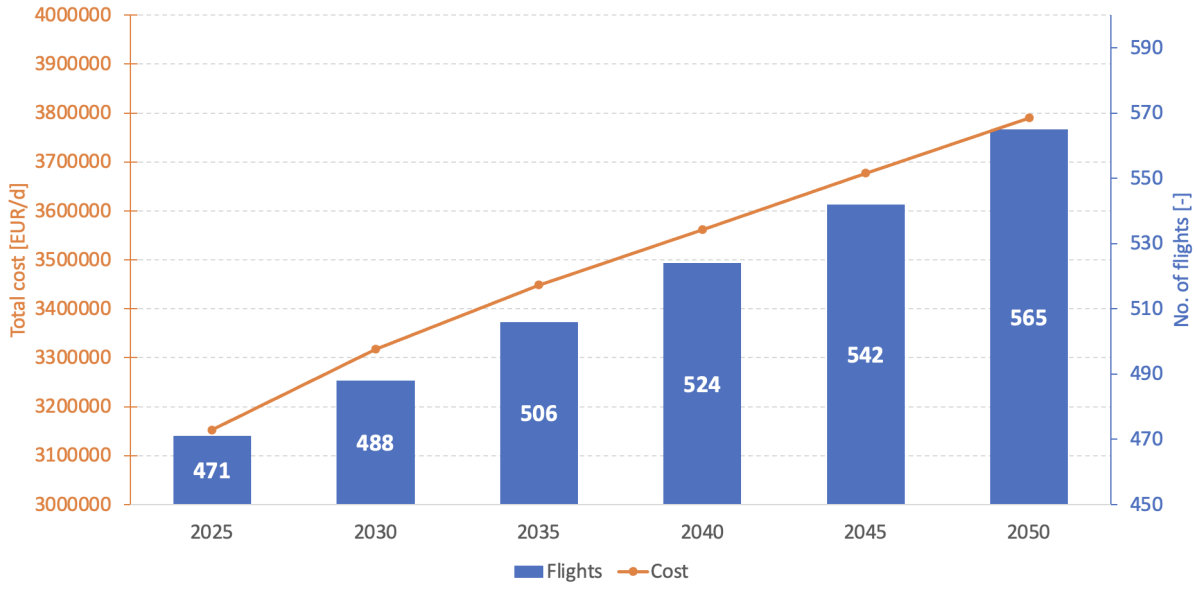


Figure 3.20: Forecast of cost trend at CDG in the next years

# Conclusion and future developments

In this thesis, a methodology able to size the infrastructure in support of liquid hydrogen-powered aircraft has been developed. It is based on suitable models of the generator, storage tank, dispensing units and aircraft properties, and on the flight schedule at the target airport. An optimization is performed in order to find the infrastructural needs to perform smooth operations, minimizing the total cost.

Some of the main conclusions drawn from the study can be summarized as follows:

- In all the cases considered, energy is the predominant cost item, primarily due to the energy expenditure required for the production of hydrogen through water electrolysis. The plant, therefore, requires a power grid that can supply the energy needed to meet the production demand. However, it is mandatory that power generation be zero-emission, so as not to negate the ecological benefit of adopting hydrogen propulsion.
- All elements of the plant requires much greater performance than currently exists. However, this should not be seen as a limitation, but highlights the need for fast technological development that can ensure the necessary performance of ground facilities in time for large-scale adoption of hydrogen-powered aircraft.
- Looking at the main value that allows summarizing the economic burden of this revolution, i.e. the cost per kilogram of hydrogen, this seems to decrease when the production of hydrogen increases in the Athens case. Indeed here, moving from the LDD to the MDD, where the daily production is tripled, there is a decrease in the parameter of 6%. However, going from the Athens case to the Malpensa case, where the production is 30 times greater, the parameter decreases by only 13%, going from €4.71 to €4.11. Then, a further increase in production shows that there is no longer any decrease in the cost per kilogram, and it settles around the value of €4.10 for all subsequent simulations. This suggests that from a certain point onward, the amount of production becomes insignificant in influencing the cost per kilogram. Hence, reducing the parameter can only be achieved by acting on the energy cost, which, from sensitivity analyses, appears to be the only one that truly influences

the final results. So in order to reduce the cost per kilogram and reach the expected value of $ 1/kg in one decade, it is necessary to lower energy costs by reducing the energy requirements of the production plant or by lowering energy costs, e.g. by producing part of the energy on-site with renewable systems.

- Regarding energy pricing, there tends to be no significant benefit in using bi-hourly pricing, other than a small decrease in energy costs. However, the adoption of this tariff would require even larger elements and thus even higher costs for the plant. Furthermore, there would be no advantage whatsoever if the discount at nighttime were to fall below a certain proportion (20-15%).

Future analyses should address the other solutions that were not explored in this study. Starting with the generation plant, it could be considered serving several airports, not too far apart, with a single generation plant that could meet the demand of all of them. However, this solution would require the resolution of several new requirements, starting with the need to ensure an efficient distribution of hydrogen to the airports. This solution could be advantageous, especially for not-too-large airports that would not benefit from as large an investment as that required for on-site hydrogen production. Another aspect that should be analyzed further is the storage system. Depending on the airport's needs, it might be advantageous to consider several smaller tanks instead of one large tank. Depending on the layout and size of the airport, there could be one main tank operating throughout the year and one or more secondary tanks that only enter into service when demand is greatest. Or multiple tanks, that fill in parallel, placed at strategic points in the airport. Another key aspect to investigate is the hydrogen distribution system within the airport. Especially for large airports, distribution via tanker trucks is not advantageous, but a pipeline system should be considered. However, this system cannot be adopted until the technology required for cryogenically sealed pipelines is sufficiently mature.

In general, this work could be improved in the future by using more accurate input data, particularly regarding airport requirements and cost estimation. The goal of this work is not to offer definitive and certain data, but to provide a first approximation of the scale of such a facility and, more importantly, a practical tool that can be customized to specific requirements due to its remarkable adaptability and versatility, which allows it to go beyond civil airports to include private airfields and military bases as well.

# Bibliography

[1] Sources and emissions of air pollutants in europe. Technical report, European Environment Agency, November 2022.

[2] Younseok Choi and Jinkwang Lee. Estimation of liquid hydrogen fuels in aviation. *Aerospace*, 9(10):564, 2022.

[3] Clean Sky et al. Hydrogen-powered aviation: A fact-based study of hydrogen technology, economics, and climate impact by 2050. page 17.

[4] European Commission, Directorate-General for Mobility, Transport, Directorate-General for Research, and Innovation. *Flightpath 2050 : Europe's vision for aviation : maintaining global leadership and serving society's needs*. Publications Office, 2011.

[5] A Contreras, S Yiğit, K Özay, and TN Veziroğlu. Hydrogen as aviation fuel: a comparison with hydrocarbon fuels. *International Journal of Hydrogen Energy*, 22(10-11):1053–1060, 1997.

[6] Karen Kwon. Hydrogen: coming to an aircraft near you. *AEROSPACE AMERICA*, 60(7-8), 2022.

[7] Clean Sky et al. Hydrogen-powered aviation: A fact-based study of hydrogen technology, economics, and climate impact by 2050. 2020.

[8] Bryan S Pivovar, Mark F Ruth, Deborah J Myers, and Huyen N Dinh. Hydrogen: targeting $1/kg in 1 decade. *The Electrochemical Society Interface*, 30(4):61, 2021.

[9] Linda Capuano. Annual energy outlook 2019. *Washington, DC: US Energy Information Administration*, 2019.

[10] Julian Hoelzen, M Flohr, Daniel Silberhorn, Jonas Mangold, A Bensmann, and Richard Hanke-Rauschenbach. H2-powered aviation at airports–design and economics of lh2 refueling systems. *Energy Conversion and Management: X*, 14:100206, 2022.

[11] Airbus. Zero emission journey. https://www.airbus.com/en/innovation/zero-emission-journey/hydrogen/zeroe.

[12] H2FLY. https://www.h2fly.de.

[13] Carrie Hampel. H2fly  stuttgart airport to build centre for h2 aviation. *electrive*, 01 2023.

[14] Ginger Gardiner. Universal hydrogen uses dry braided carbon preform tanks as part of plan to decarbonize aviation. *CompositesWorld*, 2020.

[15] Mitch Jacoby. Fuel-cell cars finally drive off the lot. *Chem. Eng. News Arch*, 95:28, 2017.

[16] J Trainor and D Joyce. Capitol hyundai of san jose celebrates first fuel cell customer delivery in northern california. *Hyundai News*, 2016.

[17] Remzi Can Samsun, Michael Rex, Laurent Antoni, and Detlef Stolten. Deployment of fuel cell vehicles and hydrogen refueling station infrastructure: a global overview and perspectives. *Energies*, 15(14):4975, 2022.

[18] H2iseo hydrogen valley. *FNMgroup.com*, 2021.

[19] Ahmed G Elkafas, Massimo Rivarolo, Eleonora Gadducci, Loredana Magistri, and Aristide F Massardo. Fuel cell systems for maritime: A review of research development, commercial products, applications, and perspectives. *Processes*, 11(1):97, 2022.

[20] Steel production with green hydrogen at dalmine plant in italy. *Techint.com*, 2021.

[21] Clean Sky et al. Hydrogen-powered aviation: A fact-based study of hydrogen technology, economics, and climate impact by 2050. pages 24–25.

[22] Jennifer Kurtz, Sam Sprik, and Thomas H Bradley. Review of transportation hydrogen infrastructure performance and reliability. *International Journal of Hydrogen Energy*, 44(23):12010–12023, 2019.

[23] A Garcia Garriga, Giusi Quartarone, Siena Iovino, Lorenzo Trainelli, Alberto Rolando, CED Riboldi, Costanza Mariani, Mauro Mancini, et al. An overview of the scalability investigation of hybrid electric concepts for next-generation aircraft (siena) project. In *11th EASN International Conference*, 2021.

[24] Canan Acar and Ibrahim Dincer. Review and evaluation of hydrogen production options for better environment. *Journal of cleaner production*, 218:835–849, 2019.

[25] Youssef Naimi and Amal Antar. Hydrogen generation by water electrolysis. *Advances in hydrogen generation technologies*, 1:3, 2018.

[26] Cevahir Tarhan and Mehmet Ali Çil. A study on hydrogen, the clean energy of the future: Hydrogen storage methods. *Journal of Energy Storage*, 40:102676, 2021.

[27] Sean M Riedl. Development of a hydrogen refueling station design tool. *International Journal of Hydrogen Energy*, 45(1), 2020.

[28] U.S. Department of Energy, Office of Energy Efficiency Renewable Energy. Hydrogen Production: Basics. `https://www.energy.gov/eere/fuelcells/hydrogen-production-basics`, 2021.

[29] National Renewable Energy Laboratory. Handbook for Handling, Storing, and Dispensing Hydrogen. Technical Report NREL/TP-5400-73433, 2020.

[30] Clean Hydrogen Annex to GB decision no. CleanHydrogen-GB-2022-02. Strategic research and innovation agenda 2021–2027, 2 2022.

[31] A Krenn and D Desenberg. Return to service of a liquid hydrogen storage sphere. In *IOP Conference Series: Materials Science and Engineering*, volume 755. IOP Publishing, 2020.

[32] Demaco Hydrogen. Liquid hydrogen storage: increasingly larger storage tanks, 2021.

[33] NCE Maritime CleanTech. Norwegian future value chains for liquid hydrogen. *Report. URL: https://maritimecleantech. no/wp-content/uploads/2016/11/Report-liquid-hydrogen. pdf*, pages 26–27, 2019.

[34] G Daniel Brewer. *Hydrogen aircraft technology*. Routledge, 2017.

[35] Jiaojiao Wang, Yanzhong Li, Lei Wang, Siqi Xia, Jianhua Ren, Hongwei Mao, and Yuanyuan Xu. Numerical investigation on subcooled pool film boiling of liquid hydrogen in different gravities. *International Journal of Hydrogen Energy*, 46(2), 2021.

[36] Saif ZS Al Ghafri, Adam Swanger, Vincent Jusko, Arman Siahvashi, Fernando Perez, Michael L Johns, and Eric F May. Modelling of liquid hydrogen boil-off. *Energies*, 15(3), 2022.

[37] Wade A Amos. Costs of storing and transporting hydrogen. Technical report, National Renewable Energy Lab.(NREL), Golden, CO (United States), 1999.

[38] Fardin Ghaffari-Tabrizi, Jan Haemisch, and Daniela Lindner. Reducing hydrogen boil-off losses during fuelling by pre-cooling cryogenic tank. *Hydrogen*, 3(2), 2022.

[39] Artur Bauer, Thomas Mayer, Malte Semmel, Martin Alberto Guerrero Morales, and

Joerg Wind. Energetic evaluation of hydrogen refueling stations with liquid or gaseous stored hydrogen. *International Journal of Hydrogen Energy*, 44(13), 2019.

[40] A Kalanidhi. Boil-off in long-term stored liquid hydrogen. *International journal of hydrogen energy*, 13(5), 1988.

[41] WU Notardonato, AM Swanger, JE Fesmire, KM Jumper, WL Johnson, and TM Tomsik. Zero boil-off methods for large-scale liquid hydrogen tanks using integrated refrigeration and storage. In *IOP conference series: materials science and engineering*, volume 278. IOP Publishing, 2017.

[42] Adam Swanger. world's largest liquid hydrogen tank nearing completion. *Cold Facts*, 38(2), 2022.

[43] Office of Environmental Health and Safety. Cryogenic liquid safety: Hazards and safe handling of cryogenic liquids. *Wayne State University*, 2023.

[44] Craig A Stephens, Gregory J Hanna, and Leslie Gong. Thermal-fluid analysis of the fill and drain operations of a cryrogenic fuel tank. In *SEM Structural Testing Technology at High Temperature 2 Conference*, number NASA-TM-104273, 1993.

[45] L Jones, C Wuschke, and TZ Fahidy. Model of a cryogenic liquid-hydrogen pipeline for an airport ground distribution system. *International journal of hydrogen energy*, 8(8), 1983.

[46] Jean André, Stéphane Auray, Jean Brac, Daniel De Wolf, Guy Maisonnier, Mohamed-Mahmoud Ould-Sidi, and Antoine Simonnet. Design and dimensioning of hydrogen transmission pipeline networks. *European Journal of Operational Research*, 229(1), 2013.

[47] Christopher Yang and Joan Ogden. Determining the lowest-cost hydrogen delivery mode. *International Journal of Hydrogen Energy*, 32(2), 2007.

[48] Lois Benquet. Airbus and arianegroup to pioneer liquid hydrogen technology. *Airbus Summit*, 12 2022.

[49] Frank A Grainger. Los angeles international airport. *Journal of the Air Transport Division*, 85(4), 1959.

[50] Jonas Mangold, Daniel Silberhorn, Nicolas Moebs, Niclas Dzikus, Julian Hoelzen, Thomas Zill, and Andreas Strohmayer. Refueling of lh2 aircraft—assessment of turnaround procedures and aircraft design implication. *Energies*, 15(7):20, 2022.

[51] Neutrium. https://neutrium.net/equipment/pump-power-calculation/, 2012.

[52] Jian Gan, Yanan Wang, Deming Wang, and Kang Zhang. Research on the law of head loss of jet pumps in the cavitation state. *ACS omega*, 7(15):12661–12679, 2022.

[53] E Shashi Menon. *Working Guide to Pump and Pumping Stations: Calculations and Simulations*. Gulf Professional Publishing, 2009.

[54] Lorenzo Trainelli, Francesco Salucci, Carlo ED Riboldi, Alberto Rolando, and Federico Bigoni. Optimal sizing and operation of airport infrastructures in support of electric-powered aviation. *Aerospace*, 8(2), 2021.

[55] Enel Energia for the free market. What is the pun and what is it for, 2022.

[56] Gestore Mercati Energetici, 2023.

[57] Trading Economics. Italy forecast, 2023.

[58] DIEU Direzione Infrastrutture Energia e Unbundling. Delibera 22 dicembre 2022 564/2020/r/eel. *ARERA*, 12 2022.

[59] Flight International. Guide to feederline aircraft. 1972.

[60] Massimiliano Del Grano. Master thesis: Optimal approach to the preliminary sizing of hydrogen-driven transport aircraft. *Politecnico di Milano*, 2021.

[61] Maria Chiara Massaro, Roberta Biga, Artem Kolisnichenko, Paolo Marocco, Alessandro Hugo Antonio Monteverde, and Massimo Santarelli. Potential and technical challenges of on-board hydrogen storage technologies coupled with fuel cell systems for aircraft electrification. *Journal of Power Sources*, 2023.

[62] Gabriele Sirtori. Master thesis: Environmental benefits introducing hybrid propulsion on 70 and 19-seat aircraft. *Politecnico di Milano*, 2021.

[63] Mike Menzies and CE MIChemE. Hydrogen: The burning question. *Chem. Eng*, 2019.

[64] International Air Transport Association et al. Liquid hydrogen as a potential low-carbon fuel for aviation. *International Air Transport Association: Montreal, QC, Canada*, 2019.

[65] Luca Caccetta. Master thesis: Preliminary sizing of hydrogen- burning jet aircraft. *Politecnico di Milano*, 2022.

[66] aia.gr. Athens international airport "el.venizelos" facts figures.

[67] Eurostat. Eurostat database: Airport traffic data by reporting airport and airlines.

[68] Eurocontrol. Daily traffic variation - airports (2022).

[69] Flightlabs. https://www.goflightlabs.com/e.

[70] Assaeroporti. Statistiche dati di traffico aeroportuale italiano.

[71] Union des aéroports Français. Statistiques annuelles.

[72] A ICAO. Focus on the production of renewable energy at the airport site. *Québec, Canada: International Civil Aviation Organization*, 2017.

[73] Wikipedia. List of cities in Europe by sunshine duration — Wikipedia, the free encyclopedia, 2023. [Online; accessed 13-April-2023].

[74] IRENA. Renewable power generation cost in 2020. `https://www.irena.org/-/media/Files/IRENA/Agency/Publication/2021/Jun/IRENA_Power_Generation_Costs_2020.pdf`.

[75] AP Matzarakis and VD Katsoulis. Sunshine duration hours over the greek region. *Theoretical and Applied Climatology*, 83:107–120, 2006.

[76] Transect. Solar farm land requirements. `https://www.transect.com/resources/solar-farm-land-requirements`, accessed 2023.

[77] EUROCONTROL. Eurocontrol aviation outlook 2050. page 8, 2022.

# A | Appendix A

Table A.1: Flight schedule – Athens Airport – 15th July 2022

| Time | Flight | To | IATA code | Airline | Distance [km] | Aircraft |
|---|---|---|---|---|---|---|
| 06:00:00 | OA60 | Paros | PAS | Olympic Air | 146 | ATR42 |
| 06:40:00 | OA30 | Leros | LRS | Olympic Air | 373 | DHC8 |
| 06:45:00 | GQ300 | Mytilene | MJT | Sky Express | 262 | ATR72 |
| 06:50:00 | GQ420 | Zakynthos | ZTH | Sky Express | 270 | ATR42 |
| 06:50:00 | GQ470 | Paros | PAS | Sky Express | 146 | ATR72 |
| 06:50:00 | OA240 | Samos | SMI | Olympic Air | 262 | ATR42 |
| 07:00:00 | GQ270 | Corfu | CFU | Sky Express | 396 | ATR42 |
| 07:05:00 | OA50 | Zakynthos | ZTH | Olympic Air | 270 | ATR42 |
| 07:05:00 | GQ340 | Santorini | JTR | Sky Express | 218 | ATR72 |
| 07:10:00 | OA40 | Ikaria | JIK | Olympic Air | 213 | ATR42 |
| 07:15:00 | GQ250 | Chania | CHQ | Sky Express | 267 | ATR72 |
| 07:15:00 | GQ220 | Kos | KGS | Sky Express | 445 | ATR72 |
| 07:15:00 | GQ290 | Alexandroupoli | AXD | Sky Express | 367 | ATR42 |
| 07:20:00 | GQ240 | Chios | JKH | Sky Express | 197 | ATR72 |
| 07:30:00 | GQ210 | Heraklion | HER | Sky Express | 308 | ATR42 |
| 07:30:00 | OA270 | Chios | JKH | Olympic Air | 197 | DHC8 |
| 07:45:00 | GQ410 | Milos | MLO | Sky Express | 145 | ATR72 |
| 07:50:00 | GQ408 | Naxos | JNX | Sky Express | 248 | ATR72 |
| 07:55:00 | OA160 | Ioannina | IOA | Olympic Air | 334 | DHC8 |
| 07:55:00 | GQ230 | Mykonos | JMK | Sky Express | 135 | ATR42 |
| 08:00:00 | OA372 | Mykonos | JMK | Olympic Air | 135 | ATR42 |
| 08:20:00 | OA62 | Paros | PAS | Olympic Air | 146 | DHC8 |
| 08:40:00 | OA20 | Milos | MLO | Olympic Air | 145 | DHC8 |
| 09:05:00 | GQ30 | Kalymnos | JKL | Sky Express | 285 | ATR72 |
| 09:30:00 | OA14 | Naxos | JNX | Olympic Air | 248 | DHC8 |
| 09:45:00 | GQ460 | Karpathos | AOK | Sky Express | 400 | ATR42 |
| 10:00:00 | GQ310 | Samos | SMI | Sky Express | 262 | ATR72 |
| 10:00:00 | GQ342 | Santorini | JTR | Sky Express | 218 | ATR42 |
| 10:00:00 | OA32 | Leros | LRS | Olympic Air | 373 | DHC8 |
| 10:05:00 | OA222 | Kos | KGS | Olympic Air | 445 | ATR42 |
| 10:05:00 | GQ400 | Naxos | JNX | Sky Express | 248 | ATR42 |
| 10:10:00 | GQ20 | Syros | JSY | Sky Express | 228 | ATR72 |
| 10:20:00 | OA44 | Sitia | JSH | Olympic Air | 358 | DHC8 |
| 10:20:00 | OA70 | Paros | PAS | Olympic Air | 146 | DHC8 |
| 10:30:00 | GQ344 | Santorini | JTR | Sky Express | 218 | ATR42 |
| 10:30:00 | GQ430 | Skiathos | JSI | Sky Express | 143 | ATR42 |
| 11:00:00 | GQ242 | Chios | JKH | Sky Express | 197 | ATR42 |
| 11:00:00 | OA272 | Chios | JKH | Olympic Air | 197 | DHC8 |
| 11:05:00 | OA242 | Samos | SMI | Olympic Air | 262 | DHC8 |

Continued on next page

**Table A.1 – continued from previous page**

| Time | Flight | To | IATA code | Airline | Distance [km] | Aircraft |
|---|---|---|---|---|---|---|
| 11:10:00 | OA28 | Milos | MLO | Olympic Air | 145 | ATR42 |
| 11:20:00 | OA92 | Paros | PAS | Olympic Air | 146 | ATR42 |
| 11:40:00 | GQ472 | Paros | PAS | Sky Express | 146 | ATR72 |
| 12:00:00 | GQ320 | Lemnos | LXS | Sky Express | 246 | ATR42 |
| 12:00:00 | OA16 | Naxos | JNX | Olympic Air | 248 | ATR42 |
| 12:15:00 | GQ272 | Corfu | CFU | Sky Express | 396 | ATR72 |
| 12:30:00 | GQ402 | Naxos | JNX | Sky Express | 248 | ATR42 |
| 12:50:00 | GQ260 | Kefalonia | EFL | Sky Express | 303 | ATR42 |
| 12:50:00 | GQ346 | Santorini | JTR | Sky Express | 218 | ATR72 |
| 13:00:00 | OA64 | Paros | PAS | Olympic Air | 146 | ATR42 |
| 13:10:00 | GQ232 | Mykonos | JMK | Sky Express | 135 | ATR42 |
| 13:30:00 | GQ348 | Santorini | JTR | Sky Express | 218 | ATR72 |
| 13:30:00 | OA22 | Milos | MLO | Olympic Air | 145 | ATR42 |
| 13:35:00 | OA292 | Kefalonia | EFL | Olympic Air | 303 | DHC8 |
| 13:40:00 | OA90 | Paros | PAS | Olympic Air | 146 | DHC8 |
| 13:40:00 | GQ302 | Mytilene | MJT | Sky Express | 262 | ATR42 |
| 13:55:00 | OA42 | Milos | MLO | Olympic Air | 145 | DHC8 |
| 14:00:00 | GQ350 | Santorini | JTR | Sky Express | 218 | ATR72 |
| 14:15:00 | OA10 | Naxos | JNX | Olympic Air | 248 | DHC8 |
| 14:15:00 | OA56 | Kythira | KIT | Olympic Air | 202 | DHC8 |
| 14:45:00 | GQ10 | Astypalaia | JTY | Sky Express | 262 | ATR42 |
| 14:50:00 | OA74 | Paros | PAS | Olympic Air | 146 | ATR42 |
| 15:00:00 | OA368 | Santorini | JTR | Olympic Air | 218 | ATR42 |
| 15:00:00 | GQ212 | Heraklion | HER | Sky Express | 308 | ATR72 |
| 15:40:00 | GQ450 | Ikaria | JIK | Sky Express | 213 | ATR42 |
| 15:45:00 | GQ474 | Paros | PAS | Sky Express | 146 | ATR72 |
| 15:45:00 | OA72 | Paros | PAS | Olympic Air | 146 | DHC8 |
| 15:50:00 | OA24 | Milos | MLO | Olympic Air | 145 | ATR42 |
| 16:00:00 | GQ406 | Naxos | JNX | Sky Express | 248 | ATR42 |
| 16:15:00 | OA2 | Karpathos | AOK | Olympic Air | 400 | ATR42 |
| 16:30:00 | GQ352 | Santorini | JTR | Sky Express | 218 | ATR42 |
| 16:30:00 | OA18 | Naxos | JNX | Olympic Air | 248 | ATR42 |
| 16:40:00 | GQ262 | Kefalonia | EFL | Sky Express | 303 | ATR72 |
| 16:50:00 | GQ354 | Santorini | JTR | Sky Express | 218 | ATR42 |
| 16:50:00 | OA246 | Samos | SMI | Olympic Air | 262 | DHC8 |
| 16:55:00 | OA48 | Skyros | SKU | Olympic Air | 127 | DHC8 |
| 16:55:00 | OA68 | Paros | PAS | Olympic Air | 146 | DHC8 |
| 17:00:00 | GQ254 | Chania | CHQ | Sky Express | 267 | ATR72 |
| 17:20:00 | OA266 | Lemnos | LXS | Olympic Air | 246 | ATR42 |
| 17:55:00 | GQ214 | Heraklion | HER | Sky Express | 308 | ATR72 |
| 18:00:00 | OA166 | Ioannina | IOA | Olympic Air | 334 | ATR42 |
| 18:05:00 | OA66 | Paros | PAS | Olympic Air | 146 | ATR42 |
| 18:10:00 | OA26 | Milos | MLO | Olympic Air | 145 | DHC8 |
| 18:45:00 | OA6 | Karpathos | AOK | Olympic Air | 400 | ATR42 |
| 18:45:00 | GQ404 | Naxos | JNX | Sky Express | 248 | ATR72 |
| 18:45:00 | GQ412 | Milos | MLO | Sky Express | 145 | ATR72 |
| 18:45:00 | GQ476 | Paros | PAS | Sky Express | 146 | ATR42 |
| 19:00:00 | OA996 | Izmir | ADB | Olympic Air | 284 | ATR42 |
| 19:40:00 | OA360 | Santorini | JTR | Olympic Air | 218 | DHC8 |
| 19:50:00 | OA278 | Chios | JKH | Olympic Air | 197 | ATR42 |
| 20:05:00 | OA154 | Kavalla | KVA | Olympic Air | 335 | ATR42 |

Continued on next page

**Table A.1 – continued from previous page**

| Time | Flight | To | IATA code | Airline | Distance [km] | Aircraft |
|---|---|---|---|---|---|---|
| 20:15:00 | GQ234 | Mykonos | JMK | Sky Express | 135 | ATR42 |
| 20:15:00 | GQ274 | Corfu | CFU | Sky Express | 396 | ATR72 |
| 20:15:00 | OA52 | Zakynthos | ZTH | Olympic Air | 270 | DHC8 |
| 20:15:00 | GQ304 | Mytilene | MJT | Sky Express | 262 | ATR42 |
| 20:15:00 | OA296 | Kefalonia | EFL | Olympic Air | 303 | DHC8 |
| 20:20:00 | GQ216 | Heraklion | HER | Sky Express | 308 | ATR42 |
| 20:25:00 | OA382 | Mykonos | JMK | Olympic Air | 135 | ATR42 |
| 20:30:00 | GQ294 | Alexandroupoli | AXD | Sky Express | 367 | ATR42 |
| 20:40:00 | OA78 | Skiathos | JSI | Olympic Air | 143 | ATR42 |
| 20:45:00 | GQ224 | Kos | KGS | Sky Express | 445 | ATR72 |
| 21:00:00 | GQ322 | Lemnos | LXS | Sky Express | 246 | ATR72 |
| 21:00:00 | GQ462 | Karpathos | AOK | Sky Express | 400 | ATR72 |
| 21:00:00 | GQ244 | Chios | JKH | Sky Express | 197 | ATR72 |
| 21:00:00 | GQ440 | Kythira | KIT | Sky Express | 202 | ATR72 |
| 21:40:00 | OA362 | Santorini | JTR | Olympic Air | 218 | ATR42 |
| 22:50:00 | GQ218 | Heraklion | HER | Sky Express | 308 | ATR42 |

Table A.2: Flight schedule – Athens Airport – 25th December 2022

| Time | Flight | To | IATA code | Airline | Distance [km] | Aircraft |
|---|---|---|---|---|---|---|
| 09:05:00 | OA3002 | Rhodes | RHO | Olympic Air | 405 | DHC8 |
| 09:10:00 | OA222 | Kos | KGS | Olympic Air | 445 | DHC8 |
| 09:50:00 | OA142 | Alexandroupoli | AXD | Olympic Air | 367 | DHC8 |
| 10:05:00 | OA240 | Samos | SMI | Olympic Air | 262 | ATR42 |
| 10:35:00 | OA370 | Mykonos | JMK | Olympic Air | 135 | ATR42 |
| 10:40:00 | OA12 | Naxos | JNX | Olympic Air | 248 | ATR42 |
| 10:45:00 | OA274 | Chios | JKH | Olympic Air | 197 | DHC8 |
| 11:00:00 | GQ242 | Chios | JKH | Sky Express | 197 | ATR72 |
| 12:55:00 | GQ302 | Mytilene | MJT | Sky Express | 262 | ATR42 |
| 13:05:00 | OA252 | Mytilene | MJT | Olympic Air | 262 | DHC8 |
| 13:25:00 | OA366 | Santorini | JTR | Olympic Air | 218 | DHC8 |
| 13:40:00 | GQ30 | Kalymnos | JKL | Sky Express | 285 | ATR72 |
| 15:05:00 | OA246 | Samos | SMI | Olympic Air | 262 | DHC8 |
| 15:45:00 | OA64 | Paros | PAS | Olympic Air | 146 | DHC8 |
| 16:40:00 | GQ310 | Samos | SMI | Sky Express | 262 | ATR42 |
| 16:45:00 | GQ230 | Mykonos | JMK | Sky Express | 135 | ATR42 |
| 16:55:00 | GQ214 | Heraklion | HER | Sky Express | 308 | ATR72 |
| 17:00:00 | OA358 | Santorini | JTR | Olympic Air | 218 | DHC8 |
| 17:15:00 | GQ344 | Santorini | JTR | Sky Express | 218 | ATR72 |
| 17:30:00 | OA224 | Kos | KGS | Olympic Air | 445 | DHC8 |
| 18:20:00 | OA266 | Lemnos | LXS | Olympic Air | 246 | ATR42 |
| 18:30:00 | OA154 | Kavalla | KVA | Olympic Air | 335 | ATR42 |
| 18:30:00 | OA166 | Ioannina | IOA | Olympic Air | 334 | ATR42 |
| 19:10:00 | OA276 | Chios | JKH | Olympic Air | 197 | DHC8 |
| 19:30:00 | GQ304 | Mytilene | MJT | Sky Express | 262 | ATR72 |
| 19:45:00 | GQ224 | Kos | KGS | Sky Express | 445 | ATR72 |
| 20:00:00 | GQ216 | Heraklion | HER | Sky Express | 308 | ATR42 |
| 20:05:00 | GQ294 | Alexandroupoli | AXD | Sky Express | 367 | ATR72 |
| 20:10:00 | GQ274 | Corfu | CFU | Sky Express | 396 | ATR42 |
| 20:15:00 | GQ256 | Chania | CHQ | Sky Express | 267 | ATR42 |

Table A.3: Flight schedule – Malpensa Airport – 5th September 2022

| Time | Flight | To | IATA code | Airline | Distance [km] | Aircraft |
|---|---|---|---|---|---|---|
| 02:20:00 | TK6394 | Istanbul | IST | Turkish Airlines | 1675 | A321 |
| 05:55:00 | TP821 | Lisbon | LIS | Tap Air Portugal | 1686 | A320 |
| 06:00:00 | FR2752 | Madrid | MAD | Ryanair | 1190 | A320 |
| 06:00:00 | EN1863 | Munich | MUC | Air Dolomiti | 349 | E190 |
| 06:00:00 | NO1004 | Djerba | DJE | Neos | 1316 | B737 |
| 06:00:00 | NO1620 | Fuerteventura | FUE | Neos | 2792 | B737 |
| 06:00:00 | U22591 | Marrakesh | RAK | Easyjet | 2139 | B737 |
| 06:00:00 | U22795 | Faro | FAO | Easyjet | 1684 | A319 |
| 06:00:00 | U22861 | Lamezia Terme | SUF | Easyjet | 931 | A321 |
| 06:00:00 | U22951 | Mykonos | JMK | Easyjet | 1615 | A319 |
| 06:05:00 | FR6616 | Kalamata | KLX | Ryanair | 1429 | A321 |
| 06:15:00 | FR5968 | Aarhus | AAR | Ryanair | 1194 | A321 |
| 06:15:00 | LH259 | Frankfurt | FRA | Lufthansa | 519 | A321 |
| 06:20:00 | FR3416 | Brindisi | BDS | Ryanair | 892 | B737 |
| 06:20:00 | U22691 | Ibiza | IBZ | Easyjet | 970 | A321 |
| 06:30:00 | U22777 | Paris | CDG | Easyjet | 640 | B737 |
| 06:30:00 | W65593 | Lamezia Terme | SUF | Wizz Air | 931 | A320 |
| 06:40:00 | FR2770 | Bari | BRI | Ryanair | 788 | A321 |
| 06:40:00 | FR5515 | Catania | CTA | Ryanair | 1012 | B737 |
| 06:40:00 | KL1628 | Amsterdam | AMS | Klm | 830 | E190 |
| 06:45:00 | U22733 | Malaga | AGP | Easyjet | 1497 | A321 |
| 06:50:00 | 2L1639 | Zurich | ZRH | Helvetic Airways | 218 | E190 |
| 06:50:00 | W65541 | Athens | ATH | Wizz Air | 1464 | A320 |
| 06:55:00 | TK1878 | Istanbul | IST | Turkish Airlines | 1675 | A321 |
| 07:00:00 | FR5972 | Naples | NAP | Ryanair | 658 | B737 |
| 07:00:00 | NO1672 | Sharm El-Sheikh | SSH | Neos | 2953 | B737 |
| 07:00:00 | U22551 | Munich | MUC | Easyjet | 349 | A319 |
| 07:00:00 | U22563 | Tel Aviv | TLV | Easyjet | 2656 | A319 |
| 07:00:00 | U22889 | Naples | NAP | Easyjet | 658 | A321 |
| 07:00:00 | W65788 | London | LGW | Wizz Air | 961 | A321 |
| 07:05:00 | OS518 | Wien | VIE | Austrian | 626 | E190 |
| 07:05:00 | U22653 | Copenhagen | CPH | Easyjet | 1162 | A321 |
| 07:05:00 | U22831 | Bari | BRI | Easyjet | 788 | A320 |
| 07:10:00 | U22805 | Palermo | PMO | Easyjet | 888 | A320 |
| 07:10:00 | W65589 | Naples | NAP | Wizz Air | 658 | B737 |
| 07:15:00 | U22587 | Reina Sofia | TFS | Easyjet | 2960 | A320 |
| 07:25:00 | LO322 | Warsaw | WAW | Lot - Polish Airlines | 1146 | E170 |
| 07:25:00 | U28190 | London | LGW | Easyjet | 961 | A319 |
| 07:30:00 | NO1024 | Monastir | MIR | Neos | 1087 | B737 |
| 08:05:00 | BA583 | London | LHR | British Airways | 961 | A319 |
| 08:05:00 | FR4948 | Malaga | AGP | Ryanair | 1497 | A321 |
| 08:20:00 | EW2821 | Stuttgart | STR | Eurowings | 369 | A319 |
| 08:20:00 | LG6992 | Luxembourg | LUX | Luxair | 536 | E190 |
| 08:25:00 | U22891 | Naples | NAP | Easyjet | 658 | A321 |
| 08:30:00 | SN3154 | Brussels | BRU | Brussels Airlines | 699 | A320 |
| 08:30:00 | W65579 | Palermo | PMO | Wizz Air | 888 | B737 |
| 08:40:00 | EN8269 | Munich | MUC | Air Dolomiti | 349 | E190 |
| 08:40:00 | EW825 | Cologne | CGN | Eurowings | 631 | A320 |
| 08:40:00 | W65640 | Bari | BRI | Wizz Air | 788 | A320 |
| 08:55:00 | LW9216 | Wien | VIE | Lauda Europe | 626 | A320 |
| 08:55:00 | PQ6608 | Tirana | TIA | Skyup Airlines | 975 | B737 |

Continued on next page

**Table A.3 – continued from previous page**

| Time | Flight | To | IATA code | Airline | Distance [km] | Aircraft |
|---|---|---|---|---|---|---|
| 09:00:00 | U29855 | Catania | CTA | Easyjet | 1012 | B737 |
| 09:05:00 | EW9827 | Dusseldorf | DUS | Eurowings | 666 | A320 |
| 09:05:00 | LH247 | Frankfurt | FRA | Lufthansa | 519 | A321 |
| 09:10:00 | 2B330 | Tirana | TIA | Albawings | 975 | B737 |
| 09:10:00 | NO4789 | Tirana | TIA | Neos | 975 | B737 |
| 09:15:00 | U22919 | Lampedusa | LMP | Easyjet | 1146 | A321 |
| 09:25:00 | U22755 | Bordeaux | BOD | Easyjet | 770 | A321 |
| 09:30:00 | FR1070 | Catania | CTA | Ryanair | 1012 | B737 |
| 09:35:00 | W65575 | Catania | CTA | Wizz Air | 1012 | A320 |
| 09:40:00 | U22867 | Lamezia Terme | SUF | Easyjet | 931 | A321 |
| 09:45:00 | FR8754 | London | STN | Ryanair | 961 | B737 |
| 09:55:00 | BJ6058 | Rome | FCO | Nouvelair Tunisie | 476 | A320 |
| 09:55:00 | BJ6059 | Rome | FCO | Nouvelair Tunisie | 476 | A320 |
| 10:00:00 | VY9433 | Paris | ORY | Vueling | 640 | A321 |
| 10:05:00 | U22759 | Barcelona | BCN | Easyjet | 726 | A321 |
| 10:10:00 | VY6331 | Barcelona | BCN | Vueling | 726 | A321 |
| 10:15:00 | OS512 | Wien | VIE | Austrian | 626 | A320 |
| 10:20:00 | FR6825 | Manchester | MAN | Ryanair | 1214 | A320 |
| 10:20:00 | U22837 | Bari | BRI | Easyjet | 788 | B737 |
| 10:25:00 | AF1831 | Paris | CDG | Air France | 640 | BCS3 |
| 10:30:00 | FR1423 | Alicante | ALC | Ryanair | 1126 | A321 |
| 10:30:00 | U28192 | London | LGW | Easyjet | 961 | B737 |
| 10:35:00 | LO318 | Warsaw | WAW | Lot - Polish Airlines | 1146 | E170 |
| 10:35:00 | UX1066 | Madrid | MAD | Air Europa | 1190 | A321 |
| 10:35:00 | U22875 | Cagliari | CAG | Easyjet | 695 | A321 |
| 10:40:00 | FR5914 | Naples | NAP | Ryanair | 658 | A321 |
| 10:40:00 | LX1613 | Zurich | ZRH | Swiss | 218 | A320 |
| 10:45:00 | TK1874 | Istanbul | IST | Turkish Airlines | 1675 | A321 |
| 10:50:00 | PS312 | Kiev | KBP | Uia | 1728 | E190 |
| 10:55:00 | A3661 | Athens | ATH | Aegean Airlines | 1464 | A321 |
| 10:55:00 | FR1150 | Palermo | PMO | Ryanair | 888 | A321 |
| 11:00:00 | U22715 | Lisbon | LIS | Easyjet | 1686 | A320 |
| 11:05:00 | AY1752 | Helsinki | HEL | Finnair | 1940 | A321 |
| 11:10:00 | U22845 | Catania | CTA | Easyjet | 1012 | A320 |
| 11:15:00 | FR2179 | Catania | CTA | Ryanair | 1012 | A321 |
| 11:15:00 | LH249 | Frankfurt | FRA | Lufthansa | 519 | A321 |
| 11:15:00 | U22725 | Amsterdam | AMS | Easyjet | 830 | A321 |
| 11:20:00 | FR6182 | Bari | BRI | Ryanair | 788 | A320 |
| 11:20:00 | SK1686 | Copenhagen | CPH | Sas | 1162 | A320 |
| 11:25:00 | FR1434 | Lamezia Terme | SUF | Ryanair | 931 | A320 |
| 11:25:00 | W65505 | Cagliari | CAG | Wizz Air | 695 | A320 |
| 11:35:00 | U22821 | Brindisi | BDS | Easyjet | 892 | B737 |
| 11:40:00 | FR4561 | Cagliari | CAG | Ryanair | 695 | A321 |
| 11:45:00 | TU757 | Tunis | TUN | Tunisair | 966 | A319 |
| 11:45:00 | U22711 | Nantes | NTE | Easyjet | 848 | A321 |
| 11:50:00 | TP827 | Lisbon | LIS | Tap Air Portugal | 1686 | A319 |
| 12:00:00 | U22829 | Bari | BRI | Easyjet | 788 | A321 |
| 12:00:00 | U22905 | Olbia | OLB | Easyjet | 506 | B737 |
| 12:00:00 | U24830 | Naples | NAP | Easyjet | 658 | B737 |
| 12:00:00 | NO1006 | Djerba | DJE | Neos | 1316 | B737 |
| 12:10:00 | LY382 | Tel Aviv | TLV | El Al | 2656 | B737 |

Continued on next page

**Table A.3 – continued from previous page**

| Time | Flight | To | IATA code | Airline | Distance [km] | Aircraft |
|---|---|---|---|---|---|---|
| 12:20:00 | U22963 | Heraklion | HER | Easyjet | 1755 | B737 |
| 12:25:00 | W65613 | Lamezia Terme | SUF | Wizz Air | 931 | B737 |
| 12:30:00 | FR9 | Berlin | BER | Ryanair | 843 | A320 |
| 12:35:00 | EN1855 | Munich | MUC | Air Dolomiti | 349 | E190 |
| 12:45:00 | U22807 | Palermo | PMO | Easyjet | 888 | A319 |
| 12:50:00 | KL1630 | Amsterdam | AMS | Klm | 830 | B737 |
| 12:50:00 | U22783 | Paris | CDG | Easyjet | 640 | A321 |
| 12:50:00 | U22863 | Lamezia Terme | SUF | Easyjet | 931 | A319 |
| 13:00:00 | AT955 | Casablanca | CMN | Royal Air Maroc | 1935 | B737 |
| 13:00:00 | U22797 | Sharm El-Sheikh | SSH | Easyjet | 2953 | A319 |
| 13:00:00 | VY6333 | Barcelona | BCN | Vueling | 726 | A321 |
| 13:05:00 | VY6378 | Ibiza | IBZ | Vueling | 970 | A321 |
| 13:10:00 | FR7540 | Barcelona | BCN | Ryanair | 726 | A321 |
| 13:15:00 | BA573 | London | LHR | British Airways | 961 | A319 |
| 13:20:00 | U22913 | Fuerteventura | FUE | Easyjet | 2792 | A321 |
| 13:35:00 | U22853 | Catania | CTA | Easyjet | 1012 | A320 |
| 13:35:00 | W65619 | Prague | PRG | Wizz Air | 646 | B737 |
| 13:40:00 | AF1331 | Paris | CDG | Air France | 640 | A318 |
| 13:45:00 | U22607 | Athens | ATH | Easyjet | 1464 | A319 |
| 13:45:00 | U22823 | Brindisi | BDS | Easyjet | 892 | B737 |
| 13:50:00 | ME236 | Beirut | BEY | Middle East Airlines | 2580 | A320 |
| 14:00:00 | DY1877 | Oslo | OSL | Norwegian Air Shuttle Aoc | 1612 | B737 |
| 14:00:00 | NO1460 | Reina Sofia | TFS | Neos | 2960 | B737 |
| 14:15:00 | W66610 | Tirana | TIA | Wizz Air | 975 | A321 |
| 14:30:00 | IB3253 | Madrid | MAD | Iberia | 1190 | A320 |
| 14:30:00 | MS704 | Cairo | CAI | Egyptair | 2576 | B737 |
| 14:40:00 | LH253 | Frankfurt | FRA | Lufthansa | 519 | A321 |
| 14:40:00 | SK4718 | Oslo | OSL | Sas | 1612 | E190 |
| 14:40:00 | U22847 | Catania | CTA | Easyjet | 1012 | A320 |
| 14:40:00 | XQ893 | Izmir | ADB | Sunexpress | 1722 | B737 |
| 14:45:00 | U22809 | Palermo | PMO | Easyjet | 888 | A320 |
| 14:55:00 | 2L1629 | Zurich | ZRH | Helvetic Airways | 218 | E190 |
| 14:55:00 | TK1896 | Istanbul | IST | Turkish Airlines | 1675 | A321 |
| 15:00:00 | VY6341 | Barcelona | BCN | Vueling | 726 | A321 |
| 15:05:00 | U22921 | Manchester | MAN | Easyjet | 1214 | A319 |
| 15:30:00 | BA3290 | London | LCY | British Airways | 961 | A320 |
| 15:30:00 | FR2962 | Brussels | BRU | Ryanair | 699 | A321 |
| 15:30:00 | FR8734 | Bucharest | OTP | Ryanair | 1335 | A320 |
| 15:30:00 | U22855 | Catania | CTA | Easyjet | 1012 | A319 |
| 15:30:00 | U22895 | Naples | NAP | Easyjet | 658 | A320 |
| 15:30:00 | 9U894 | Chisinau | KIV | Air Moldova | 1519 | A320 |
| 15:35:00 | FR1811 | Reina Sofia | TFS | Ryanair | 2960 | B737 |
| 15:40:00 | U22907 | Olbia | OLB | Easyjet | 506 | A319 |
| 15:40:00 | W68052 | Vilnius | VNO | Wizz Air | 1535 | A321 |
| 15:45:00 | U22879 | Cagliari | CAG | Easyjet | 695 | A319 |
| 16:00:00 | BA585 | London | LHR | British Airways | 961 | A319 |
| 16:00:00 | FR1436 | Lamezia Terme | SUF | Ryanair | 931 | B737 |
| 16:00:00 | U22722 | Amsterdam | AMS | Easyjet | 830 | A319 |
| 16:10:00 | EW7827 | Hamburg | HAM | Eurowings | 902 | A320 |
| 16:10:00 | U22727 | Amsterdam | AMS | Easyjet | 830 | A319 |
| 16:20:00 | FR1438 | Palermo | PMO | Ryanair | 888 | B737 |

Continued on next page

**Table A.3 – continued from previous page**

| Time | Flight | To | IATA code | Airline | Distance [km] | Aircraft |
|---|---|---|---|---|---|---|
| 16:20:00 | U24832 | Naples | NAP | Easyjet | 658 | A321 |
| 16:25:00 | FR5936 | Naples | NAP | Ryanair | 658 | A321 |
| 16:35:00 | BT9825 | Dusseldorf | DUS | Air Baltic | 666 | BCS3 |
| 16:35:00 | U22761 | Barcelona | BCN | Easyjet | 726 | A319 |
| 16:35:00 | W65565 | Reykjavik | KEF | Wizz Air | 2827 | A320 |
| 16:40:00 | U22735 | Malaga | AGP | Easyjet | 1497 | B737 |
| 16:40:00 | U22987 | Mahon | MAH | Easyjet | 740 | B737 |
| 16:45:00 | W62334 | Budapest | BUD | Wizz Air | 788 | A320 |
| 16:50:00 | FR979 | Brindisi | BDS | Ryanair | 892 | A321 |
| 16:50:00 | FR1455 | Dublin | DUB | Ryanair | 1418 | A321 |
| 16:50:00 | U28194 | London | LGW | Easyjet | 961 | A319 |
| 16:55:00 | U22959 | Santorini | JTR | Easyjet | 1692 | A321 |
| 16:55:00 | W65515 | Reina Sofia | TFS | Wizz Air | 2960 | A321 |
| 17:15:00 | LH1857 | Munich | MUC | Lufthansa | 349 | A320 |
| 17:25:00 | U22787 | Paris | CDG | Easyjet | 640 | B737 |
| 17:30:00 | U22286 | London | LTN | Easyjet | 961 | A321 |
| 17:30:00 | U22849 | Catania | CTA | Easyjet | 1012 | A319 |
| 17:35:00 | OS514 | Wien | VIE | Austrian | 626 | A321 |
| 17:35:00 | TP823 | Lisbon | LIS | Tap Air Portugal | 1686 | A321 |
| 17:40:00 | BA593 | London | LHR | British Airways | 961 | A320 |
| 17:40:00 | W65583 | Bari | BRI | Wizz Air | 788 | A321 |
| 17:45:00 | AT951 | Casablanca | CMN | Royal Air Maroc | 1935 | B737 |
| 17:45:00 | W65581 | Palermo | PMO | Wizz Air | 888 | A321 |
| 17:50:00 | MS706 | Cairo | CAI | Egyptair | 2576 | B737 |
| 17:50:00 | W65547 | Santorini | JTR | Wizz Air | 1692 | B737 |
| 17:55:00 | AF1731 | Paris | CDG | Air France | 640 | E170 |
| 17:55:00 | U22857 | Alghero | AHO | Easyjet | 551 | B737 |
| 18:10:00 | VY6335 | Barcelona | BCN | Vueling | 726 | A321 |
| 18:15:00 | U22685 | Edinburgh | EDI | Easyjet | 1453 | A320 |
| 18:25:00 | FR8732 | Seville | SVQ | Ryanair | 1549 | A320 |
| 18:25:00 | U22941 | Mykonos | JMK | Easyjet | 1615 | A321 |
| 18:30:00 | PS314 | Kiev | KBP | Uia | 1728 | B737 |
| 18:35:00 | NO1676 | Marsa Alam | RMF | Neos | 3209 | B737 |
| 18:40:00 | U28198 | London | LGW | Easyjet | 961 | A320 |
| 18:45:00 | FR347 | Heraklion | HER | Ryanair | 1755 | A321 |
| 18:50:00 | A3665 | Athens | ATH | Aegean Airlines | 1464 | A321 |
| 18:50:00 | BA567 | London | LHR | British Airways | 961 | E190 |
| 18:50:00 | LH255 | Frankfurt | FRA | Lufthansa | 519 | A319 |
| 19:00:00 | AY1756 | Helsinki | HEL | Finnair | 1940 | A320 |
| 19:15:00 | UX1062 | Madrid | MAD | Air Europa | 1190 | B737 |
| 19:20:00 | FR8718 | London | STN | Ryanair | 961 | A320 |
| 19:30:00 | KL1634 | Amsterdam | AMS | Klm | 830 | B737 |
| 19:30:00 | W65786 | London | LGW | Wizz Air | 961 | A321 |
| 19:35:00 | U22865 | Lamezia Terme | SUF | Easyjet | 931 | A319 |
| 19:35:00 | U22881 | Cagliari | CAG | Easyjet | 695 | A321 |
| 19:35:00 | U26442 | London | LGW | Easyjet | 961 | B737 |
| 19:40:00 | AF1131 | Paris | CDG | Air France | 640 | A320 |
| 19:40:00 | LH257 | Frankfurt | FRA | Lufthansa | 519 | A319 |
| 19:40:00 | TK1876 | Istanbul | IST | Turkish Airlines | 1675 | A321 |
| 19:40:00 | U22835 | Bari | BRI | Easyjet | 788 | A320 |
| 19:45:00 | LO320 | Warsaw | WAW | Lot - Polish Airlines | 1146 | E170 |

Continued on next page

**Table A.3 – continued from previous page**

| Time | Flight | To | IATA code | Airline | Distance [km] | Aircraft |
|---|---|---|---|---|---|---|
| 19:45:00 | U22827 | Brindisi | BDS | Easyjet | 892 | A321 |
| 19:45:00 | U22897 | Naples | NAP | Easyjet | 658 | B737 |
| 19:55:00 | U22585 | Prague | PRG | Easyjet | 646 | B737 |
| 20:05:00 | SK688 | Copenhagen | CPH | Sas | 1162 | E190 |
| 20:10:00 | BA2837 | London | LGW | British Airways | 961 | E190 |
| 20:10:00 | EN8279 | Munich | MUC | Air Dolomiti | 349 | E190 |
| 20:15:00 | FR5513 | Catania | CTA | Ryanair | 1012 | B737 |
| 20:15:00 | 2L1623 | Zurich | ZRH | Helvetic Airways | 218 | E190 |
| 20:15:00 | U22811 | Palermo | PMO | Easyjet | 888 | A319 |
| 20:20:00 | ET713 | Rome | FCO | Ethiopian Airlines | 476 | B737 |
| 20:20:00 | FR1444 | Valencia | VLC | Ryanair | 1030 | A321 |
| 20:20:00 | VY9435 | Paris | ORY | Vueling | 640 | A321 |
| 20:30:00 | TP829 | Lisbon | LIS | Tap Air Portugal | 1686 | A319 |
| 20:30:00 | U22747 | Palma de Mallorca | PMI | Easyjet | 847 | A321 |
| 20:35:00 | OS516 | Wien | VIE | Austrian | 626 | A321 |
| 20:40:00 | EW9821 | Dusseldorf | DUS | Eurowings | 666 | A319 |
| 20:50:00 | FR1580 | Palma de Mallorca | PMI | Ryanair | 847 | A320 |
| 21:00:00 | SM2804 | Cairo | CAI | Air Cairo | 2576 | A320 |
| 21:05:00 | FR1015 | Palermo | PMO | Ryanair | 888 | A320 |
| 21:05:00 | U22767 | Barcelona | BCN | Easyjet | 726 | A320 |
| 21:10:00 | LG6998 | Luxembourg | LUX | Luxair | 536 | E190 |
| 21:10:00 | U22719 | Lisbon | LIS | Easyjet | 1686 | B737 |
| 21:20:00 | U24834 | Naples | NAP | Easyjet | 658 | A319 |
| 21:20:00 | VY6337 | Barcelona | BCN | Vueling | 726 | A320 |
| 21:25:00 | W68404 | Naples | NAP | Wizz Air | 658 | A321 |
| 21:30:00 | U22851 | Catania | CTA | Easyjet | 1012 | B737 |
| 21:30:00 | W62336 | Budapest | BUD | Wizz Air | 788 | B737 |
| 21:30:00 | W65577 | Catania | CTA | Wizz Air | 1012 | B737 |
| 21:35:00 | U22791 | Paris | CDG | Easyjet | 640 | B737 |
| 21:45:00 | EI437 | Dublin | DUB | Aer Lingus | 1418 | A320 |
| 21:50:00 | FR8737 | London | STN | Ryanair | 961 | B737 |
| 22:00:00 | SN3160 | Brussels | BRU | Brussels Airlines | 699 | A319 |
| 22:50:00 | ZT1807 | Cologne | CGN | Titan Airways | 631 | A321 |
| 23:00:00 | LY388 | Tel Aviv | TLV | El Al | 2656 | B737 |
| 23:50:00 | FI593 | Reykjavik | KEF | Icelandair | 2827 | B737 |

Table A.4: Flight schedule – Malpensa Airport – 25th January 2022

| Time | Flight | To | IATA code | Airline | Distance [km] | Aircraft |
|---|---|---|---|---|---|---|
| 02:30:00 | WT8340 | Madrid | MAD | Swiftair | 1190 | B737 |
| 03:00:00 | WT4286 | Budapest | BUD | Swiftair | 788 | B737 |
| 03:30:00 | BO949 | Cagliari | CAG | Bluebird Nordic | 695 | B737 |
| 03:50:00 | WT7550 | Athens | ATH | Swiftair | 1464 | B737 |
| 05:40:00 | W65535 | Marrakesh | RAK | Wizz Air | 2139 | A320 |
| 06:10:00 | W65579 | Palermo | PMO | Wizz Air | 888 | A320 |
| 06:10:00 | W65567 | Yerevan | EVN | Wizz Air | 2951 | A320 |
| 06:13:00 | ZT1806 | Naples | NAP | Titan Airways | 658 | A321 |
| 06:20:00 | TP821 | Lisbon | LIS | Tap Air Portugal | 1686 | A321 |
| 06:25:00 | FR7555 | Barcelona | BCN | Ryanair | 726 | A320 |
| 06:30:00 | TK6157 | Istanbul | IST | Turkish Airlines | 1675 | A321 |
| 06:40:00 | W65593 | Lamezia Terme | SUF | Wizz Air | 931 | A320 |

Continued on next page

**Table A.4 – continued from previous page**

| Time | Flight | To | IATA code | Airline | Distance [km] | Aircraft |
|---|---|---|---|---|---|---|
| 06:45:00 | FR7387 | Catania | CTA | Ryanair | 1012 | A321 |
| 06:55:00 | FR1423 | Alicante | ALC | Ryanair | 1126 | A321 |
| 06:55:00 | W65788 | London | LGW | Wizz Air | 961 | A321 |
| 07:00:00 | U22805 | Palermo | PMO | Easyjet | 888 | B737 |
| 07:05:00 | FR1811 | Reina Sofia | TFS | Ryanair | 2960 | A320 |
| 07:05:00 | OS518 | Wien | VIE | Austrian | 626 | A320 |
| 07:05:00 | TK1878 | Istanbul | IST | Turkish Airlines | 1675 | A321 |
| 07:05:00 | U28188 | London | LGW | Easyjet | 961 | A321 |
| 07:05:00 | TK6157 | Istanbul | IST | Turkish Airlines | 1675 | A321 |
| 07:20:00 | TK6419 | Istanbul | IST | Turkish Airlines | 1675 | A321 |
| 07:45:00 | FR7407 | Lamezia Terme | SUF | Ryanair | 931 | A321 |
| 07:45:00 | U22861 | Lamezia Terme | SUF | Easyjet | 931 | B737 |
| 08:00:00 | U22563 | Tel Aviv | TLV | Easyjet | 2656 | A321 |
| 08:05:00 | FR7377 | Naples | NAP | Ryanair | 658 | B737 |
| 08:30:00 | EW2821 | Stuttgart | STR | Eurowings | 369 | A319 |
| 08:35:00 | FR6182 | Bari | BRI | Ryanair | 788 | A321 |
| 08:35:00 | SN3154 | Brussels | BRU | Brussels Airlines | 699 | A320 |
| 08:40:00 | U22779 | Paris | CDG | Easyjet | 640 | A319 |
| 08:45:00 | W66608 | Tirana | TIA | Wizz Air | 975 | A321 |
| 08:55:00 | U22891 | Naples | NAP | Easyjet | 658 | A321 |
| 09:05:00 | W65575 | Catania | CTA | Wizz Air | 1012 | A320 |
| 09:10:00 | FR8880 | Palermo | PMO | Ryanair | 888 | A321 |
| 09:15:00 | EW9827 | Dusseldorf | DUS | Eurowings | 666 | A319 |
| 09:15:00 | VY9433 | Paris | ORY | Vueling | 640 | A320 |
| 09:25:00 | JU541 | Belgrade | BEG | Air Serbia | 888 | A320 |
| 09:55:00 | FR5517 | Catania | CTA | Ryanair | 1012 | B737 |
| 10:10:00 | VY6331 | Barcelona | BCN | Vueling | 726 | A321 |
| 10:15:00 | OS512 | Wien | VIE | Austrian | 626 | A321 |
| 10:25:00 | FR8741 | London | STN | Ryanair | 961 | B737 |
| 10:25:00 | LO318 | Warsaw | WAW | Lot - Polish Airlines | 1146 | E190 |
| 10:35:00 | U22845 | Catania | CTA | Easyjet | 1012 | A321 |
| 10:40:00 | AF1831 | Paris | CDG | Air France | 640 | E190 |
| 10:40:00 | 2L1613 | Zurich | ZRH | Helvetic Airways | 218 | E190 |
| 10:40:00 | UX1066 | Madrid | MAD | Air Europa | 1190 | B737 |
| 10:45:00 | TK1874 | Istanbul | IST | Turkish Airlines | 1675 | A321 |
| 10:45:00 | TU757 | Tunis | TUN | Tunisair | 966 | A320 |
| 10:45:00 | TU756 | Rome | FCO | Tunisair | 476 | A319 |
| 10:45:00 | TU757 | Rome | FCO | Tunisair | 476 | A319 |
| 10:55:00 | LH247 | Frankfurt | FRA | Lufthansa | 519 | A320 |
| 11:05:00 | A3661 | Athens | ATH | Aegean Airlines | 1464 | A321 |
| 11:05:00 | W65553 | Pristina | PRN | Wizz Air | 1005 | B737 |
| 11:20:00 | AY1752 | Helsinki | HEL | Finnair | 1940 | A321 |
| 11:20:00 | LY382 | Tel Aviv | TLV | El Al | 2656 | B737 |
| 11:20:00 | SK1686 | Copenhagen | CPH | Sas | 1162 | A320 |
| 11:30:00 | FR7395 | Brindisi | BDS | Ryanair | 892 | A320 |
| 11:35:00 | BA573 | London | LHR | British Airways | 961 | A321 |
| 11:35:00 | TP827 | Lisbon | LIS | Tap Air Portugal | 1686 | A320 |
| 11:55:00 | FR6825 | Manchester | MAN | Ryanair | 1214 | B737 |
| 12:00:00 | U22595 | Rovaniemi | RVN | Easyjet | 2537 | A321 |
| 12:20:00 | AF1131 | Paris | CDG | Air France | 640 | B737 |
| 12:30:00 | W65691 | Jeddah | JED | Wizz Air | 3818 | A320 |

Continued on next page

**Table A.4 – continued from previous page**

| Time | Flight | To | IATA code | Airline | Distance [km] | Aircraft |
|---|---|---|---|---|---|---|
| 12:45:00 | AT352 | Brussels | BRU | Royal Air Maroc | 699 | B737 |
| 12:50:00 | FR9 | Berlin | BER | Ryanair | 843 | A320 |
| 12:50:00 | VY6333 | Barcelona | BCN | Vueling | 726 | A321 |
| 13:10:00 | U22783 | Paris | CDG | Easyjet | 640 | A319 |
| 13:15:00 | FR2964 | Brussels | BRU | Ryanair | 699 | A320 |
| 13:25:00 | U28192 | London | LGW | Easyjet | 961 | A319 |
| 13:35:00 | FR6993 | Bari | BRI | Ryanair | 788 | A321 |
| 13:35:00 | MS704 | Cairo | CAI | Egyptair | 2576 | B737 |
| 13:40:00 | FR7470 | Valencia | VLC | Ryanair | 1030 | B737 |
| 13:50:00 | FR6326 | Dublin | DUB | Ryanair | 1418 | B737 |
| 13:50:00 | W65561 | Tel Aviv | TLV | Wizz Air | 2656 | A321 |
| 14:05:00 | BT630 | Riga | RIX | Air Baltic | 1638 | BCS3 |
| 14:25:00 | TK1896 | Istanbul | IST | Turkish Airlines | 1675 | A321 |
| 14:30:00 | U22567 | Tel Aviv | TLV | Easyjet | 2656 | A320 |
| 14:35:00 | LH253 | Frankfurt | FRA | Lufthansa | 519 | E190 |
| 14:40:00 | IB3253 | Madrid | MAD | Iberia | 1190 | A319 |
| 14:55:00 | ZB2004 | Tirana | TIA | Air Albania | 975 | A320 |
| 15:00:00 | NO288 | Rome | FCO | Neos | 476 | B737 |
| 15:15:00 | U22851 | Catania | CTA | Easyjet | 1012 | B737 |
| 15:30:00 | FR7415 | Palermo | PMO | Ryanair | 888 | A320 |
| 15:30:00 | IR750 | Tehran | IKA | Iran Air | 3687 | A319 |
| 15:40:00 | SV210 | Jeddah | JED | Saudia | 3818 | A320 |
| 15:50:00 | U22807 | Palermo | PMO | Easyjet | 888 | B737 |
| 16:05:00 | FR4561 | Cagliari | CAG | Ryanair | 695 | A320 |
| 16:05:00 | W65607 | Sharm El-Sheikh | SSH | Wizz Air | 2953 | A320 |
| 16:20:00 | W63796 | Chisinau | KIV | Wizz Air | 1519 | A321 |
| 16:45:00 | W65615 | Amman | AMM | Wizz Air | 2809 | A320 |
| 16:55:00 | AT951 | Casablanca | CMN | Royal Air Maroc | 1935 | B737 |
| 17:05:00 | EN1857 | Munich | MUC | Air Dolomiti | 349 | E190 |
| 17:20:00 | FR778 | Lamezia Terme | SUF | Ryanair | 931 | A321 |
| 17:30:00 | BA585 | London | LHR | British Airways | 961 | A319 |
| 17:40:00 | FR9959 | Luqa | MLA | Ryanair | 1159 | A320 |
| 17:45:00 | TP829 | Lisbon | LIS | Tap Air Portugal | 1686 | A321 |
| 17:50:00 | FR8737 | London | STN | Ryanair | 961 | A320 |
| 17:55:00 | FR7376 | Palermo | PMO | Ryanair | 888 | A320 |
| 17:55:00 | VY6335 | Barcelona | BCN | Vueling | 726 | A320 |
| 18:00:00 | AF1731 | Paris | CDG | Air France | 640 | A319 |
| 18:00:00 | A3553 | Saloniki | SKG | Aegean Airlines | 1239 | A321 |
| 18:00:00 | FR5519 | Catania | CTA | Ryanair | 1012 | B737 |
| 18:00:00 | W65585 | Catania | CTA | Wizz Air | 1012 | B737 |
| 18:10:00 | FR1205 | Seville | SVQ | Ryanair | 1549 | A321 |
| 18:10:00 | U28198 | London | LGW | Easyjet | 961 | A319 |
| 18:15:00 | UX1062 | Madrid | MAD | Air Europa | 1190 | B737 |
| 18:30:00 | EN8813 | Frankfurt | FRA | Air Dolomiti | 519 | E190 |
| 18:45:00 | A3665 | Athens | ATH | Aegean Airlines | 1464 | A321 |
| 18:50:00 | LX1623 | Zurich | ZRH | Swiss | 218 | A320 |
| 18:50:00 | TK1876 | Istanbul | IST | Turkish Airlines | 1675 | A321 |
| 18:55:00 | AY1756 | Helsinki | HEL | Finnair | 1940 | A320 |
| 19:10:00 | IB3265 | Madrid | MAD | Iberia | 1190 | A319 |
| 19:25:00 | KL1634 | Amsterdam | AMS | Klm | 830 | E190 |
| 19:30:00 | SM804 | Cairo | CAI | Air Cairo | 2576 | A320 |

Continued on next page

**Table A.4 – continued from previous page**

| Time | Flight | To | IATA code | Airline | Distance [km] | Aircraft |
|---|---|---|---|---|---|---|
| 19:40:00 | U22835 | Bari | BRI | Easyjet | 788 | A319 |
| 19:45:00 | LO320 | Warsaw | WAW | Lot - Polish Airlines | 1146 | E170 |
| 19:55:00 | AF1231 | Paris | CDG | Air France | 640 | A321 |
| 19:55:00 | FR5972 | Naples | NAP | Ryanair | 658 | A320 |
| 20:00:00 | NO292 | Rome | FCO | Neos | 476 | B737 |
| 20:00:00 | SK688 | Copenhagen | CPH | Sas | 1162 | A320 |
| 20:10:00 | U22847 | Catania | CTA | Easyjet | 1012 | A321 |
| 20:20:00 | ET713 | Rome | FCO | Ethiopian Airlines | 476 | B737 |
| 20:25:00 | EW9821 | Dusseldorf | DUS | Eurowings | 666 | A319 |
| 20:30:00 | OS516 | Wien | VIE | Austrian | 626 | A320 |
| 20:45:00 | FR3416 | Brindisi | BDS | Ryanair | 892 | A321 |
| 20:50:00 | U22729 | Amsterdam | AMS | Easyjet | 830 | B737 |
| 21:10:00 | LG6998 | Luxembourg | LUX | Luxair | 536 | B737 |
| 21:10:00 | VY6337 | Barcelona | BCN | Vueling | 726 | A320 |
| 21:20:00 | FR2758 | Madrid | MAD | Ryanair | 1190 | A321 |
| 21:25:00 | U22899 | Naples | NAP | Easyjet | 658 | A319 |
| 21:30:00 | FR5063 | Catania | CTA | Ryanair | 1012 | B737 |
| 21:50:00 | LW9216 | Wien | VIE | Lauda Europe | 626 | A320 |
| 22:00:00 | BO623 | Catania | CTA | Bluebird Nordic | 1012 | B737 |
| 22:35:00 | W62336 | Budapest | BUD | Wizz Air | 788 | A321 |
| 22:50:00 | ZT1807 | Cologne | CGN | Titan Airways | 631 | A321 |

# Acknowledgements

In conclusione di questo lungo percorso, desidero esprimere la mia più sincera gratitudine al mio relatore, il professor Lorenzo Trainelli e al correlatore il professor Carlo E.D. Riboldi, per avermi dato la possibilità di collaborare a questo progetto e per il continuo supporto e l'indispensabile aiuto datomi durante l'intero lavoro di tesi. Desidero inoltre ringraziare di cuore il mio tutor Gabriele Sirtori, per il suo essenziale sostegno non solo a livello professionale, ma anche personale, per l'estrema disponibilità e per i preziosi consigli. Infine, ringrazio il collega Jonathan Tarocco per aver gettato le solide basi su cui si fonda il lavoro qui presentato.

Un grazie infinito va alla mia famiglia. A Mamma e Papà per l'amore incondizionato e perché senza di loro non sarei nulla, a Elisabetta e Davide per essermi sempre stati accanto in ogni momento della mia vita. Il ringraziamento più grande è per voi quattro che avete sempre creduto in me più di quanto abbia mai fatto io stesso. Grazie alle mie nonne che ho la fortuna di avere qui con me oggi, e ai miei nonni che sempre le accompagnano. Grazie a Giulia, da sempre punto fermo e certezza indubbia. Grazie a Francesco, per l'amicizia sincera e per il supporto costante che dura dal primo anno. Grazie agli amici di Galatone per il legame indissolubile che resiste al tempo e alla distanza e senza il quale sarei perso, e agli amici di Milano che sono stati per me essenziali, come una famiglia lontano da casa. E per finire ringrazio tutte le persone che ho incontrato nel percorso e che, anche per un solo momento, hanno contribuito a rendere questi gli anni più belli della mia vita, finora.